27669

NATIONAL LIBRARY
OTTAWA

CANADA

BIBLIOTHÈQUE NATIONALE
OTTAWA

NAME OF AUTHOR. Ahmed H. Hussein

TITLE OF THESIS. Electromagnetic Interaction of Polarized Neutrons With Heavy Nuclei

UNIVERSITY. of Alberta

DEGREE FOR WHICH THESIS WAS PRESENTED. Ph. D.

YEAR THIS DEGREE GRANTED. 1976

Permission is hereby granted to THE NATIONAL LIBRARY OF CANADA to microfilm this thesis and to lend or sell copies of the film.

The author reserves other publication rights, and neither the thesis nor extensive extracts from it may be printed or otherwise reproduced without the author's written permission.

(Signed) A. H. Hussein

PERMANENT ADDRESS:

Nuclear Research
Centre, U. of A.
Edmonton, Alta

DATED. Aug. 12 19 76

NL-91 (10-68)

INFORMATION TO USERS

THIS DISSERTATION HAS BEEN MICROFILMED EXACTLY AS RECEIVED

This copy was produced from a microfiche copy of the original document. The quality of the copy is heavily dependent upon the quality of the original thesis submitted for microfilming. Every effort has been made to ensure the highest quality of reproduction possible.

PLEASE NOTE: Some pages may have indistinct print. Filmed as received.

Canadian Theses Division
Cataloguing Branch
National Library of Canada
Ottawa, Canada K1A 0N4

AVIS AUX USAGERS

LA THESE A ETE MICROFILMEE TELLE QUE NOUS L'AVONS RECUE

Cette copie a été faite à partir d'une microfiche du document original. La qualité de la copie dépend grandement de la qualité de la thèse soumise pour le microfimage. Nous avons tout fait pour assurer une qualité supérieure de reproduction.

NOTA BENE: La qualité d'impression de certaines pages peut laisser à désirer. Microfilmée telle que nous l'avons reçue.

Division des thèses canadiennes
Direction du catalogage
Bibliothèque nationale du Canada
Ottawa, Canada K1A 0N4

THE UNIVERSITY OF ALBERTA

ELECTROMAGNETIC INTERACTION OF POLARIZED NEUTRONS WITH HEAVY NUCLEI

by

AHMED HASSAN HUSSEIN (C)

A THESIS

SUBMITTED TO THE FACULTY OF GRADUATE STUDIES AND RESEARCH

IN PARTIAL FULFILLMENT OF THE REQUIREMENTS FOR THE DEGREE

OF DOCTOR OF PHILOSOPHY

IN

PHYSICS

DEPARTMENT OF PHYSICS

EDMONTON, ALBERTA

SPRING 1976

THE UNIVERSITY OF ALBERTA

FACULTY OF GRADUATE STUDIES AND RESEARCH

The undersigned certify that they have read, and recommend to the Faculty of Graduate Studies and Research, for acceptance, a thesis entitled ELECTROMAGNETIC INTERACTION OF POLARIZED NEUTRONS WITH HEAVY NUCLEI submitted by Ahmed Hassan Hussein in partial fulfillment of the requirements for the degree of Doctor of Philosophy in Physics.

J.M. Cameron
Co-supervisor

[illegible]
Co-supervisor

D.J. Jongh

Helmy S. Shif

P.P. Comyach

[illegible]
External Examiner

Date: Mar. 10, 1976

ABSTRACT

A facility has been designed and built to produce 10 MeV polarized neutrons. This facility was used to measure the polarization and cross section of 10 MeV neutrons scattered from Pb and Bi in the angular range of 1.5-65°.

No significant difference has been found between the measurements of the small angle polarization of 10 MeV neutrons scattered from Pb and Bi, in contrast to the situation at 2.5 MeV reported previously. Furthermore, DWBA calculation using only the nuclear and Mott-Schwinger interactions give good agreement with the data.

Comparison of the experimental results with predictions using three different global optical potentials proved that the Becchetti and Greenlees potential can best describe both the differential cross section and polarization in the scattering of 10 MeV neutrons from heavy elements.

ACKNOWLEDGEMENT

The successful conclusion of the work reported in this thesis is due to the efforts of a large number of people. I was able to go forward all the time by the direct and positive involvement of some of these people and also by the negative attitude of others. I would like to thank them all.

I would like to express my gratitude and special thanks to the following people.

Dr. G.C. Neilson for his support and encouragement. He was always available for advice and consultation.

Dr. J.M. Cameron for his active participation in all phases of the work. He gave freely of his time for discussion and support and during many weeks of experimental runs.

Dr. Helmy Sherif for his contribution which extends beyond nuclear physics. Helmy is a good friend, we spent long hours on interesting discussions about nuclear physics, physics in general, politics and "life". His contributions to this work were numerous and very useful. I would like to thank him, in particular, for allowing me to use his computer programs.

Dr. Y. Selim, of the University of Alexandria, Egypt, who was the first to direct me to the exciting world of polarization!

Dr. S.T. Lam, Mr. J. Soukup and Dr. H. Fielding for their continuous invaluable support and help.

Dr. S.B. Woods and Mr. T. Vallian for their help in sorting out the troubles of the superconducting solenoid. It was a pleasure to work with them.

The late C.F. Green for his efforts in building the detector shield.

The graduate students, summer students, post doctors, academic and non academic staff of the Nuclear Research Center for their help and support specially by taking some of the numerous night shifts used for data collection. Special thanks to Jim Pasos who was always available for night shifts.

Mrs. Mary Yiu for her efficient trouble free typing of this thesis.

The Egyptian and Canadian people for their financial support during my long years of education through the University of Alexandria and the University of Alberta.

Finally I would like to express my gratitude to my parents and the rest of my family in Egypt for things I could not possibly list here.

TABLE OF CONTENTS

		Page
CHAPTER 1	INTRODUCTION	1
CHAPTER 2	POLARIZATION	5
	2.1 Introduction	5
	2.2 Density Matrix for Spin $\frac{1}{2}$	7
	2.3 Observables for $\vec{\frac{1}{2}}+A \rightarrow \vec{\frac{1}{2}}+B$	11
	2.4 Measurements in $\vec{\frac{1}{2}}+A \rightarrow \vec{\frac{1}{2}}+A$ Experiments	26
CHAPTER 3	THE POLARIZED NEUTRON FACILITY	34
	3.1 Polarized Neutron Source	34
	3.2 Spin Rotation	38
	3.3 Shielding	43
	3.3.1 Source Shielding	46
	3.3.2 The Large Scattering Angle Shield	49
	3.3.3 Small Scattering Angle Shield	54
CHAPTER 4	NEUTRON-NUCLEUS ELECTROMAGNETIC INTERACTION	61
	4.1 Introduction	61
	4.2 Theoretical Calculations	70
CHAPTER 5	MEASUREMENT OF POLARIZATION AND CROSS SECTION OF 10 MeV NEUTRONS SCATTERED FROM LEAD AND BISMUTH	79
	5.1 Introduction	79
	5.2 Scatterers	82

		Page
CHAPTER 5	(cont'd)	
	5.3 Detectors	82
	5.4 Angular Calibration	92
	5.5 Experimental Results	100
CHAPTER 6	COMPARISON WITH THEORETICAL CALCULATIONS	115
	6.1 Introduction	115
	6.2 The Program Code "TASHTASH"	119
CHAPTER 7	CONCLUSIONS	129
APPENDIX A	MULTIPLE SCATTERING CORRECTIONS	133
	A.1 Introduction	133
	A.2 The Program PMS1	136
	A.3 The Modified Program	147
APPENDIX B	THE SUPERCONDUCTING SOLENOID SYSTEM	150
	B.1 The Solenoid and the Persistent Switch	150
	B.2 The Power Supply	161
	B.3 The Cryostat	161
REFERENCES		166

LIST OF TABLES

Table		Page
3.1	Properties of neutrons produced by $^{9}Be(^{4}He,\vec{n})^{12}C$ and $^{3}H(d,\vec{n})^{4}He$.	36
3.2	Comparison between solenoids used to rotate spin of 24.0 MeV neutrons by 90°.	42
6.1	Optical model parameters used in theoretical calculations.	118
B.1	Specifications of the superconducting solenoid system.	151
B.2	Measurements of the magnetic field along the axis of the solenoid at two different points.	159

LIST OF FIGURES

Figure		Page
2.1	Definition of projectile and outgoing particle sets of axes.	14
2.2	Definition of polarization of the incident beam in the projectile set of axes. The scattering is in the x-z plane.	16
2.3	Definition of spin rotation parameter β.	24
2.4	a) Relation between spin and orbital angular momentum. b) Experimental set up of a double scattering experiment.	28
3.1	Typical time-of-flight spectrum of neutron produced by $^{9}Be(^{4}He,n)^{12}C$ reaction taken at the laboratory angle of 30°.	40
3.2	General experimental set up.	45
3.3	Source shielding.	48
3.4	Large angle experimental set up.	51
3.5	Detector shield.	53
3.6	Basic types of scattering geometry.	56
3.7	Experimental set up for small angle scattering.	60
5.1	Basic principle of the long detector.	84
5.2	Detectors' holder for small angle scattering measurements.	88
5.3	Block diagram of time-of-flight electronics with n-γ separation.	91
5.4	Typical time-of-flight spectra for the elastic scattering of 10 MeV polarized neutrons from Pb at scattering angle of 1.5°.	94

Figure		Page
5.5	The same spectrum shown in figure 5.4d. The straight line under the 10 MeV peak is the average linear background.	96
5.6	Neutron absorption in the scatterer as a function of detector position.	99
5.7	Small angle polarization of 10 MeV neutrons scattered from Pb and Bi.	104
5.8	Small angle polarization of 10 MeV neutrons scattered from Pb and Bi corrected for multiple scattering and finite geometry effects.	106
5.9	Small angle asymmetry of 5.57 MeV neutrons scattered from Pb and Bi.	108
5.10	Small angle differential cross section of 10 MeV neutrons scattered from Pb and Bi.	110
5.11	Large angle polarization of 10 MeV neutrons scattered from Pb and Bi.	112
5.12	Large angle differential cross section of 10 MeV neutrons scattered from Pb and Bi.	114
6.1	Comparison between theoretical calculations and small angle polarization measurements.	121
6.2	Comparison between theoretical calculations and small angle differential cross section.	123
6.3	Comparison between theoretical calculations and large angle polarization measurements.	125
6.4	Comparison between theoretical calculations and large angle differential cross section.	127
A.1	Experimental geometry simulated by the Monte Carlo code PMS1.	138

Figure		Page
B.1	Schematic circuit diagram for the superconducting solenoid and the persistent switch.	153
B.2	The profile of the axial magnetic field of the superconducting solenoid.	158
B.3	Schematic diagram of the liquid helium cryostat.	164

CHAPTER 1

INTRODUCTION

The production of a well collimated mono energetic neutron beam is very difficult and as a result there is a paucity of experiments involving the scattering of fast neutrons. Good collimation requires very well designed massive shielding. Many charged particle reactions which produce neutrons result in more than one energy group of neutrons. An efficient separation of these groups requires a high resolution time-of-flight system. Thus a high intensity pulsed beam of charged particles must be used to initiate the reaction.

The difficulties in producing good beam are further magnified when one tries to produce polarized neutrons. In addition to the above mentioned difficulties one will have to face the fact that in a nuclear reaction the maxima of polarization and cross section are out of phase i.e. the polarization will attain its maximum value when the cross section is at its minimum. Thus to produce a polarized neutron beam, one has to maximize the beam current, production target thickness, the scatterer size and detector efficiency and optimize the geometry without jeopardizing the quality of the neutron beam.

The 6 MeV Van der Graaff accelerator of the University of Alberta, has a 0.3 n.s, pulsed beam and is ideally suited to produce fast neutron beams. The reaction $^{9}Be(^{4}He,n)^{12}C$ has been used as the neutron source in this work. With a ^{4}He energy of 5.45 MeV one obtains 10 MeV neutrons with 0.44 ± 0.03 polarization at a laboratory reaction angle of 30°. Using a target of 0.8 mg/cm^2 one has an energy spread of 500 KeV and a flux of 6×10^{6} neutrons/sec.μa.sr. Various combinations of source and detector shielding were used to allow the scattering angular range from 60° to 1.5° to be studied. A Monte Carlo computer code was modified to correct, for multiple scatter effects, not only the large angle polarization data but also the small angle measurements as well. Such corrections become very important for very small scattering angles.

The polarized neutron facility, described above, has been used to compare the elastic scattering of 10 MeV neutrons from Bismuth (Bi) and Lead (Pb). In the small angle region, the long range forces dominate the interaction between the incident neutron and the scattering nucleus. The interaction between the magnetic moment of the neutron and the Coulomb field of the nucleus (M-S interaction) and the interaction between the neutron induced electric moment and the nuclear Coulomb field are examples of such long range forces that may contribute

to the small angle region. The existence of the M-S force has been well established experimentally and theoretically. However, the existence of the interaction between the induced electric moment of the neutron and the Coulomb field of the nucleus is still controversial. A further difficulty arises from the results reported by Drigo et al (Dr 73). They found a difference between the polarization of 2.45 MeV neutrons scattered from Pb and Bi in the angular region where the long range forces are dominant. This difference could not be accounted for using the nuclear forces and the above mentioned long range forces. If such a difference is real it may be very important and might be an indication of the existence of another long range force. So it is not clear if one can predict the small angle observables by simple theoretical treatment which includes only the M-S and nuclear forces.

There are three "global" optical model potential sets of parameters which are frequently used to describe the scattering of neutrons in the energy range of 10-30 MeV from Pb and Bi. Recently Bucher and Hollandsworth (Bu 75 and Bu 75a) reported that two of these sets, namely Rosen et al (Ro 62) and Wilmore and Hodgson (Wi 64), do not produce the same cross section for the scattering of 7-14 MeV neutrons from Pb and Bi in the angular range of 2.5-15°. It is thus of some importance

to compare these three potentials to see which provides the best description of the scattering of 10 MeV neutrons.

In an attempt to answer the questions mentioned above, the polarization and cross section of 10 MeV neutrons have been measured in the angular range of 1.5°-65° and the results are reported in this thesis.

CHAPTER 2

POLARIZATION

2.1 Introduction

Nuclear reactions involving polarization measurements are very important tools in nuclear physics investigations. In this chapter we will introduce the necessary formalism for the description of polarization. The discussion will be restricted to spin 1/2 particles and spin zero targets.

A particle with spin $\vec{S}$ will have z-component quantum number m_s. Quantum mechanically m_s is allowed to take only the discrete values +S, S-1, ... -S. If S = 1/2 then $m_s = \pm 1/2$. This means that the spin vector can be parallel or antiparallel to the (+ve) z-direction. A particle with spin 1/2 can exist only in one of two spin states +1/2 or "spin-up" state or -1/2 or "spin-down" state. In an ensemble of particles, however, a fraction of the particles in the ensemble can have spin up and the rest will, of course, have spin down. "Polarization" is the quantity normally used as a measure for the distribution of spin states in an ensemble of particles. Let $N_\uparrow$ and $N_\downarrow$ be the number of particles with spin up and spin down respectively. If $N_\uparrow = N_\downarrow$ then the ensemble is unpolarized. If either $N_\uparrow$ or $N_\downarrow$ is zero then the ensemble is fully polarized.

If P is the polarization of the ensemble then P = 0 for the unpolarized case and $|P| = 1$ for the fully polarized case. If $N_\uparrow$ and $N_\downarrow$ are not equal but neither of them is zero, then the assembly is partially polarized and $0 < |P| < 1$ and P will be given by:

$$P = \frac{N_\uparrow - N_\downarrow}{N_\uparrow + N_\downarrow} \quad .$$

Ohlsen (Oh 72) has suggested the following classification of nuclear reactions and scattering experiments, which involve polarized particles,

i) $A(b,\vec{c})D$ polarization experiments.

ii) $A(\vec{b},c)D$ analysing power experiments.

iii) $A(\vec{b},\vec{c})D$ polarization transfer experiments.

In an experiment of type (i) a beam of particles b will interact with a target A to produce a polarized beam of particles c (the arrow above the letter indicates that the beam is polarized). The polarization of $\vec{c}$ can be measured using an "analyser" that is sensitive to the polarization of $\vec{c}$. If the projectile beam "b" is unpolarized, then this kind of reaction is called a "polarizer". In type (ii) experiments the polarization of particle $\vec{b}$ is usually known and by measuring the "left-right" asymmetry one can obtain the "analysing power" of the target nucleus and the process is called an "analyser". In the work described in this thesis a

charged particle reaction of type (i) is used to produce a polarized neutron beam and the elastic scattering of type (ii) is used to measure the analysing power of some nuclei. In type (iii) experiments the polarization of particle $\vec{b}$ is usually known and that of particle $\vec{c}$ is usually measured using an "analyser".

2.2 Density Matrix for Spin 1/2

In the rest of this chapter we will mainly follow an article by Ohlsen (Oh 72). A Pauli spinor of the form:

$$\chi = \begin{pmatrix} a_1 \\ a_2 \end{pmatrix}$$

can be used to represent a spin 1/2 particle. This is a representation of a fully polarized particle, which means that the spin vector points along a definite direction. If that direction is chosen as the quantization (z) axis, then the spinor will have $a_2 = 0$. The expectation value of any observable corresponding to any hermetian operator Ω is:

$$\langle\Omega\rangle = \chi^*\Omega\chi = (a_1^* \; a_2^*) \begin{pmatrix} \Omega_{11} & \Omega_{12} \\ \Omega_{21} & \Omega_{22} \end{pmatrix} \begin{pmatrix} a_1 \\ a_2 \end{pmatrix}$$

$$= |a_1|^2 \, \Omega_{11} + |a_2|^2 \Omega_{22} + 2 \, \mathrm{Re} \, \Omega_{12} a_1 a_2^* \qquad (2.1)$$

Note that $\Omega_{21} = \Omega_{12}^*$ for hermetian operators.
One can, now, define the density matrix as

$$\rho = \begin{pmatrix} |a_1|^2 & a_1 a_2^* \\ a_2 a_1^* & |a_2|^2 \end{pmatrix} . \tag{2.2}$$

It is convenient to rewrite (2.1) as:

$$\langle\Omega\rangle = \mathrm{Tr}\ \rho\Omega \quad . \tag{2.3}$$

All the above results can now be generalized to an ensemble of N identical particles. The Pauli spinor has to be specified for each particle

$$\chi^{(n)} = \begin{pmatrix} a_1^{(n)} \\ a_2^{(n)} \end{pmatrix} \tag{2.4}$$

where the n-superscript refers to the nth particle. The average of the expectation value of the operator Ω now operating on the ensemble is:

$$\overline{\langle\Omega\rangle} = \sum_{n=1}^{N} \chi^{\dagger(n)} \Omega \chi^{(n)} = \mathrm{Tr}\ \rho\Omega \tag{2.5}$$

and ρ in this case will be given as:

$$\rho = \frac{1}{N} \begin{pmatrix} \sum_{n=1}^{N} |a_1^{(n)}|^2 & \sum_{n=1}^{N} a_1^{(n)} a_2^{(n)*} \\ \sum_{n=1}^{N} a_2^{(n)} a_1^{(n)*} & \sum_{n=1}^{N} |a_2^{(n)}|^2 \end{pmatrix} \tag{2.6}$$

The rest of the discussion will be restricted to ensembles, and the bar indicating ensemble averages will be dropped.

The state of polarization of an ensemble can be specified by Pauli spin operators defined as:

$$\sigma_x = 2S_x = \begin{pmatrix} 0 & 1 \\ 1 & 0 \end{pmatrix}$$

$$\sigma_y = 2S_y = \begin{pmatrix} 0 & -i \\ i & 0 \end{pmatrix} \qquad (2.7)$$

$$\sigma_z = 2S_z = \begin{pmatrix} 1 & 0 \\ 0 & -1 \end{pmatrix}$$

S_x, S_y and S_z are spin angular momentum operators. Applying equation (2.5) to σ_x, σ_y and σ_z we get:

$$p_x = \langle\sigma_x\rangle = \mathrm{Tr}\ \rho\sigma_x = \frac{1}{N}\sum_{n=1}^{N} 2\ \mathrm{Re}(a_1^{(n)} a_2^{(n)*})$$

$$p_y = \langle\sigma_y\rangle = \mathrm{Tr}\ \rho\sigma_y = \frac{1}{N}\sum_{n=1}^{N} 2\ \mathrm{Im}(a_1^{(n)} a_2^{(n)*}) \qquad (2.8)$$

$$p_z = \langle\sigma_z\rangle = \mathrm{Tr}\ \rho\sigma_z = \frac{1}{N}\sum_{n=1}^{N} (|a_1^{(n)}|^2 - |a_2^{(n)}|^2) \ .$$

The expectation value of the unit matrix I gives the normalization of the density matrix, i.e.

$$\langle I\rangle = \mathrm{Tr}\ \rho = \frac{1}{N}\sum(|a_1^{(n)}|^2 + |a_2^{(n)}|^2) = 1 \ . \qquad (2.9)$$

This normalization of the density matrix follows from

the assumption that each Pauli spinor is normalized. It is possible to drop the factor 1/N in all the above definitions if Tr ρ is taken to indicate the total number of particles in the ensemble.

Equations (2.8) will put limits of ± 1 on p_x, p_y and p_z. The set of operators I, σ_x, σ_y and σ_z forms a complete set of hermetian matrices for the spin 1/2 2×2 space. So, any other operator in this space is a linear combination of these operators. Thus p_x, p_y and p_z provide a complete description of the polarization of any spin 1/2 ensemble.

Since ρ is a 2×2 matrix then it can be expanded in terms of the basic set I, σ_x, σ_y and σ_z, as

$$\rho = \sum_j c_j \sigma_j \tag{2.10}$$

where $j = 0,1,2,3$ and $\sigma_o = I$, $\sigma_1 = \sigma_x$, $\sigma_2 = \sigma_y$ and $\sigma_3 = \sigma_z$. Since

$$\text{Tr } \sigma_i \sigma_j = 2\delta_{ij} \tag{2.11}$$

then:

$$\text{Tr } \rho\sigma_j = 2c_j = \langle \sigma_j \rangle = p_j \tag{2.12}$$

and

$$\begin{aligned} \rho &= \tfrac{1}{2}(I + p_x\sigma_x + p_y\sigma_y + p_z\sigma_z) \\ &\equiv \tfrac{1}{2}\left(I + \sum_{j=1}^{3} p_j\sigma_j\right) . \end{aligned} \tag{2.13}$$

2.3 Observables For $\vec{\frac{1}{2}}+A \rightarrow \vec{\frac{1}{2}}+B$

This kind of interaction has its most general form in experiments dealing with the interaction of polarized particles with non-polarized nuclei. In neutron scattering experiments one usually deals with a thick scatterer with a large possibility that the neutron will scatter more than once before leaving the scatterer. In any multiple scattering polarization corrections, the above interaction is the basic interaction, and all its observables are needed to perform the corrections as will be explained in Appendix A of this thesis.

It is important to start our discussion by defining the coordinate system. It is customary to define a set of axes for the projectile and another set for the outgoing particles. For the projectile a set of axes can be chosen such that the z-axis is taken along the momentum vector $\vec{k}_i$; the y-axis normal to the scattering plane is defined by $\vec{k}_i \wedge \vec{k}_f$ where $\vec{k}_f$ is the momentum vector of the outgoing particles, and x-axis such as to form a right-handed coordinate system. The unit vectors of this system will be called $\hat{p}$, $\hat{n}$ and $\hat{k}$ corresponding to x, y and z directions respectively. For the outgoing particle the set of axes x', y' and z' can be defined in a similar way. The z'-axis will be taken along $\vec{k}_f$, and the y'-axis will be along the same direction as the y-axis and similarly x' will form a right-handed system. The unit

vectors will be $\hat{p}'$, $\hat{n}'$ and $\hat{k}'$. Fig. 2.1 shows such systems.

To define the polarization of the incident beam let us consider fig. 2.2. The coordinate system is defined as mentioned above. $\hat{S}$ is a general quantization axis of the incident beam. $\hat{\ell}$ is the projection of $\hat{S}$ in the xy plane. Let $\hat{S}$ make an angle β with z-axis (the incident beam direction) and ϕ is the angle between $\hat{\ell}$ and the y axis. Then β and ϕ can be defined vectorially as

$$\cos \beta = \hat{S} \cdot \hat{k}_i \qquad (2.14)$$

and

$$\cos \phi = (\hat{S} \wedge \hat{k}_i) \cdot (\hat{n} \wedge \hat{k}_i) \ . \qquad (2.15)$$

The angle ϕ is very important and it is taken to be positive in the sense of a right-handed screw with x-axis going into y. Now if $\hat{S}$ is pointing in a direction such that $\hat{\ell}$ is parallel to y-axis then $\phi = 0$ and if $\hat{\ell}$ is antiparallel to y-axis then $\phi = 180°$. Similarly $\phi = 90°$ and 270 if $\hat{\ell}$ is antiparallel and parallel to the x-axis respectively. In nuclear reactions involving unpolarized projectiles the polarization vector of the outgoing particles is always perpendicular to the scattering plane formed by $\vec{k}_i$ and $\vec{k}_f$ i.e. $\hat{S}$ will be along the $\hat{y}(\hat{n})$ axis, this means that ϕ will be either 0 or 180°.

Figure 2.1 - Definition of projectile and outgoing particle sets of axes.

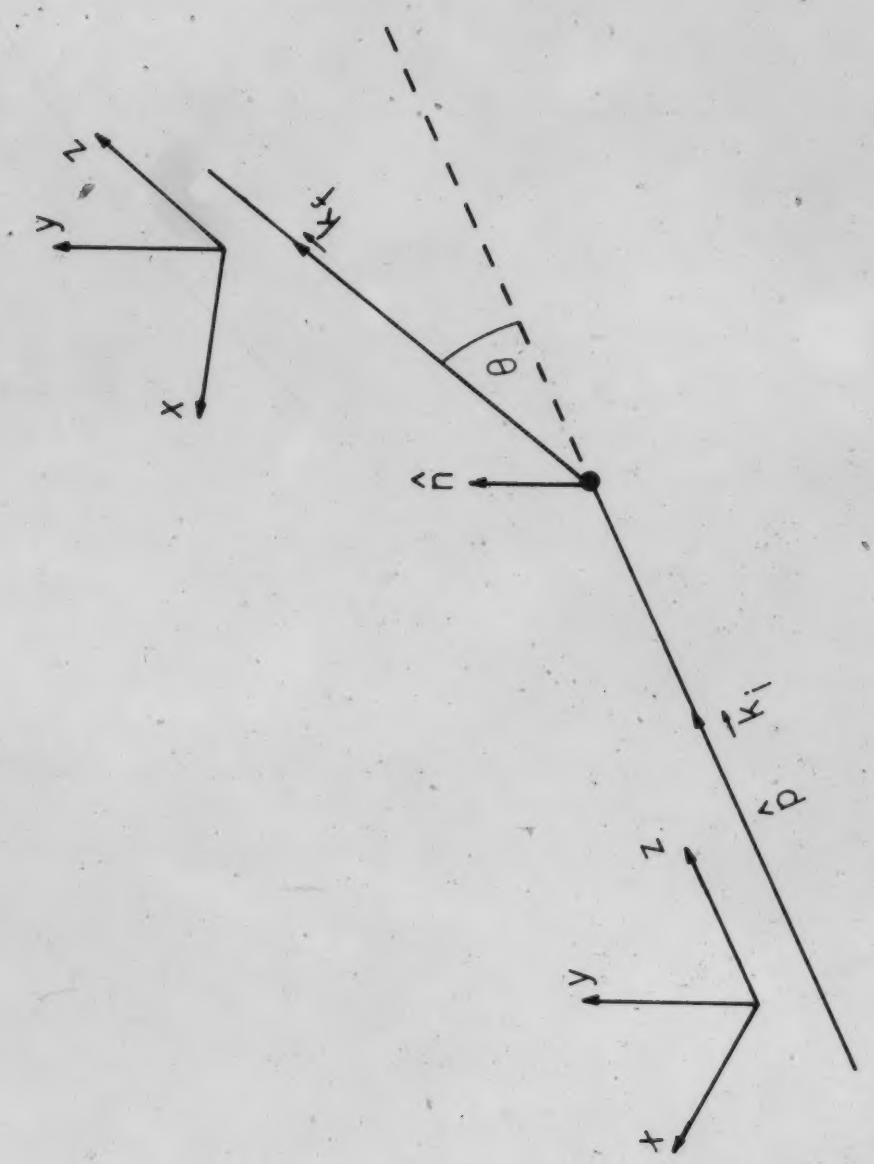
z
y
x
$\vec{r}_t$
θ
$\vec{r}_i$
$\vec{\rho}$
z
y
x

Figure 2.2 - Definition of the polarization of the incident beam in the projectile set of axes. The scattering is in the x-z plane.

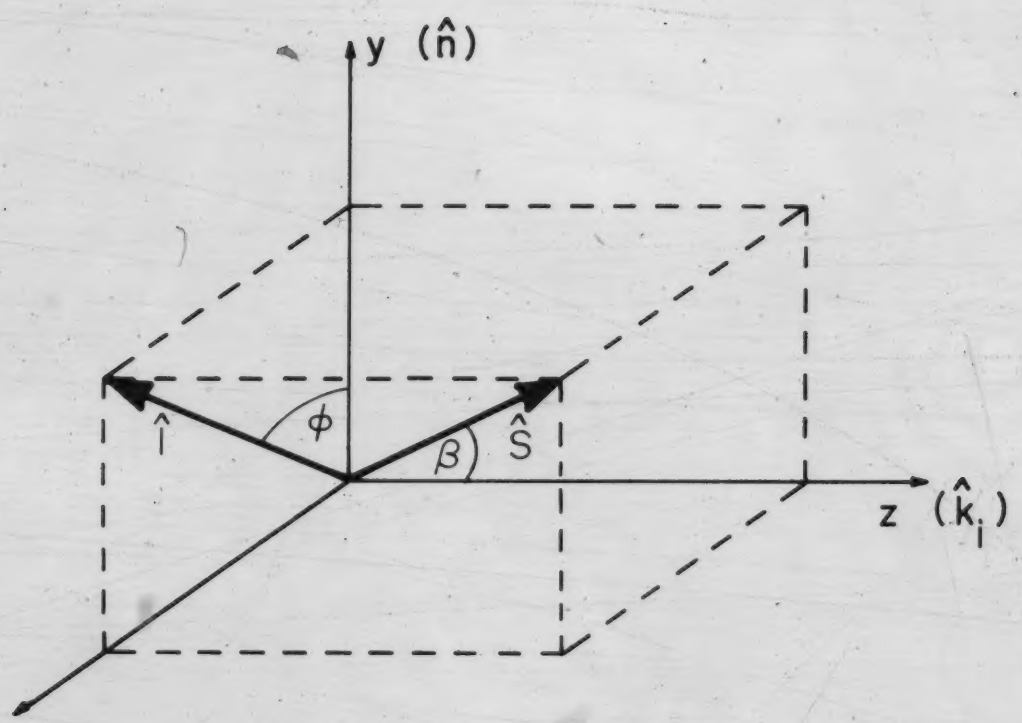
y (n̂)
î
φ
β
Ŝ
z (k̂ᵢ)

We will turn our attention now to the scattering process of the form $\vec{\tfrac{1}{2}}+A \rightarrow \vec{\tfrac{1}{2}}+B$. Let χ_f be the spinor describing the outgoing particle spin. This spinor can be related to χ_i, the spinor describing the projectile spin, through the relation

$$\chi_f = M\chi_i \tag{2.16}$$

where M is a 2×2 matrix whose elements are, in general, functions in energy and angle. χ_i is defined in the projectile frame where χ_f is defined in the outgoing particle frame, as defined above. Assuming A and B are spin-zero nuclei, then the density matrix describing the initial state is:

$$\rho_i = \sum_{n=1}^{N} \chi_i^{(n)} [\chi_i^{(n)}]^{\dagger} \tag{2.17}$$

where $[\chi_i^{(n)}]^{\dagger}$ is the hermetian conjugate of $\chi_i^{(n)}$. Similarly, for the final state,

$$\rho_f = \sum_{n=1}^{N} \chi_f^{(n)} [\chi_f^{(n)}]^{\dagger} . \tag{2.18}$$

N is the total number of particles in each ensemble. Since,

$$\chi_f^{\dagger} = \chi_i^{\dagger} M^{\dagger}$$

then equation (2.18) becomes:

$$\rho_f = M\rho_i M^{\dagger} . \tag{2.19}$$

Now the scattering cross section is given by:

$$I(\theta,\phi) = Tr(\rho_f)/Tr(\rho_i)$$

$$= Tr(M\rho_i M^\dagger)/Tr(\rho_i) \quad . \qquad (2.20)$$

If ρ_i is now normalized to unity then

$$I(\theta,\phi) = Tr(M\rho_i M^\dagger) \quad . \qquad (2.21)$$

This is the cross-section for the scattering of a polarized beam. If the incident beam is unpolarized then

$$\rho_i = \frac{1}{2}\begin{pmatrix} 1 & 0 \\ 0 & 1 \end{pmatrix} \qquad (2.22)$$

and this will give:

$$I_o(\theta) = \frac{1}{2} Tr(MM^\dagger) \quad . \qquad (2.23)$$

Using equation (2.13) equation (2.21) becomes:

$$I(\theta,\phi) = \frac{1}{2} Tr[M(1 + \sum_{j=1}^{3} p_j\sigma_j)M^\dagger]$$

$$= \frac{1}{2} Tr\ MM^\dagger + \frac{1}{2} \sum_{j=1}^{3} p_j\ Tr(M\sigma_j M^\dagger) \quad . \qquad (2.24)$$

Using equation (2.23) we get:

$$I(\theta,\phi) = I_o(\theta)(1 + \sum_{j=1}^{3} p_j A_j(\theta)) \qquad (2.25)$$

where

$$A_j(\theta) = \frac{\text{Tr } M\sigma_j M^\dagger}{\text{Tr } MM^\dagger} \quad . \tag{2.26}$$

The quantity $A_j(\theta)$ is called the analysing power of the scattering for the jth component of the initial polarization. Similar relations for the outgoing polarization can be established. One can write equations (2.8) for the outgoing polarization as:

$$P_{k'} \equiv \langle \sigma_{k'} \rangle = \text{Tr } \rho_f \sigma_{k'} / \text{Tr } \rho_f$$

$$\therefore \quad P_{k'} \cdot \text{Tr } \rho_f = \text{Tr } \rho_f \sigma_{k'} \quad .$$

Using equations (2.20) (notice that ρ_i is normalized) and (2.24) one gets

$$P_{k'} \, I(\theta,\phi) = I_o(\theta)\left[P_{k'}(\theta) + \sum_{j=1}^{3} p_j K_j^{k'}(\theta)\right] \tag{2.27}$$

where

$$P_{k'}(\theta) = \frac{\text{Tr } MM^\dagger \sigma_{k'}}{\text{Tr } MM^\dagger} \tag{2.28}$$

and

$$K_j^{k'}(\theta) = \frac{\text{Tr } M\sigma_j M^\dagger \sigma_{k'}}{\text{Tr } MM^\dagger} \tag{2.29}$$

where $P_{k'}(\theta)$ is the kth component of polarization which would be produced by an unpolarized beam, and $K_j^{k'}(\theta)$ is the polarization transfer coefficient that relates the

jth initial polarization component to the kth final polarization component. It is easy now to rewrite equations (2.25) and (2.27) as:

$$
\begin{aligned}
&I(\theta,\phi) = I_o(\theta)[1 + p_x A_x(\theta) + p_y A_y(\theta) + p_z A_z(\theta)] \\
&p_k, I(\theta,\phi) = I_o(\theta)[P_x,(\theta) + p_x K_x^{x'}(\theta) + p_y K_y^{x'}(\theta) + p_z K_z^{x'}(\theta)] \\
&p_y, I(\theta,\phi) = I_o(\theta)[P_y,(\theta) + p_x K_x^{y'}(\theta) + p_y K_y^{y'}(\theta) + p_z K_z^{y'}(\theta)] \\
&p_z, I(\theta,\phi) = I_o(\theta)[P_z,(\theta) + p_x K_x^{z'}(\theta) + p_y K_y^{z'}(\theta) + p_z K_z^{z'}(\theta)] \ .
\end{aligned}
\tag{2.30}
$$

Equations (2.30) are the most general forms that are allowed by the conservation of angular momentum. Moreover, if parity conservation, rotation invariance and the relation between the reaction and its inverse are imposed on equations (2.30), they will be reduced to:

$$
\begin{aligned}
&I(\theta,\phi) = I_o(\theta)[1 + p_y A_y(\theta)] \\
&p_x, I(\theta,\phi) = I_o(\theta)[p_x K_x^{x'}(\theta) + p_z K_z^{x'}(\theta)] \\
&p_y, I(\theta,\phi) = I_o(\theta)[P_y,(\theta) + p_y K_y^{y'}(\theta)] \\
&p_z, I(\theta,\phi) = I_o(\theta)[p_x K_x^{z'}(\theta) + p_z K_z^{z'}(\theta)] \ .
\end{aligned}
\tag{2.31}
$$

In a nuclear reaction where the reaction and its inverse are identical (elastic scattering) time reversal invariance

shows that:

$$K_x^{x'} = K_z^{z'} \quad ,$$

$$A_y = P_{y'} \quad , \qquad (2.32)$$

and $$K_x^{z'} = - K_z^{x'}$$

which means that

$$I(\theta,\phi) = I_o(\theta)[1 + p_y P_{y'}(\theta)] \quad . \qquad (2.33)$$

Now p_y is the component of the incident particle polarization along the y-axis in the incident particle frame and $P_{y'}(\theta)$ is the y-component of the polarization of the outgoing particles which would be produced by an unpolarized beam. This means that both p_y and $P_{y'}(\theta)$ are perpendicular to the reaction plane and the angle between them is ϕ. In this case ϕ will be either 0 or 180°. Now one can write equation (2.33) as:

$$I(\theta,\phi) = I_o(\theta)[1 + \vec{P}_1 \cdot \vec{P}_2] = I_o(\theta)[1 + P_1 P_2 \cos \phi] \qquad (2.34)$$

$$I(\theta,0) = I_o(\theta)[1 + P_1 P_2] \qquad (2.35)$$

$$I(\theta,180) = I_o(\theta)[1 - P_1 P_2] \qquad (2.36)$$

where $P_1 = p_y$ and $P_{y'}(\theta) = P_2$.

From equations (2.35) and (2.36) one can get the familiar equation for the asymmetry

$$\varepsilon = \frac{I(\theta,0) - I(\theta,180)}{I(\theta,0) + I(\theta,180)} = P_1 P_2 \quad . \qquad (2.37)$$

In the scattering of spin-1/2 particles from spin zero nuclei, the polarization component in the reaction (x-z) plane will rotate through a certain angle "β" after collision. Moreover, the magnitude of that component will be reduced by a factor of $(1 - P_{y'}^2)^{\frac{1}{2}}$. As shown in fig. 2.3 the angle β is given by:

$$\beta = \beta_f - \beta_i + \theta$$

where θ is the laboratory scattering angle. Then

$$\tan(\beta-\theta) = \tan(\beta_f - \beta_i)$$

$$= (\tan \beta_f - \tan \beta_i)/1 + \tan \beta_f \tan \beta_i$$

since $\tan \beta_f = \frac{p_{x'}}{p_{z'}}$ and $\tan \beta_i = \frac{p_x}{p_z}$.

Then by using equations (2.31) and (2.32) we get:

$$\tan(\beta-\theta) = \frac{K_z^{x'}}{K_x^{x'}} \quad . \qquad (2.38)$$

If we take now a single z-axis along the projectile momentum for both the incident and outgoing particle frames, then we get:

$$K_x^{x'} = K_z^{z'} = K_x^x \cos\theta + K_z^x \sin\theta$$

$$K_z^{x'} = -K_x^{z'} = K_z^x \cos\theta - K_x^x \sin\theta \quad . \qquad (2.39)$$

Figure 2.3 - Definition of spin rotation parameter β.

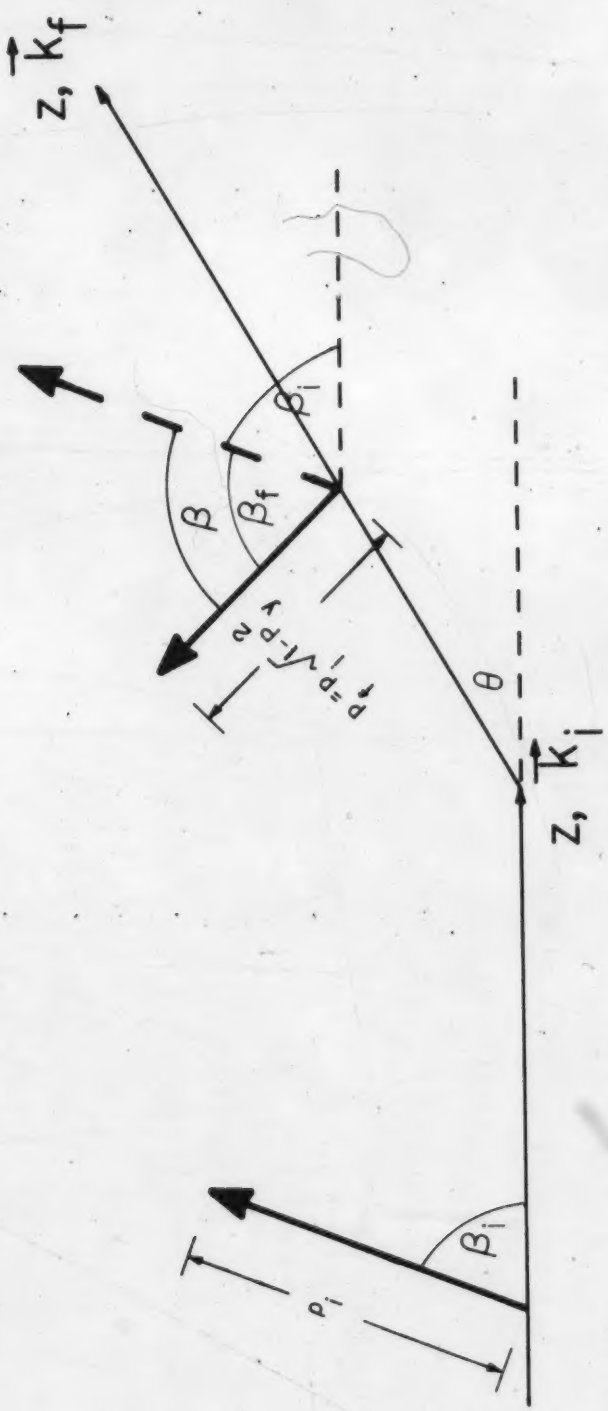
z, $\vec{k}_f$
β
β_f
β_i
$\rho = \rho / \sqrt{1-\rho^2}$
θ
z, $\vec{k}_i$
β_i
ρ_i

Using equation (2.38) one gets:

$$\tan(\beta-\theta) = \frac{\tan\theta - K_z^x/K_x^x}{1 + \tan\theta\, K_z^x/K_x^x}$$

or

$$\tan\beta = K_z^x/K_x^x$$

and

$$\sin\beta = K_z^x \qquad \cos\beta = K_x^x \quad . \tag{2.40}$$

Equations (2.31), for the polarization of the scattered particles, can be rewritten, with the help of equations (2.33) and (2.38), as:

$$p_{x'} = \frac{\sqrt{1 - P_{y'}^2(\theta)}}{1 + p_y P_{y'}(\theta)} [p_x\cos(\theta-\beta) - p_z\sin(\theta-\beta)]$$

$$p_{y'} = \frac{P_{y'}(\theta) + p_y}{1 + p_y P_{y'}(\theta)} \tag{2.41}$$

$$p_{z'} = \frac{\sqrt{1 - P_{y'}^2(\theta)}}{1 + p_y P_{y'}(\theta)} [p_x\sin(\theta-\beta) + p_z\cos(\theta-\beta)] \quad .$$

All the necessary observables for the elastic scattering of a polarized beam of spin 1/2-particles have been defined. These observables can be defined in terms of the M-matrix.

The M-matrix can be defined as:

$$M = A + B\sigma_y = \begin{pmatrix} A & -iB \\ iB & A \end{pmatrix} \tag{2.42}$$

Using equations (2.23), (2.28), (2.29), (2.40) and (2.42), we get:

$$I_o(\theta) = |A|^2 + |B|^2 \tag{2.43}$$

$$P_{y'}(\theta) = \frac{2\,\mathrm{Re}(AB^*)}{|A|^2 + |B|^2} \tag{2.44}$$

$$\sin\beta = \frac{2\,\mathrm{Im}(AB^*)}{(|A|^2 + |B|^2)\sqrt{1 + P_{y'}^2(\theta)}} \tag{2.45}$$

$$\cos\beta = \frac{|A|^2 - |B|^2}{(|A|^2 + |B|^2)\sqrt{1 - P_{y'}^2(\theta)}} \tag{2.46}$$

2.4 Measurements In $\vec{\tfrac{1}{2}}+A \to \vec{\tfrac{1}{2}}+A$ Experiments

The elastic scattering of a polarized beam of spin-1/2 particle can, in its simplest form, be used to measure the polarized cross-section $I(\theta,\phi)$ given by equation (2.34). If $I(\theta,\phi)$ is measured at two different azimuthal angles ϕ_1 and ϕ_2 then it is possible to obtain the quantity P_1P_2. Given the product P_1P_2 it is possible to determine one if the other is known.

The experimental set up for such measurement is illustrated in fig. 2.4b. The first scatterer is actually a source of a polarized beam which will scatter on the second scatterer. The R and L detectors are set to measure the polarized cross-section at $+\theta_2$ and $-\theta_2$. If P_1, the polarization of the incident beam, is perpendicular to the scattering plane then as mentioned in

Figure 2.4 - a) Relation between spin and orbital angular momentum.

b) Experimental set up of a double scattering experiment.

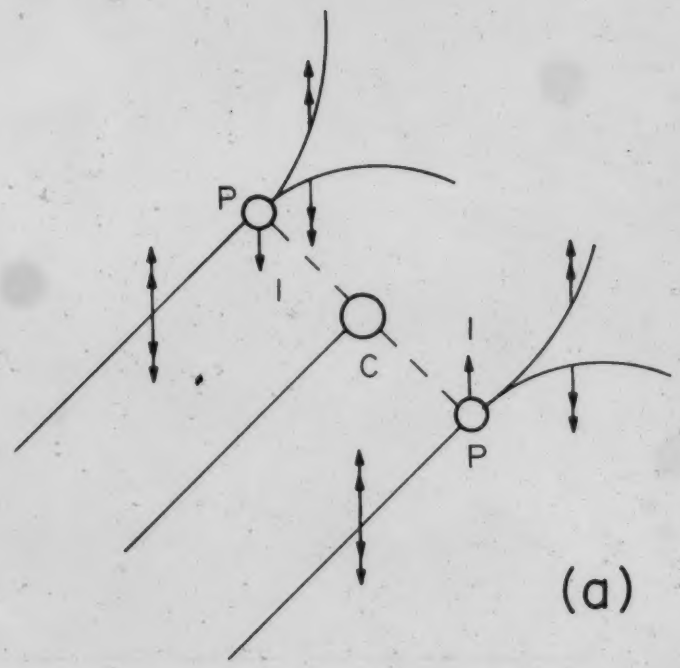
P
I
C
I
P

(a)

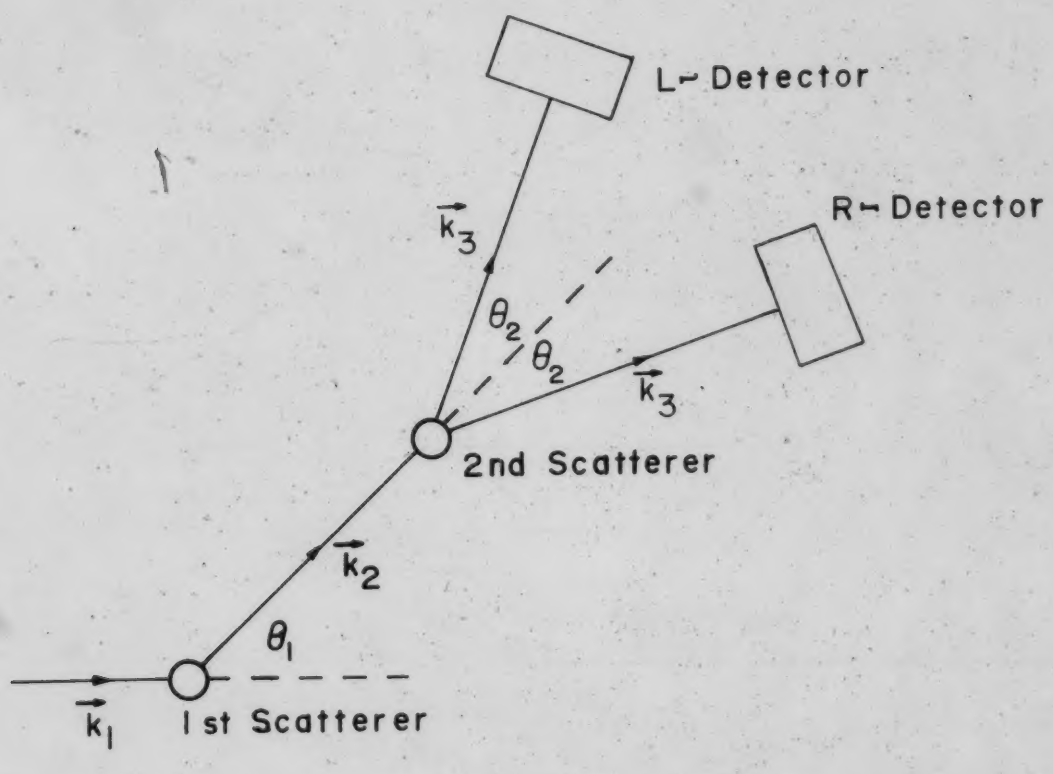
L- Detector
R- Detector
$\vec{k}_3$
θ_2
θ_2
$\vec{k}_3$
2nd Scatterer
$\vec{k}_2$
θ_1
$\vec{k}_1$
1st Scatterer

(b)

section 2.3, the angle ϕ should be 0 and 180°; this can be shown by a classical argument (Ma 70) using fig.2.4a. In that figure a beam of, spin-1/2 and orbital angular momentum $\vec{\ell}$, particles moves toward a nucleus "c". Those particles with orbital angular momentum vector $\vec{\ell}$ points downward will have a trajectory which will take them, say, to the left of the nucleus while those with $\vec{\ell}$ points upward will go to the right-hand side of the nucleus. Each particle of the beam will have its spin aligned parallel or antiparallel to $\vec{\ell}$. Now if the scattering force has a component which is proportional to $\vec{\ell}.\vec{S}$ (spin-orbit force) then a particle in the parallel orientation will feel a different magnitude of the force than another particle in the antiparallel orientation. This will result in a preferential scattering to the left for one spin state and to the right for the other state. This means that after scattering the distribution of spin states will change and this distribution can simply be measured by counting the number of particles scattered at a certain polar angle twice, once at the right-hand side of the incident beam and once to the left-hand side. In effect, this means that we are measuring the number of particles scattered at $(\theta,0)$ and $(\theta,180)$ and these numbers will yield the cross-section if it is related to the number of particles in the incident beam and number of nuclei in the target. So, measuring

left-right asymmetry will give the product P_1P_2 as suggested by equation (2.37). This method has been used in a very large number of experiments over the last few decades. In spite of the fact that this method is very simple and direct, it suffers from few disadvantages, which will lead to false asymmetries. Hillman and Stafford (Hi 56) attributed these false asymmetries, in neutron elastic scattering experiments, to:

1) Error in aligning the detectors at exactly the same angle on both sides of the beam.
2) Difference in the count rate between the two positions due to inhomogeneous irradiation of the scatterer.
3) Change in count rate due to any difference in efficiency of the detectors due to differences in geometrical shape or electronics. This problem can be solved by using one detector and rotation of the spin of incident neutrons.
4) Difference in the background count rate at the two positions.

Hillman et al (Hi 56a) suggested a different method to avoid these problems. The method makes use of the fact that the neutron has a magnetic moment and in an axial magnetic field, perpendicular to the direction of the magnetic moment, the neutron will precess

in a direction normal to the plane containing the magnetic field and the neutron magnetic moment with a frequency ν, given by:

$$\nu = g\mu_N H/h \qquad (2.47)$$

where

g is gyromagnetic ratio,

h is Planck's constant,

μ_N is nuclear magneton,

H is the magnetic field.

Now,

$$\nu = 1/T$$

where T is the periodic time of the precession, which is the time the neutron takes to rotate 360°. So if the neutron spends in the magnetic field a time "t" then it will rotate an angle "θ" where

$$\frac{t}{T} = \frac{\theta}{360} \quad \text{or} \quad T = t \cdot \frac{360}{\theta} \; .$$

If the path length of the neutron in the magnetic field is "ℓ" and the neutron velocity is V then

$$\nu = \frac{\theta V}{360 \times \ell} \; .$$

Equation (2.47) will then become

$$H\ell = \frac{\theta}{360} \frac{hV}{g\mu_N} \; .$$

For relativistic velocities

$$H\ell = \frac{\theta}{360} \cdot \frac{hc}{g\mu_N} \frac{\beta}{\sqrt{1-\beta^2}}$$

$$= \frac{\theta}{360} \cdot 10.28 \times 10^3 \frac{\beta}{\sqrt{1-\beta^2}} \quad \text{K Gauss-cm} \qquad (2.48)$$

where $\beta = V/c$ and c is the velocity of light. Since the magnetic moment and spin of the neutron are parallel, rotation of the magnetic moment of the neutron through an angle θ will result in rotating the spin vector through the same angle. If one now adjusts the value of $H\ell$ so that θ will be 180 this will mean that neutrons in the incident beam with spin up will have a spin down after going through the magnetic field and at the same time neutrons with spin down will emerge from the magnetic field with spin up. Consequently, those neutrons scattered to the left detector with the magnetic field off will scatter to the right detector with the magnetic field on. This will mean that only one detector need be used at a fixed position and counts will be taken with field on and field off and the result will be equivalent to the use of two detectors. In other words using such a magnetic field and one detector will mean that the polarization of the incident beam will change its sign after going through the magnetic field,

and this will have exactly the same effect as changing ϕ from 0° to 180°. It is customary to rotate the polarization of the incident beam by ±90° and this will result in a reduction in the magnetic field by a factor of 1/2 over that required to rotate the spin by 180°. This procedure is very important if a conventional solenoid is used. In this case, rotating the spin vector by 90° will result in the neutron scattering which will be above and below the scattering plane instead of left-right scattering in that plane. So the detector has to be placed in the vertical plane and counts will be taken with the necessary magnetic field to rotate the spin of the incident beam by 90° and by reversing the polarity of the magnetic field the spin will be rotated -90° and this will again be equivalent to changing the sign of the beam polarization.

CHAPTER 3

THE POLARIZED NEUTRONS FACILITY

3.1 Polarized Neutrons Source

Most experiments on scattering of polarized neutrons todate have used charged particle induced reactions as sources of neutrons, usually $(p,\vec{n})$ or $(d,\vec{n})$ reactions. The ideal neutron-producing reaction would be one giving a monoenergetic neutron flux having a large differential cross section at the reaction angle where the polarization of neutrons is maximum. It would involve self supporting targets which could withstand high beam currents and would yield highly polarized neutrons. In reality, most reactions give several neutron groups, consequently, to utilize them one must use time-of-flight techniques to separate the various neutron groups. Several laboratories have been studying the use of the associated particle method for discriminating against unwanted neutron groups or other backgrounds. If this technique were effective, it would bypass the pulsed beam requirement, as fast time-of-flight measurements are then possible by employing a high current d-c beam and the associated particle for a timing pulse. Such measurements are however severely hampered by the limited count rate which can be handled by the associated particle detector.

In the last few decades, a large amount of data on the polarization of neutrons produced in reactions has been recorded. Several authors (Wa 70, Go 63, Ha 63 and Ha 60) have summarized and tabulated information relevant to polarized neutron sources. To facilitate comparison between the different sources available Walter (Wa 70) suggested two quantities $P^2\sigma$ and $P^2\sigma/s$ to be used as a figure of merit for each source. P is the polarization of the neutron beam, σ is the cross section and s is the energy lost by the charged particle in the neutron producing target.

If one is constrained to a relatively low energy for the incident charged particles, a reaction with large $P^2\sigma/s$ and a large positive Q-value would be desirable for elastic scattering experiments. A survey shows that two reactions can best satisfy these requirements, namely the $T(d,\vec{n})^4He$ and $^9Be(^4He,\vec{n})^{12}C$ reactions. In table 3.1 the properties of these two reactions, relevant to their use as polarized neutrons sources, are given.

Tritium targets can be obtained in two forms, "gas" and "solid". Solid targets containing tritium can be made by adsorbing tritium gas interstitially in some heavy metals (e.g. platinum, zirconium, titanium or ytterbium). Solid targets have been used in the early stages of this investigation and found to be inadequate for use in elastic scattering experiments.

Table 3.1

Properties of neutrons produced by $^{9}Be(^{4}He,\vec{n})^{12}C$ and $^{3}H(d,\vec{n})^{4}He$

Reaction	Q (MeV)	$E_{inc.}$ (MeV)	θ_{lab}	$E_{n_o}(\theta)$ (MeV)	$E_{n_o}-E_{n_1}$ (MeV)	$P(\theta)$	$\sigma_{lab}(\theta)$ mb/sr	S 10^{-15} eV-cm^2	$P^2\sigma/s$ 10^{-12}/ eV-sr	Target thickness (KeV)
$^{9}Be(^{4}He,\vec{n})$	+5.704	5.45	30.0	10.7	4.43	-0.44 ± 0.03 (1)	18 (2)	11.0 (3)	0.32	≈500 solid
$^{3}H(d,\vec{n})$	+17.58	6.5	30.0	22.6	-	$+0.502 \pm 0.015$ (4)	11.4 (5)	0.35 (3)	8.21	<500 gas

1. (De 73), 2. (Ob 72), 3. (Wa 70), 4. (Mu 71) and 5. (Ba 57), (Go 61) and (Go 63).

Firstly, the energy loss of deuterons was quite high. Secondly, the best ratio between the number of tritium nuclei to the number of host nuclei is around 1:1, this ratio makes these targets inferior to gas targets. Finally, the neutron background resulting from unwanted reactions was also unacceptably high.

Gas targets require the use of metal foils and thus carry the risk of leaks, which is a very serious problem, in case of tritium, because of its radioactivity. However, gas targets have the advantage that, a large ratio of ^{3}H atoms to foil atoms can be obtained.

A neutron production facility using tritium gas has now been commissioned at the Nuclear Research Center of the University of Alberta (So 71). It is hoped that, the work described in this thesis can be extended using the higher energy polarized neutrons available from this facility.

In the present work, the reaction $^{9}Be(^{4}He,\vec{n})^{12}C$ was used to produce polarized neutrons with a polarization of 0.44 ± 0.03 (De 73) at a laboratory angle of 30.0°. Using 5.40 MeV ^{4}He-particles the neutrons have an energy of 10.70 ± 0.25 MeV.

The solid beryllium targets used were prepared by evaporating commercial beryllium metal (>99% purity) onto tantalum backings (0.02" thick × $2\frac{1}{8}$" diameter).

Target thicknesses were always kept under 0.8 mg/cm^2 or less than 0.5 MeV thick for ^{4}He-energy of 5.4 MeV. These targets, provided with simple air cooling, were able to withstand beam currents of 3.5 μa for several days. Under these conditions a neutron flux of about 6×10^6 neutrons/sec.μa.sr was obtained.

Fig. 3.1 shows a neutron time-of-flight spectrum taken at a laboratory angle of 30.0° and α-energy of 5.4 MeV.

3.2 Spin Rotation

As has been mentioned in Chapter 2, Hillman et. al. (Hi 56a) were the first to use the spin precession method in neutron polarization experiments. Since that time this method has been used by several groups (e.g. Hi 56a, Du 61, Wo 62, Br 71 and Na 72). All these groups have used conventional solenoids to rotate neutron spin by ±90. Conventional solenoids suffer from the following disadvantages:

1) A very large electric current (of the order of 500 amps) is needed to produce a strong enough magnetic field to rotate the neutron spin by ±90°.

2) Due to the relatively low axial magnetic field which can be attained, conventional solenoids have to be very long, thus the scatterer has to

Figure 3.1 - Typical time-of-flight spectrum of neutrons produced by the $^{9}Be(^{4}He,\vec{n})^{12}C$ reaction taken at the laboratory angle of 30°.

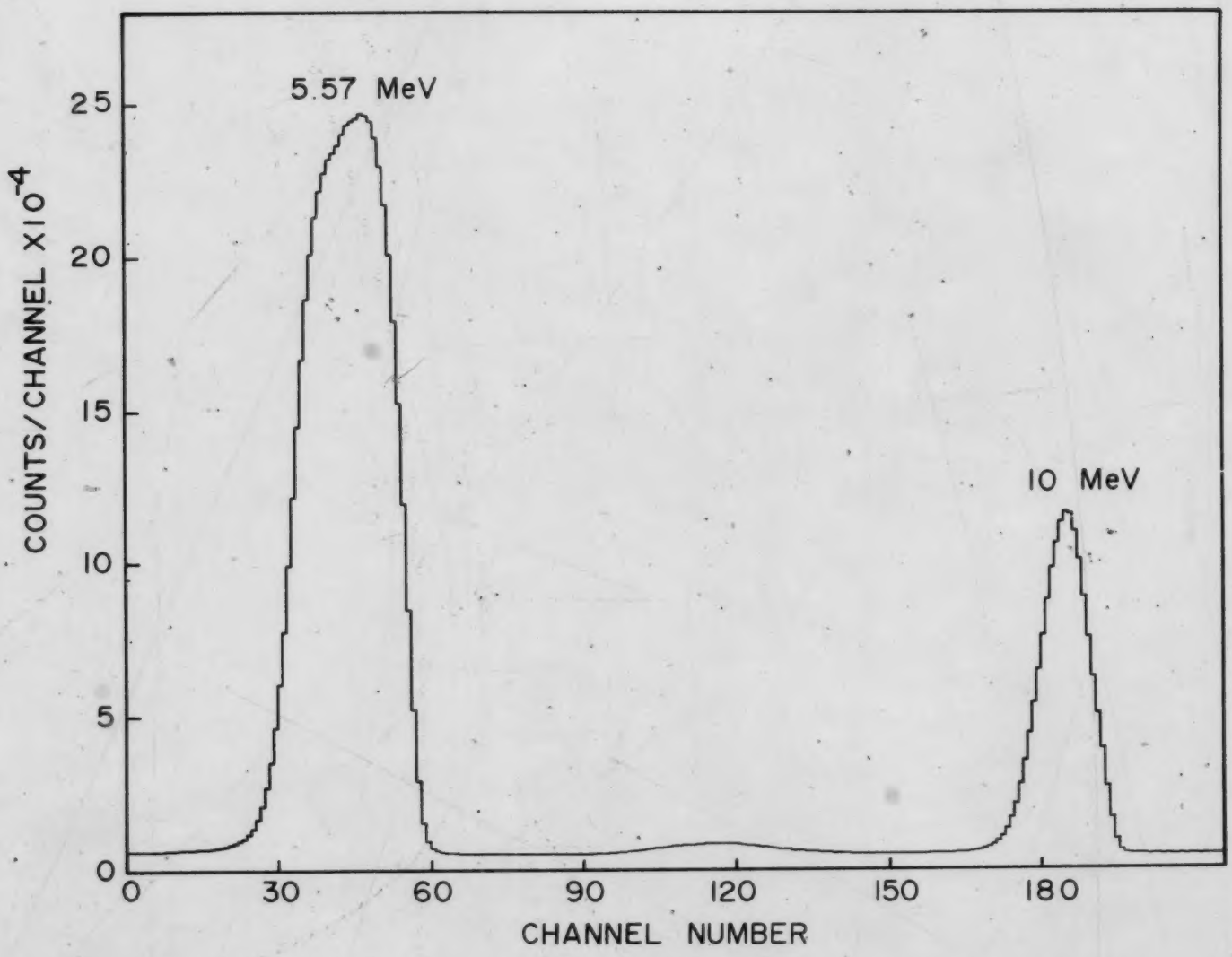
5.57 MeV
10 MeV
COUNTS/CHANNEL X10⁻⁴
0
5
10
15
20
25
0
30
60
90
120
150
180
CHANNEL NUMBER

be placed a large distance away from the neutron source. This results in a severe restriction in the neutron flux at the scatterer.

New developments in the technology of superconductors and cryogenics during the last five years make it possible now to design short superconducting solenoids to rotate neutron spins with the following advantages:

1) Superconducting solenoids could be designed to provide magnetic fields of more than 100 KG.

2) Superconducting solenoids are very efficient in transforming electric energy to magnetic energy. The number of turns per unit length is much higher for superconducting solenoids than for conventional ones. Much smaller power supplies will be suitable for superconducting solenoids. In addition, once the current flows, the supply can in fact be "disconnected" using a persistent switch.

3) The homogeneity and stability of superconducting solenoids are much better than those of conventional solenoids.

The only disadvantage of superconducting magnets is the necessity to have a large supply of liquid helium. Table 3.2 shows a comparison between some conventional

Table 3.2

Comparison Between Solenoids Used To Rotate Spin of 24.0 MeV Neutrons by 90°

Ref.	Length cm.	Bore Diameter cm.	Current I amp.	H/I KG/amp
Hi 56a	335.28	4.75	601.2	0.0029
Du 61	78.0	5.7	345.4	0.0217
Wo 62	101.6	7.62	850.0	0.0068
Br 71	54.0	7.62	615.0	0.0176
Na 72	120.0	7.5	183.8	0.0265
Present work	30.5	3.81	21.1	0.9081

solenoids and the superconducting solenoid used in the present work. All the figures in this table are given for the precession of the spin of 24.0 MeV neutrons by 90.0°.

The solenoid system which was used in this experiment was manufactured by "Superconductivity-Helium-Electronics, S.H.E. Manufacturing Corporation", London, England. It is composed of a superconducting solenoid with a persistent switch, a liquid helium dewar with a room temperature air bore along the solenoid axis and a power supply. Fig. 3.2 shows the position of the solenoid within the experimental set-up. A detailed description of the system is given in Appendix B.

3.3 Shielding

The use of time-of-flight technique in neutron scattering experiments will help in differentiating between neutron scattered from the scatterer and neutrons coming directly from the source. Unfortunately, this is not true under certain kinematic and geometrical conditions. Direct neutrons leaving the source at a larger reaction angle have energies less than those scattered into the detector, and they follow a shorter path. At some detector positions, the combination between flight path and energy will allow direct and scattered neutrons to arrive at the detector at exactly

Figure 3.2 - General experimental set up.

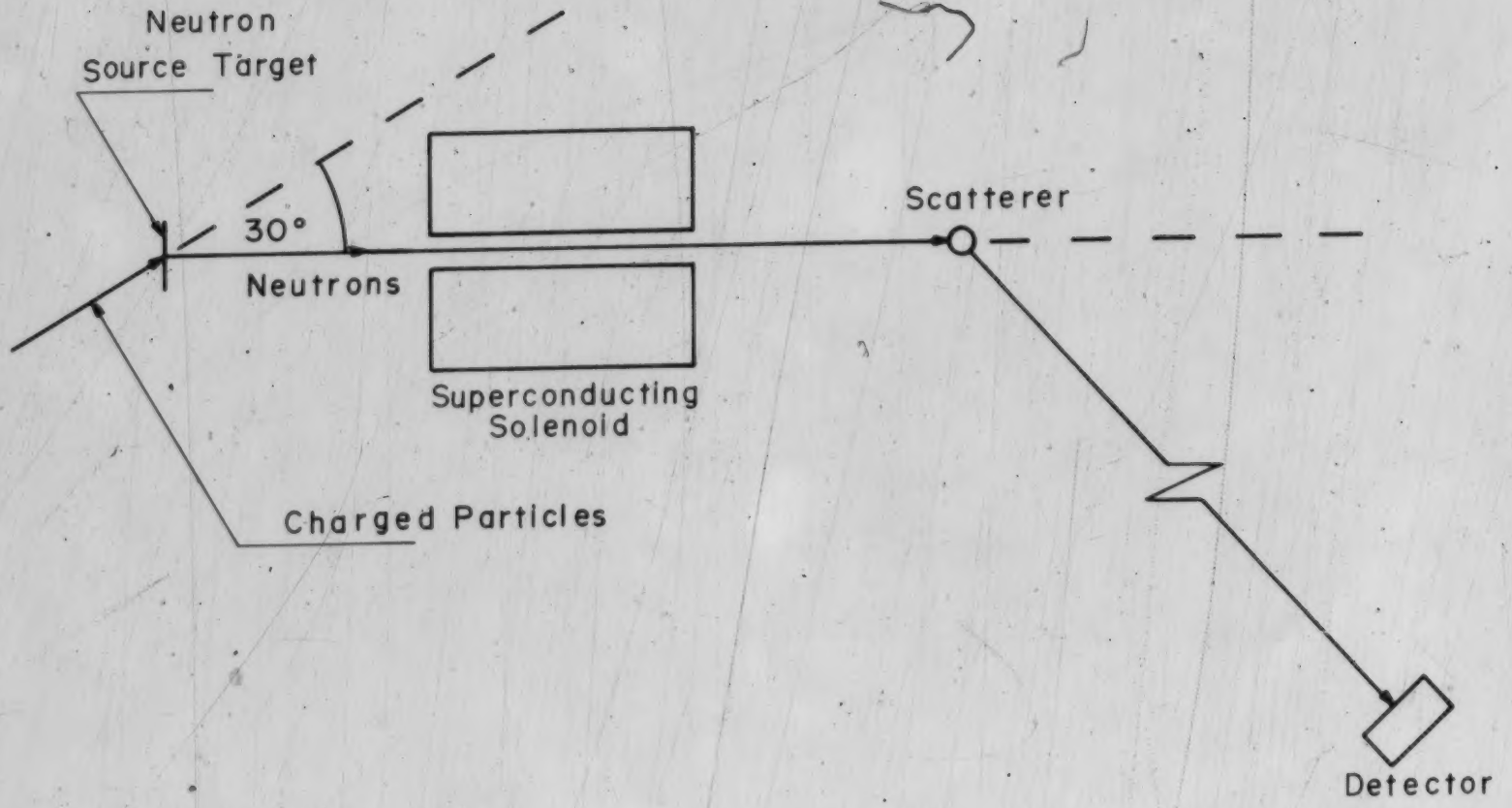
Neutron
Source Target
30°
Neutrons
Scatterer
Superconducting
Solenoid
Charged Particles
Detector

the same time. Source or detector shielding or a combination of both is the only solution to this problem. In the present work both types of shielding were used and will be described in detail in the following sections.

3.3.1 Source Shielding

Fig. 3.3 shows the local source shielding. It consists of blocks of lead, iron and "heavy metal"†. These blocks were built around the neutron source on three sides. The front is built from lead blocks (6" × 12" × 2" thick). In the middle plane the lead blocks were replaced by heavy metal blocks, and contained two tapered slots, one along the 30.0° line to collimate the neutron beam on the scatterer placed about a meter away from the source. The other slot was cut along the 0° line to allow monitoring the 0° neutron flux. This shield also helps to reduce the general background inside the target room and around other parts of the laboratory. To reduce the number of neutrons reaching the floor and bouncing back to the detector, the whole source shielding sits on the top of an aluminum tank full of water. The whole set-up, the tank and shield, is movable on six air pads.

---

† "Heavy metal" is the commercial name of the following mixture: Tungsten (90%), Copper, Nickel, Iron and Molybdenum.

Figure 3.3 - Source shielding.

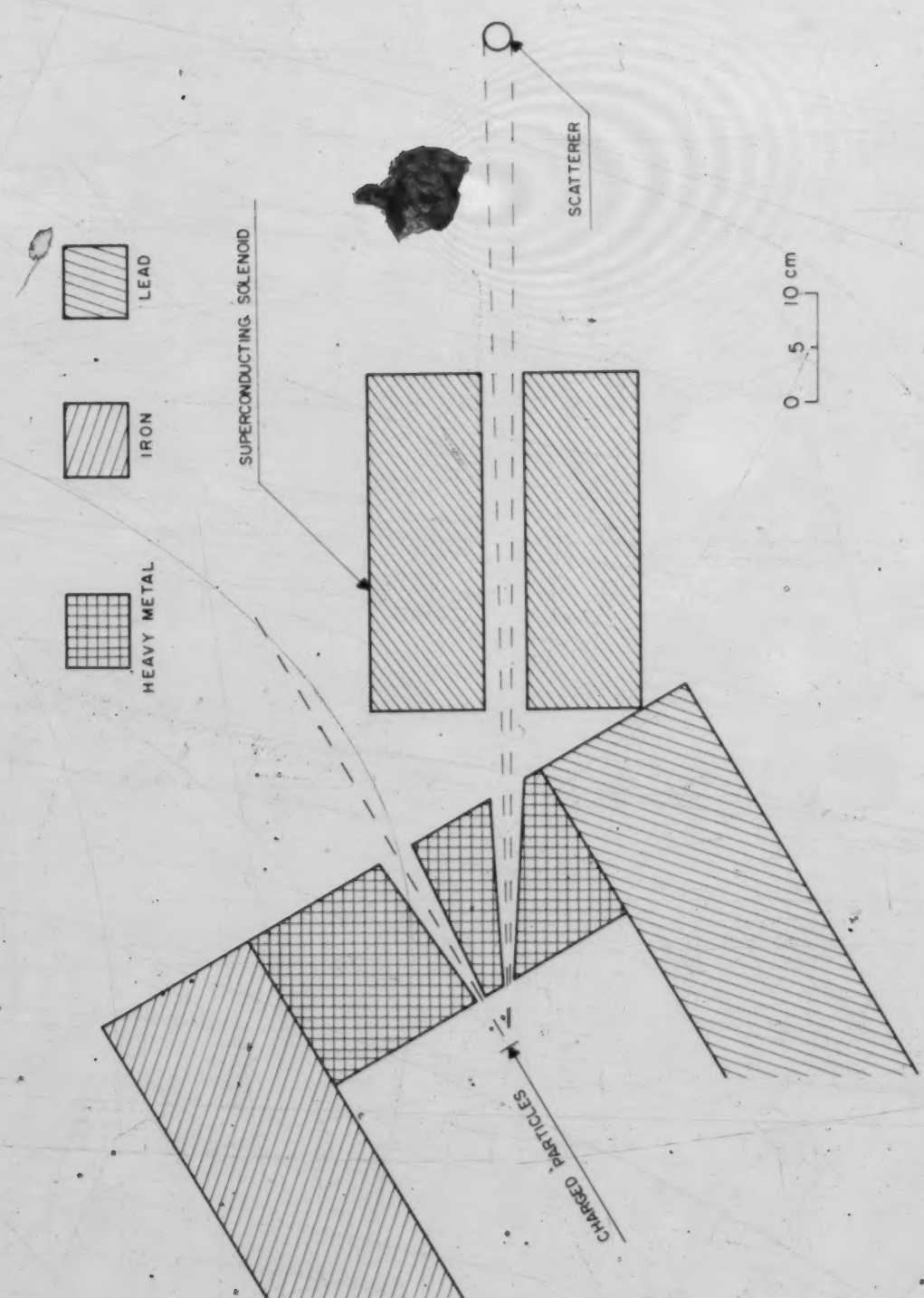
HEAVY METAL
IRON
LEAD
SUPERCONDUCTING SOLENOID
SCATTERER
0 5 10 cm
CHARGED PARTICLES

3.3.2 The Large Scattering Angle Shield

By large scattering angle we mean, scattering angles of more than 15°. The set-up is shown in fig. 3.4. Fig. 3.5 shows the details of the detector shield used.

As shown in fig. 3.5 the front part of the shield is composed of eleven iron plates. The three plates in the mid-plane were cut into two parts and their surfaces machined. The back of the shield is composed of eight iron plates arranged to form a parallelepiped with a trapezoidal base. It has two iron plates on each side, two on the top and two at the bottom. The parallelepiped is filled with paraffin wax mixed with Boron powder in the ratio 8:1 by weight. All these parts were arranged with a tapered slot in the mid-plane with the same cross-sectional area as the detector at one end and narrowing down to a little larger than the scatterer size at the front. The detector is surrounded by 2" thick lead cylinder. In this arrangement, many of those neutrons which leave the source at angles other than 30° will be absorbed or scattered in the lead and heavy metal shield around the source. They will be further reduced in number and moderated in the iron plates of the detector shield. In this way the borated wax will be effective in absorbing many of these low energy neutrons. Finally, the lead around the detector will

Figure 3.4 - Large angle experimental set up.

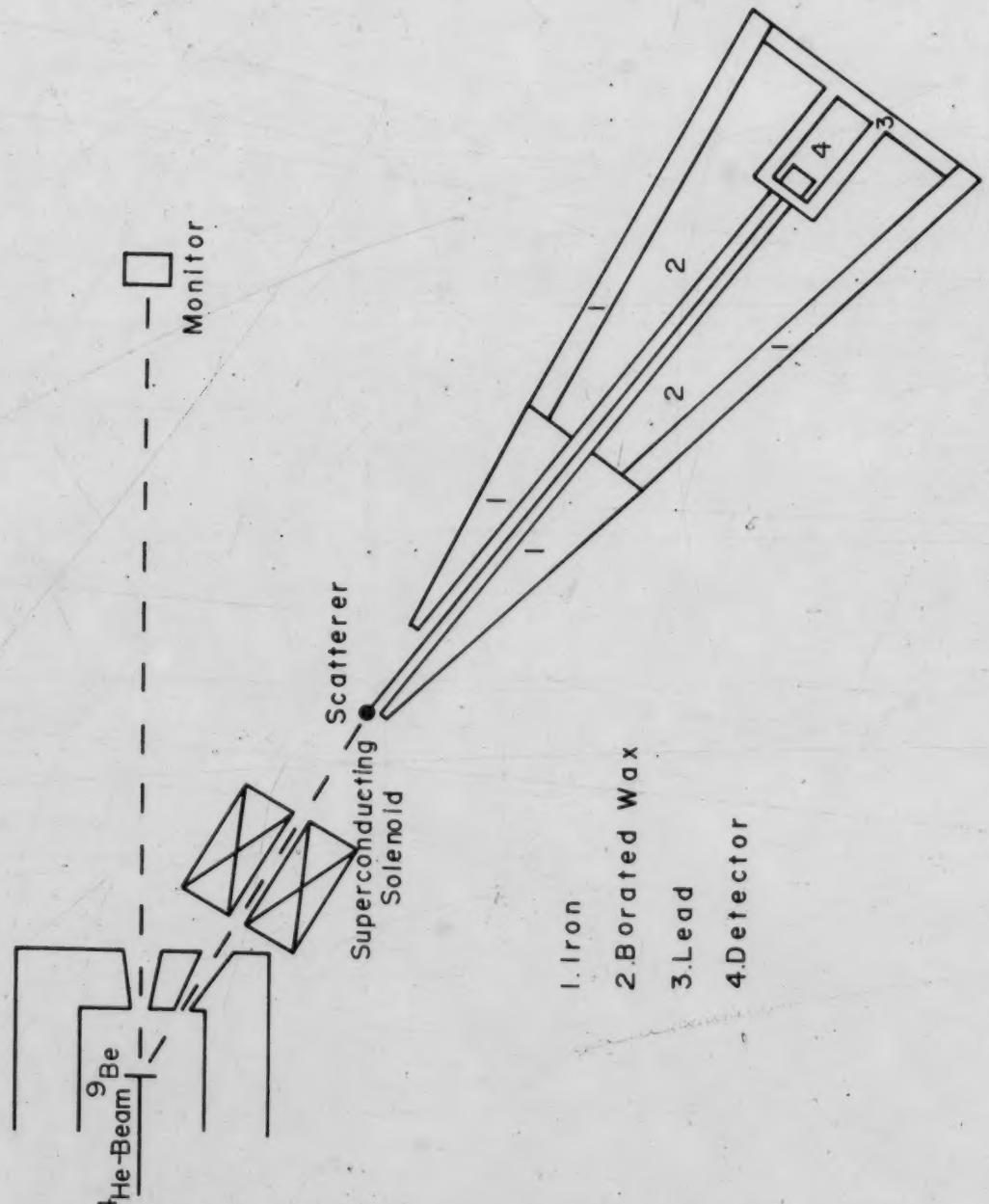
Monitor
Scatterer
Superconducting Solenoid
^{4}He-Beam
^{9}Be
1
2
2
1
1
4
3
1. Iron
2. Borated Wax
3. Lead
4. Detector

Figure 3.5 - Detector shield.

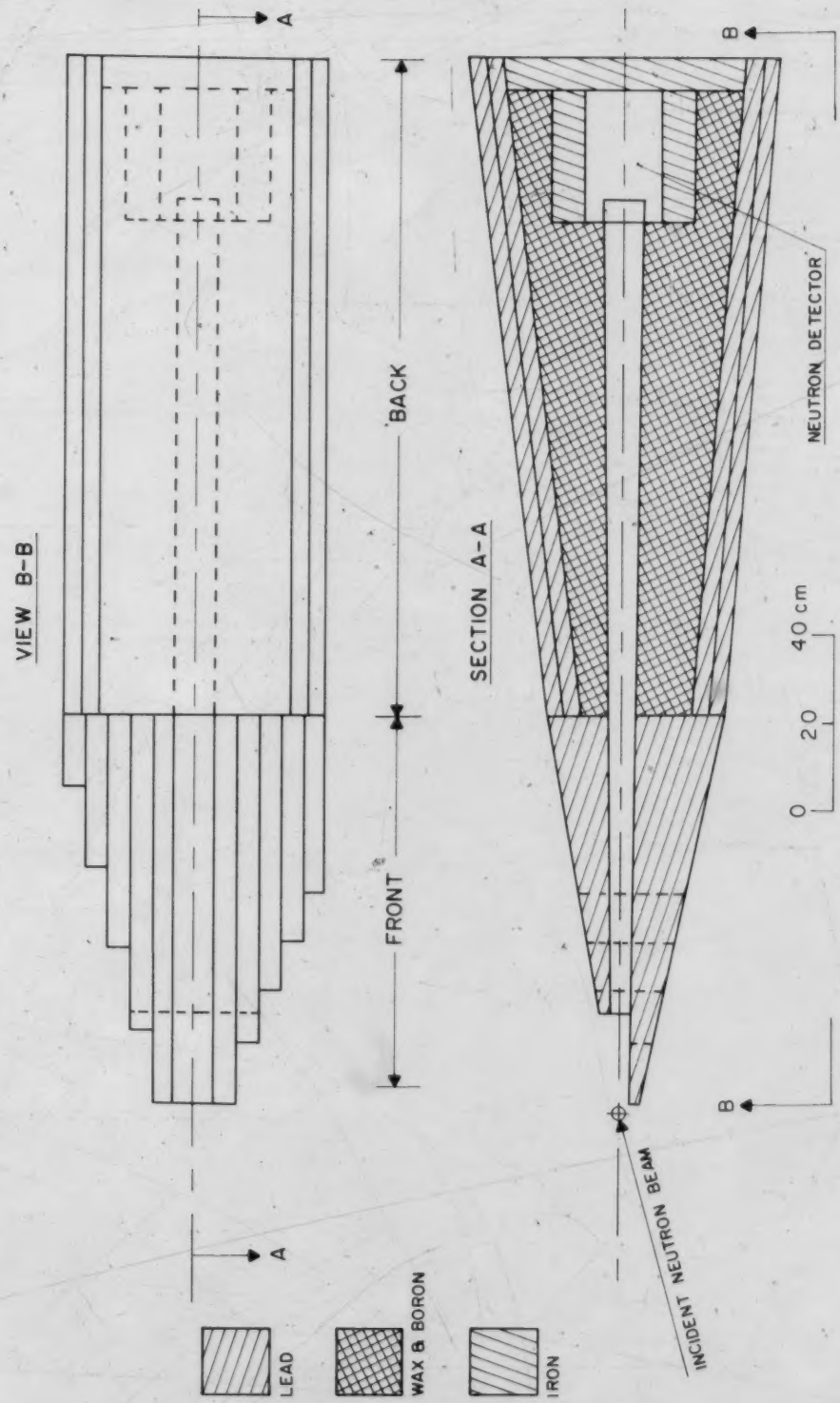
VIEW B-B
SECTION A-A
A
B
BACK
FRONT
NEUTRON DETECTOR
0
20
40 cm
INCIDENT NEUTRON BEAM
LEAD
WAX & BORON
IRON

serve as a shield against gamma-rays produced by neutron captured in the iron and borated wax. The shield is built on the top of a special frame which can be moved on four air pads. The whole structure weighs about 3.0 tons.

3.3.3 Small Scattering Angle Shield

Bucher et. al. (Bu 73) have summarized possible geometries for small angle scattering measurements. These geometries are sketched in fig. 3.6.

a) Ring Geometry: In this geometry a scatterer in the form of a ring is used. A shadow bar is placed between the source and the detector along the axis of the ring. In this arrangement the scattered counting rate is optimized since the scatterer represents the generation of a surface of constant scattering angle. However, in this geometry the measurements suffer from high contribution from air scattering. Furthermore, the minimum scattering angle will be severely limited. In addition, this geometry will not be suitable for polarization measurements because the detector will see neutrons scattered to the left and to the right simultaneously.

Bucher et. al. (Bu 73) modified the ring geometry to use more than one detector. This modification,

Figure 3.6 - Basic types of scattering geometry.

a) Ring geometry

b) Shielded source geometry

c) Shielded detector geometry

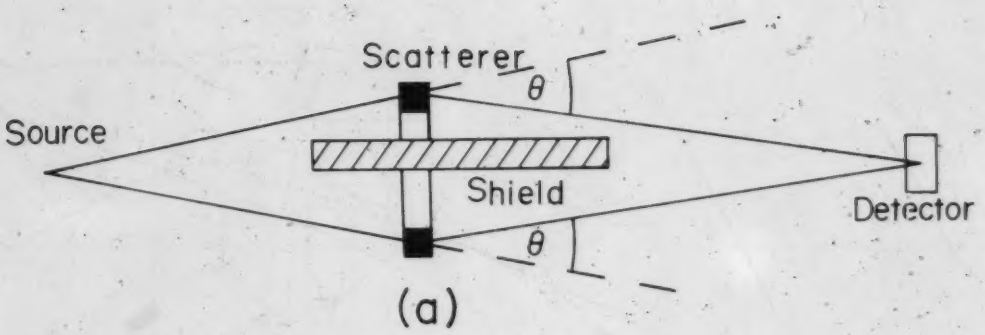

(a)

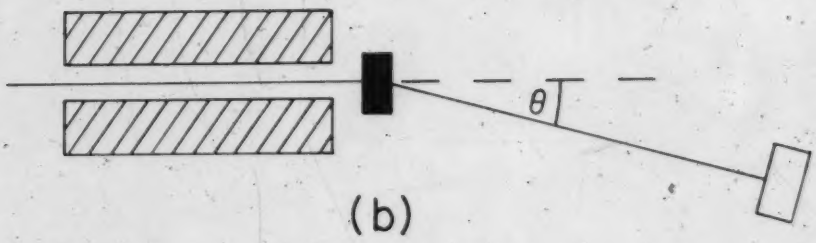

(b)

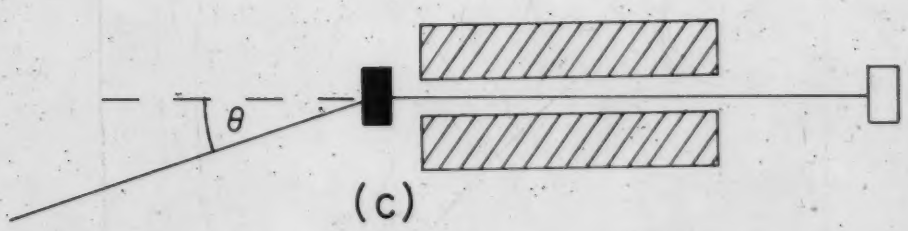

(c)

also, reduced the contribution from air scattering. In spite of these improvements to the ring geometry, it could not be used for polarization measurements, because of the same reason mentioned above.

b) Shielded Source Geometry: In this geometry the source is shielded completely allowing only a small portion of the neutrons to go through. The main advantage of this geometry is that it provides a well collimated beam with minimum background. This geometry does, however, require a massive shielding around the source.

c) Another method is the shielded detector geometry in which one shields the detector in such a way that it can see only neutrons coming from a certain direction. This method, especially when accompanied with time-of-flight measurements, will require much less shielding material than that required in the shielded source geometry. One disadvantage of this method is that one will have to build a shield for each detector restricting the number of detectors which could be used.

We have found that, for the large angle measurements, a combination of source and detector shielding a good compromise.

For small angle measurements, the need for a very well collimated beam requires a well shielded source. In addition, this geometry (shielded source)

allows one to use more than one detector simultaneously. This compensates for the loss in count rate due to the small solid angle available.

The geometry used in the small angle measurements is shown in fig. 3.7. In this set-up we used the detector shield, of the large angle set-up, to provide extra collimation of the neutron beam. Three detectors were used to record the yield at three different angles simultaneously.

Figure 3.7 - Experimental set up for small angle scattering.

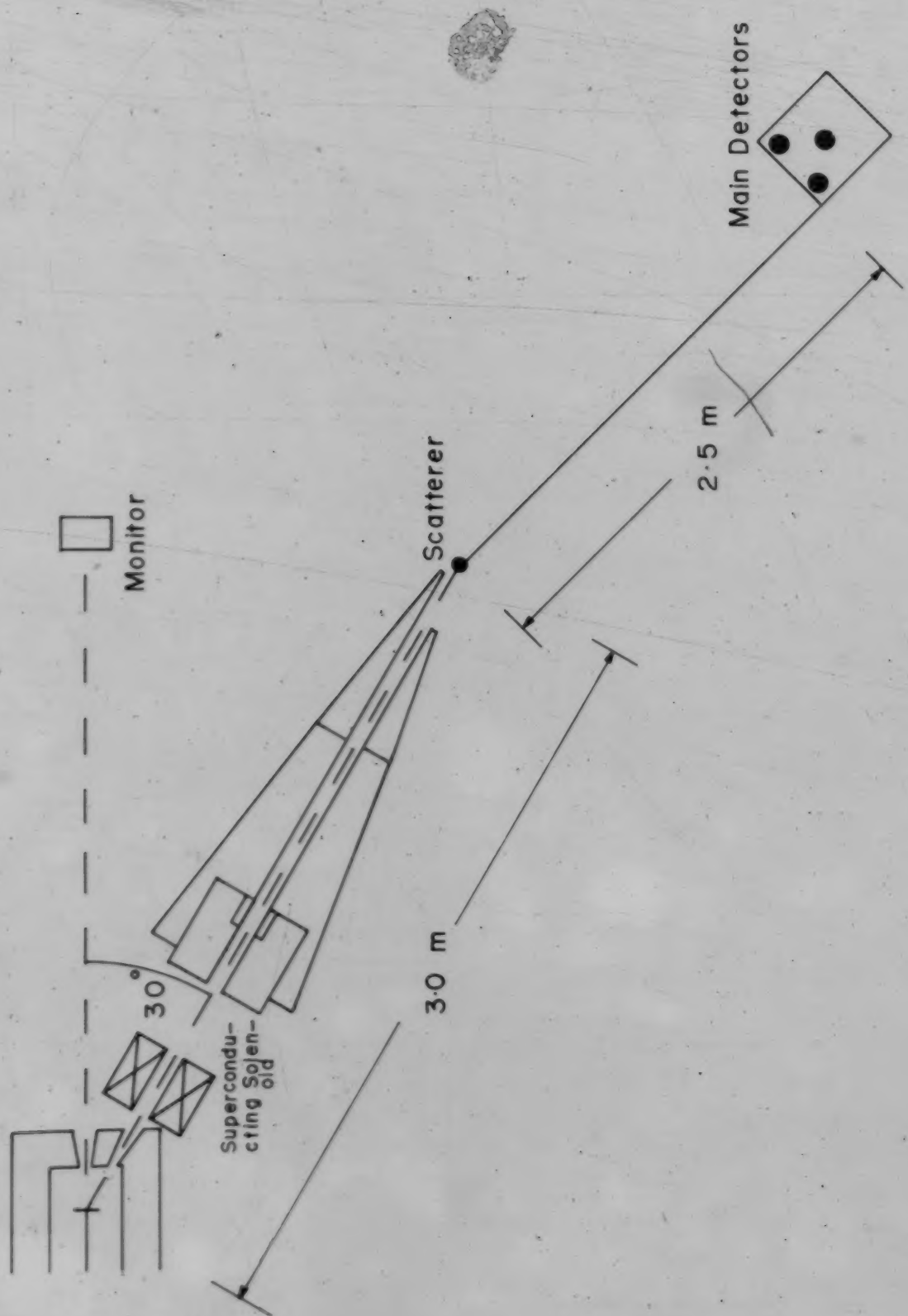
Main Detectors
2·5 m
Scatterer
Monitor
3·0 m
30°
Superconducting Solenoid

CHAPTER 4

NEUTRON-NUCLEUS ELECTROMAGNETIC INTERACTION

4.1 Introduction

The contribution of the short range nuclear forces to the scattering of neutrons at small angles is very small. One should expect a large contribution in this region from the long range interactions like the interaction between the magnetic and electric moments of the incident neutron and the electric field of the target nucleus. If these interactions, like the nuclear, are spin dependent, they are expected to affect the polarization as well as the cross-section of the scattered neutrons in their region of influence. The contribution of the interactions to the total interaction potential can be written as:

$$V(r) = V_m(r) + V_e(r)$$

where

$$V_m(r) = \hbar^2 |\mu_n| \frac{ze^2}{m^2c^2} \phi_m(r) \vec{L}\cdot\vec{S} \qquad (4.1)$$

and

$$V_e(r) = -\frac{1}{2} \phi_e(r) \vec{p}\cdot\vec{E} = -\frac{1}{2} \alpha z^2 e^2 \phi_e(r) \qquad (4.2)$$

where $V_m(r)$ is the magnetic interaction potential,

$V_e(r)$ is the electric interaction potential,

$\mu_n = -1.9135$ is the neutron magnetic moment, in nuclear magnetons,

ze is the nuclear charge,

$\phi_m(r)$ is the radial dependence of the magnetic interaction,

$\vec{L}$ is the orbital angular momentum of the neutron in units of $\hbar$,

$\vec{S}$ is the spin angular momentum of the neutron in units of $\hbar$,

$\phi_e(r)$ is the radial dependence of the electric interaction,

$\vec{p}$ is the induced electric dipole moment of the neutron,

$\vec{E}$ is the nuclear electric field of the nucleus,

α is the neutron polarizability.

Mott (Mo 29) was the first to recognize the effect of the magnetic interaction (the interaction between the magnetic moment of the projectile and the electric field of the target nucleus) on the polarization of electrons scattered from nuclei. Schwinger (Sc 48) pointed out the importance of the magnetic interaction in the neutron-nucleus interaction. From now on we will refer to this interaction as "Mott-Schwinger interaction" or "M-S interaction" for short. Schwinger used the potential of equation (4.1) in a plane wave approximation to calculate the polarization and cross-section of neutrons scattered at small angles

from heavy nuclei. His results predicted a pronounced effect in this region, e.g. a 1.0 MeV neutron beam will be, practically, completely polarized upon scattering from Pb at 1.5°. The angle of maximum polarization was given by Schwinger as

$$\theta_m \cong 2 \tan^{-1}\left[\frac{1}{2}\mu_n\left(\frac{ze^2}{\hbar c}\right)\frac{\hbar}{McR}\right] \qquad (4.3)$$

where R is the nuclear radius. On the other hand, the scattering cross-section is given by

$$\sigma(\theta) = \sigma_o(\theta) + \left[\frac{1}{2}\mu_n\left(\frac{ze^2}{\hbar c}\right)\frac{\hbar}{Mc}\right]\cot^2\left(\frac{\theta}{2}\right) \qquad (4.4)$$

where $\sigma_o(\theta)$ is the contribution of the short range nuclear interaction. Equation (4.3) shows that the angle of maximum polarization will slowly increase with the increase in the nuclear charge. The M-S contribution to the cross-section falls very rapidly with increasing scattering angle.

The M-S effect with a reversed sign should appear for protons. The large polarization produced by the M-S interaction, for protons, will be destroyed to some extent by the (strong forward) coulomb interaction. However, Eriksson (Er 56) and Heckrotte (He 56) have calculated the effect of M-S interaction on the scattering of 130 and 300 MeV protons from several nuclei using WKB approximation and found that it is noticeable up to 10°.

A considerable amount of experimental and theoretical work has been reported on small angle scattering of neutrons. There are several reasons for the special interest in studying small angle scattering of neutrons, namely -

1) These studies will contribute to the understanding of the electromagnetic long range interactions.

2) The large contribution of these interactions to the cross-section and polarization in the small angle region makes possible the design of very efficient polarized neutron sources and polarization analysers.

3) Recently Bucher and Hollandworth (Bu 75) pointed out that the selection of optical model parameters, which would at small angles accurately represent the scattering effects of the short range nuclear interactions, require a sizable body of small angle data over a broad range of energies and nuclei.

In what follows we will try to examine the experimental and theoretical evidence of the existence of the M-S and electric interactions. Voss and Willson (Vo 56) were the first to use small angle scattering as a neutron polarization analyser. They used the (p,n) reaction on Be and C to produce 100 MeV polarized neutrons. Using Schwinger's theory (Sc 48) they calculated the polarization of these neutrons upon

scattering from uranium in the angular range of $\frac{1}{4}$ - 1°. The asymmetries of neutrons scattered from uranium in this angular range were measured. Using their measurements and Schwinger's calculations they were able to estimate the polarization of neutrons produced by the (p,n) reactions. Recently this idea has been developed further and a new polarimeters has been reported (Ma 71, Ga 73 and Ga 75) in which the small angle neutron scattering from Cu, Pb and U has been used to measure the polarization of neutrons produced by the $^{2}H(d,n)^{3}He$ reaction.

Although Voss and Willson's (Vo 56) experiments proved the existence of the M-S interaction, the existence of the interaction between the induced electric moment of the neutron and the electric field of the nucleus (the electric interaction) continues to be the subject of a long standing controversy. The existence of such an interaction will manifest itself, as Aleksandrov and Bondarenko (Al 56) and Barashenkov et. al. (Ba 57a) have suggested, in an anomalous increase in the cross-section at small scattering angles which cannot be explained by the M-S interaction. The electric interaction will not affect the polarization of the scattered neutrons because the interaction potential (equation (4.2)) is spin independent. The question, of the existence of the electric interaction,

has been taken up, experimentally and theoretically, by several authors. This question has not been settled yet as we will see by examining the experimental and theoretical work available.

Aleksandrov (Al 57) measured the differential cross-section for neutrons scattered from Pu, U, Sn, Pb, Bi and Cu in the angular range of 4° to 25°. The neutron beam used was extracted from a nuclear reactor with a mean energy of 2 MeV with a large energy spread. After subtracting the quantity $\gamma^2 \cot^2(\theta/2)$ where $\gamma = \frac{1}{2} \mu_n (\hbar/mc)(ze^2/\hbar c)$ from the measured cross-section he noticed that Pu and U have a sharp rise in the cross-section at angles less than 11°. The increase in the cross-sections for the other nuclei is within the limits of the experimental error. He concluded that this rise in the cross-section could be a result of a neutron polarizability of the order of $(8.0 \pm 3.5) \times 10^{-41}$ cm^3 or due to some other reasons.

Thaler (Th 59) pointed out that, using other methods like pion-photo production sets limit on the neutron polarizability coefficient α

$$4 \times 10^{-43} \leq \alpha \leq 1.4 \times 10^{-42} \text{ cm}^3$$

and concluded that it is very unlikely that any effect on neutron-nucleus scattering can be observed.

Aleksandrov et. al. (Al 61) measured the cross-section for 0.8 and 2.8 MeV neutrons scattered from Th, U and Cu. Once again they reported a sharp increase in the scattering cross-section of U and Th nuclei at 2.8 MeV for angles less than 10° which could not be accounted for by a M-S contribution.

Dukarvich and Dyumin (Du 63) investigated the effect under improved experimental conditions using 14.2 MeV neutrons, produced by the T(d,n) reaction. A cross-section greater than the M-S cross-section was observed for Th, U and Pu and the authors suggested that the effect might be connected with specific features of fissionable nuclei.

Walt and Fossan (Wa 65) used the optical model and considered the interference between the nuclear and the electric interactions to calculate scattering cross-section of 0.57 MeV neutrons scattered from uranium. Comparing these calculations to their experimental results they estimated an upper limit for α of 2×10^{-40} cm^3. They attributed the difference between their result and that obtained by Aleksandrov et. al. (Al 61) to the fact that the interference between nuclear and electric interactions is constructive in Aleksandrov case and destructive in their case.

An extensive experimental and theoretical study of the small angle scattering of 0.83 MeV neutrons from uranium was done by Elwyn et. al. (El 66). These authors confirmed the idea that the interference between the nuclear and electric interactions (We 59) could be either constructive or destructive. They also suggested that the neutron polarizability would be somewhere between 4 & 8×10^{-40} cm^3 provided that the only interactions were nuclear, M-S and electric. They were also inclined to accept the idea that the enhancement of the cross-section at small energies is due to some fission related process. Their judgment was based on the fact that the enhancement was observed at 2.0 MeV (Al 57) and not at 0.57 MeV (Wa 65) (since the fission threshold is at about 0.6 MeV with a strong energy dependence in the cross-section).

Gorlove et. al. (Go 67 and Go 68) measured the cross-section of 4.0 MeV neutrons scattered from Cu, In, Sn, Pb, Bi and U in the angular range 2-21°. The authors concluded that their experimental results can be well described under the assumption that only nuclear and M-S interactions exist.

Kuchnir et. al. (Ku 68) measured the cross-section and polarization of 0.6-1.6 MeV neutrons scattered from U, Th, Pb, Au, W and Cd in the angular range of 1.75-15°. Adam et. al. (Ad 68) measured the

cross-section of 14.7 MeV neutrons scattered from uranium between 4-90°. The data of Adam et. al. and Kuchnir et. al. did not show any enhancement. However, Anikin and Kotukhov (An 70 and An 71) reported an improvement in fitting cross-section of 0.57-8.4 MeV neutrons scattered from U, Pb and Cu between 2.5-25°. This improvement was the result of adding an electric interaction with $\alpha = 2 \times 10^{-40}$ cm^3 to the nuclear and M-S interactions.

Palla (Pa 71) was also able to get a good fit to the 14 MeV data on U and Th using the coupled differential equation formalism of Tamura (Ta 65) which includes nuclear deformation.

It seems, from the above review, that the effect of the electric interaction on neutron-nucleus scattering is small. Although there is no strong evidence against its existence, there is however no strong evidence for its existence. It is important to mention that much of the experimental data, which exhibited an enhancement in the cross-section, have been taken with neutron beams extracted from nuclear reactors. Such beams are not monoenergetic and are usually characterized by a large energy spread. In conclusion, one can safely consider only the nuclear and the M-S interactions when making predictions of observables in small angle region for neutron-nucleus

scattering.

4.2 Theoretical Calculations

In this section we will review the theoretical calculation of the effect of the M-S interaction on neutron-nucleus scattering. Several authors used different approaches to perform the calculations. Before reviewing these different approaches we will treat the problem in detail using the plane wave Born approximation "PWBA". Schwinger (Sc 48) was the first to apply the PWBA to the problem.

The contribution of the M-S interaction to the scattering amplitude in the PWBA can be written as (De 64)

$$B_{M-S} = - \frac{m^*}{2\pi\hbar^2} \int e^{-i\vec{k}_f \cdot \vec{r}} V_m(r) e^{i\vec{k}_i \cdot \vec{r}} d\vec{r} \qquad (4.5)$$

where $\vec{k}_i$ and $\vec{k}_f$ are the initial and final wave vectors and m^* is the reduced mass. Using equation (4.1) we get

$$B_{M-S} = - \frac{m^*}{2\pi\hbar^2} |\mu_n| \hbar^2 \frac{ze^2}{m^2c^2} \int e^{-i\vec{k}_f \cdot \vec{r}} \phi_m(r) \vec{L} \cdot \vec{S} e^{i\vec{k}_i \cdot \vec{r}} d\vec{r} \, . \qquad (4.6)$$

The operator $\vec{L} \cdot \vec{S}$ can be written as

$$\vec{L} \cdot \vec{S} = \frac{1}{2} \vec{\sigma} \cdot \vec{L} = \frac{1}{2} \vec{\sigma} \cdot \vec{r} \wedge \vec{p}$$

$$= - \frac{i}{2} \vec{\sigma} \cdot (\vec{r} \wedge \vec{\nabla}) \qquad (4.7)$$

where $\vec{\sigma}$ is the Pauli spin operator and $\vec{p}$ is the linear momentum of the neutron. Substituting equation (4.7) into equation (4.6) we get

$$B_{M-S} = \frac{im^*}{4\pi} |\mu_n| \frac{ze^2}{m^2c^2} \int e^{-i\vec{k}_f \cdot \vec{r}} \phi_m(r) \vec{\sigma} \cdot (\vec{r} \wedge \vec{\nabla}) e^{i\vec{k}_i \cdot \vec{r}} d\vec{r}$$

$$= \frac{-m^*ze^2}{4\pi m^2c^2} |\mu_n| \vec{\sigma} \cdot \int e^{-i\vec{k}_f \cdot \vec{r}} \phi_m(r) \vec{r}\, e^{i\vec{k}_i \cdot \vec{r}} d\vec{r} \wedge \vec{k}_i \, .$$

Taking $\phi_m(r) = 1/r^3$ then

$$B_{M-S} = -\frac{m^*ze^2}{4\pi m^2c^2} |\mu_n| \vec{\sigma} \cdot \int e^{-i\vec{k}_f \cdot \vec{r}} \frac{\vec{r}}{r^3} e^{i\vec{k}_i \cdot \vec{r}} d\vec{r} \wedge \vec{k}_i$$

$$= K\vec{\sigma} \cdot \int e^{i\vec{q} \cdot \vec{r}} \frac{\vec{r}}{r^3} d\vec{r} \wedge \vec{k}_i$$

where

$$K = - \frac{m^*ze^2}{4\pi m^2c^2} |\mu_n|$$

and

$$\vec{q} = \vec{k}_i - \vec{k}_f \, .$$

Using the relation

$$\vec{\nabla}\left(\frac{1}{r}\right) = - \frac{1}{r^2} \hat{r} = - \frac{\vec{r}}{r^3}$$

then B_{M-S} becomes

$$B_{M-S} = K\vec{\sigma} \cdot \int e^{i\vec{q} \cdot \vec{r}} \vec{\nabla}\left(\frac{1}{r}\right) d\vec{r} \wedge \vec{k}_i \, .$$

Since

$$\int \nabla(\phi\psi)\,d\vec{r} = \int \phi\vec{\nabla}\psi\,d\vec{r} + \int \psi\vec{\nabla}\phi\,dr$$

and

$$\int \vec{\nabla}\left(\frac{e^{i\vec{q}\cdot\vec{r}}}{r}\right)\,d\vec{r} = 0$$

then

$$B_{M-S} = K\vec{\sigma}\cdot\int\frac{1}{r}\,\vec{\nabla}(e^{i\vec{q}\cdot\vec{r}})\,d\vec{r}\wedge\vec{k}_i$$

$$= iK\int\frac{1}{r}\,e^{i\vec{q}\cdot\vec{r}}\,d\vec{r}\;\vec{\sigma}\cdot(\vec{q}\wedge\vec{k}_i)$$

$$= iK\int\frac{1}{r}\,e^{i\vec{q}\cdot\vec{r}}\,d\vec{r}\;\vec{\sigma}\cdot(\vec{k}_i-\vec{k}_f)\wedge\vec{k}_i$$

$$= iK(\vec{\sigma}\cdot\hat{n})k_ik_f\sin\theta\int\frac{1}{r}\,e^{i\vec{q}\cdot\vec{r}}\,d\vec{r}$$

where

$$\hat{n} = (\vec{k}_i\wedge\vec{k}_f)/k_ik_f\sin\theta\ .$$

Now

$$\int\frac{1}{r}\,e^{i\vec{q}\cdot\vec{r}}d\vec{r} = \int_0^\infty\int_{-1}^{+1}\int_0^{2\pi} r\,e^{iqr\cos\theta'}\,dr\,d\cos\theta'\,d\phi$$

$$= 2\pi iq\int_0^\infty r^2[e^{iqr} - e^{-iqr}]\,dr$$

$$= 8\pi/q \qquad (4.8)$$

since

$$q = 2k\sin(\theta/2) \qquad (4.9)$$

where

$$k = |k_i| = |k_f|\ .$$

Using equations (4.8) and (4.9) B_{M-S} becomes

$$B_{M-S} = iK \frac{8\pi k^2 \sin(\theta/2)\cos(\theta/2)}{4k^2 \sin^2(\theta/2)} \vec{\sigma}\cdot\hat{n}$$

$$= -i \frac{m^* z e^2}{2m^2 c^2} \cot(\theta/2)\ \vec{\sigma}\cdot\hat{n} \ . \qquad (4.10)$$

Equation (2.42) can now be written as

$$M = A + (B + B_{M-S})\sigma_y \ . \qquad (4.11)$$

Using equation (4.11) in equations (2.43) and (2.44) we can get expressions for the cross-section and polarization.

Sample (Sa 56) used perturbation theory to calculate the M-S contribution. If one assumes that the M-S interaction is small, then the Schrodinger equation

$$(\nabla^2 + k^2)\psi = \varepsilon(\vec{L}\cdot\vec{S})/r^3\ \psi \qquad (4.12)$$

where

$$k = 2mE/\hbar^2 \quad \text{and} \quad \varepsilon = 2|\psi_n| \frac{ze^2}{mc^2}$$

could be reduced, according to the first order perturbation, to

$$(\nabla^2 + k^2)\psi_1 = \varepsilon(\vec{L}\cdot\vec{S})/r^3\ \psi_o \qquad (4.13)$$

where $\psi = \psi_o + \psi_1$ with ψ_o being the solution of equation (4.12) with $\varepsilon = 0$. Sample used the hard sphere

approximation to solve equation (4.13). His results agreed well with Schwinger results.

In the early 1960's numerical routines have been developed for optical model calculations of nucleon-nucleus scattering. Monahan and Elwyn (Mo 64) considered the scattering of neutrons from a spherically symmetric potential V(r) that can be written in the form

$$V(r) = V_1(r) + V_2(r) \qquad (4.14)$$

where

$$V_1(r) = 0 \quad \text{for} \quad r \geq r_c$$

and

$$V_2(r) = 0 \quad \text{for} \quad r \leq r_c \ .$$

Both $V_1(r)$ and $V_2(r)$ may contain a spin orbit term, while r_c can be chosen in such a way that $V_2(r)$ can be treated as a perturbation. It is important to mention here that a numerical solution to this problem is much more difficult than the numerical solution in case $V_2(r) = 0$ for all r. This is simply because of the range of the potentials $V_1(r)$ and $V_2(r)$. The potential $V_1(r)$ is of short range, and r_c is of the order of magnitude of the range of the nuclear forces. The inclusion of the potential $V_2(r)$, that extends to distances of the order of atomic radius, has the effect that the interval, over which the radial equation must

be integrated, is increased by several orders of magnitude. Furthermore, the number of partial waves that contribute significantly to the scattering is greatly increased. To avoid this, Monahan and Elwyn (Mo 64) derived an approximate formula for phase shifts which includes both potentials, $V_1(r)$ and $V_2(r)$. The results of these calculations showed that the effect of the M-S interaction on the polarization can extend to scattering angles as large as 24° for neutrons with energies less than 1 MeV.

Redmond (Re 65) pointed out that Monahan and Elwyn's (Mo 64) first order correction to the Born approximation can be an over-correction and proposed a more accurate approximation using a technique whereby a phase shift function is calculated at successive distances from the origin in step-wise manner.

Hogan and Seyler (Ho 69) derived expressions for scattering amplitudes using a potential like the one used by Monahan and Elwyn (Mo 64). These expressions were found to converge slowly when the M-S interaction is included, so it is accurate enough for low partial waves. Since the PWBA is accurate enough for large partial waves, it has been used to account for the contribution above a certain appropriate cut-off value. Hogan and Seyler used that approach to calculate the cross-section and polarizations for neutron with energies

of 0.5, 1.0, 7.0, 14.0 and 24.0 MeV scattered from Al, Mn, Nb and Bi. They concluded:

1) The differential cross-section is influenced only at angles ≈2° or less.

2) The polarization can be influenced at much larger angles, primarily at angles which lie near minima in the cross-section.

3) For energies and nuclei considered, the M-S influence tends to be large for large z and small E, although the "large-angle" effect is not present for E < .1 MeV.

4) Use of plane wave approximation to compute that part of the phase shifts due to the M-S potential is found to be entirely adequate for all cases considered.

A DWBA calculation for the electromagnetic effect in neutron elastic scattering was proposed and carried out by Sherif (Sh 71). In this method a potential of the form (4.14) is used with $V_1(r)$ as the short range nuclear optical potential and $V_2(r)$ as the long range weak electromagnetic potential of equation (4.1). The scattering amplitude can be written as

$$f \simeq f_o + f_{M-S} \tag{4.15}$$

where

$$f_o = \langle \phi | V_1(r) | \chi^{(+)} \rangle \tag{4.16}$$

is the scattering amplitude due to the nuclear potential alone, and

$$f_{M-S} = \langle \psi^{(-)} | V_2(r) | \chi^{(+)} \rangle \qquad (4.17)$$

is the amplitude due to the M-S interaction term. In the above equations ϕ is a plane wave, χ is the optical model distorted wave function and ψ is the total scattering wave function.

Using the DWBA one can replace ψ by χ and get:

$$f_{M-S} = \langle \chi^{(-)} | V_2(r) | \chi^{(+)} \rangle \qquad (4.18)$$

In solving equation (4.18) one will be faced with the long range problem mentioned above. If partial wave ℓ_c is chosen large enough such that

$$e^{2i\delta_{\ell_c}} = 1 \qquad (4.19)$$

where δ_{ℓ_c} is the nuclear phase shift, then all partial waves with $\ell > \ell_c$ are not affected by the nuclear potentiál and can be considered as components of a plane wave. Now χ can be expanded as

$$\chi = \sum_{\ell=0}^{\ell_c} \lambda_\ell + \sum_{\ell_c+1}^{\infty} \phi_\ell \qquad (4.20)$$

where λ_ℓ are partial waves generated using a nuclear optical potential and ϕ_ℓ are the components of a plane wave solution. The contribution of each term of

equation (4.20) is calculated in the following manner. In the region of space $0 < r \leq R_c$, where R_c is the distance from the center of the nucleus beyond which the nuclear potential vanishes, the radial part of η_ℓ is generated by the optical potential and the integration could be carried out numerically. ϕ_ℓ will have no contribution in this region.

In the region of space where $R_c < r < \infty$ the asymptotic form

$$\frac{1}{2}[(1+e^{2i\delta_\ell})j_\ell(kr) - i(1-e^{2i\delta_\ell})\eta_\ell(kr)] \qquad (4.21)$$

is used for the radial part of λ_ℓ and the integration could be done analytically. The contribution of ϕ_ℓ can be written as

$$\sum_{\ell_c+1}^{\infty} \phi_\ell = \sum_{\ell=0}^{\infty} \phi_\ell - \sum_{\ell=0}^{\ell_c} \phi_\ell$$

$$= \Phi - \sum_{\ell=0}^{\ell_c} \phi_\ell \qquad (4.22)$$

where Φ is the complete plane wave. The contribution of these two terms in (4.22) can also be carried out analytically. It is a simple process to incorporate the amplitude f_{M-S}, calculated in this way, in any optical model program.

A comparison between the DWBA method and PWBA calculation proved that the two methods differ at angles larger than about 6°.

CHAPTER 5

MEASUREMENT OF POLARIZATION AND CROSS SECTION OF 10 MeV NEUTRONS SCATTERED FROM LEAD AND BISMUTH

5.1 Introduction

Some cross sections for small angle neutron scattering ($\theta \lesssim 15°$) from Pb and Bi have been measured previously. Most of these measurements were taken at neutron energies below 4.5 MeV (Al 56, Al 57, Go 67, Ku 68, Go 68, An 70, Ma 71, Ga 73 and Ma 73). The purpose of most of these studies was to look for evidence for the existence of an interaction between the induced neutron electric moment and the Coulomb field of the nucleus. Some of these experiments were performed using neutron beams extracted from nuclear reactors, resulting in large uncertainties in the incident neutron energy. Better quality data were reported at a neutron energy of 14 MeV. The neutrons were produced by the $T(d,n)^4He$ reaction (Co 58, Du 63 and Be 73). Measurements in the energy range of 5-8 MeV have also been reported (An 70 and Bu 73). Recently, Bucher and Hollandsworth (Bu 75 Bu 75a) measured the cross section for the scattering of 7-14 MeV neutrons from Pb and Bi in the angular range of 3-15°. These authors found that equivalent local

potential of Wilmore and Hodgson (Wi 64) gave a better fit to the data than that obtained using the local optical potential of Rosen et al (Ro 65).

Small angle polarization measurements on Pb and Bi are far less numerous. Only three sets of measurements have been reported; at neutron energies of 4 MeV by Gorlove et al (Go 67 and Go 68), 3 MeV by Galloway and Maayouf (Ga 72 and Ga 73) and finally at 2.45 MeV by Drigo et al (Dr 73). Drigo's measurements showed a systematic difference between Pb and Bi. The magnitude of the polarization of neutrons scattered from Pb was significantly smaller than that of neutrons scattered from Bi.

Scattering of neutrons from Pb and Bi have been examined previously at a number of different neutron energies for angles larger than 10 degrees. The purpose of most of these measurements was to obtain differential cross sections and polarizations for optical model analysis. Most of the measurements below 9 MeV neutron energy were compiled by Perey and Perey (Pe 74). Several measurements at 14 MeV were reported and listed by Erramuspe (Er 67). Finally, the 24 MeV measurements are listed by Satchler (Sa 67).

The above review reveals a situation which can be summarized as follows:

1) There are no polarization measurements in the small angle region above 4.0 MeV neutron energy.

2) There are no cross section measurements at 10 MeV in the small angle region.

3) There is a gap at 10 MeV in the cross section and polarization data for the large angle region.

4) The difference in the polarization of 2.45 MeV neutrons scattered from Pb and Bi reported by Drigo et al (Dr 73), if confirmed, would be very important. Such a difference might be an indication of the existence of some sort of long range interaction different from the M-S interaction. Obviously, this difference need further investigation.

5) There are three sets of optical model parameters (Ro 65, Wi 64 and Be 69) which are often used to fit neutron data. The potentials are quite different and it is important to determine which represents the data best.

In the present work the facility described in Chapter 3 was used to measure the polarization and the differential cross section of 10 MeV neutrons scattered from Pb and Bi in the angular range of 1.5-65° the details of the experimental method will be given below.

5.2 Scatterers

The scatterers used were solid cylinders of Pb and Bi. Each cylinder was 3" high and 1" in diameter. The Pb cylinder weighed 426.7 gm while the Bi weighed 367.1 gm. These cylinders were made by pouring molten metals into hollow brass cylinders which had removable plugs at the bottom. After the metals had solidified the plugs were removed and the solid metal cylinders were pushed out of the brass cylinders.

5.3 Detectors

In the early stages of small angle measurements attempts were made to use a "long detector" (Ne 70). The long detector consists of NE 213 liquid scintillator encapsulated in a glass tube, three feet long and two inch in diameter. Each end of the scintillator is viewed by an RCA 8575 photomultiplier. Figure 5.1 shows a schematic diagram of the long detector as used in neutron elastic scattering experiment. As shown in the figure "t_o" is the time taken by the neutron to fly from the neutron source to the scatterer. The time "t" is the neutron flight time between the scatterer and the long detector. The time "t_1" is the sum of "t_o", "t" and the transit time "t_x" of the light, produced inside the scintillator, over the distance "x".

Figure 5.1 - Basic principle of the long detector.

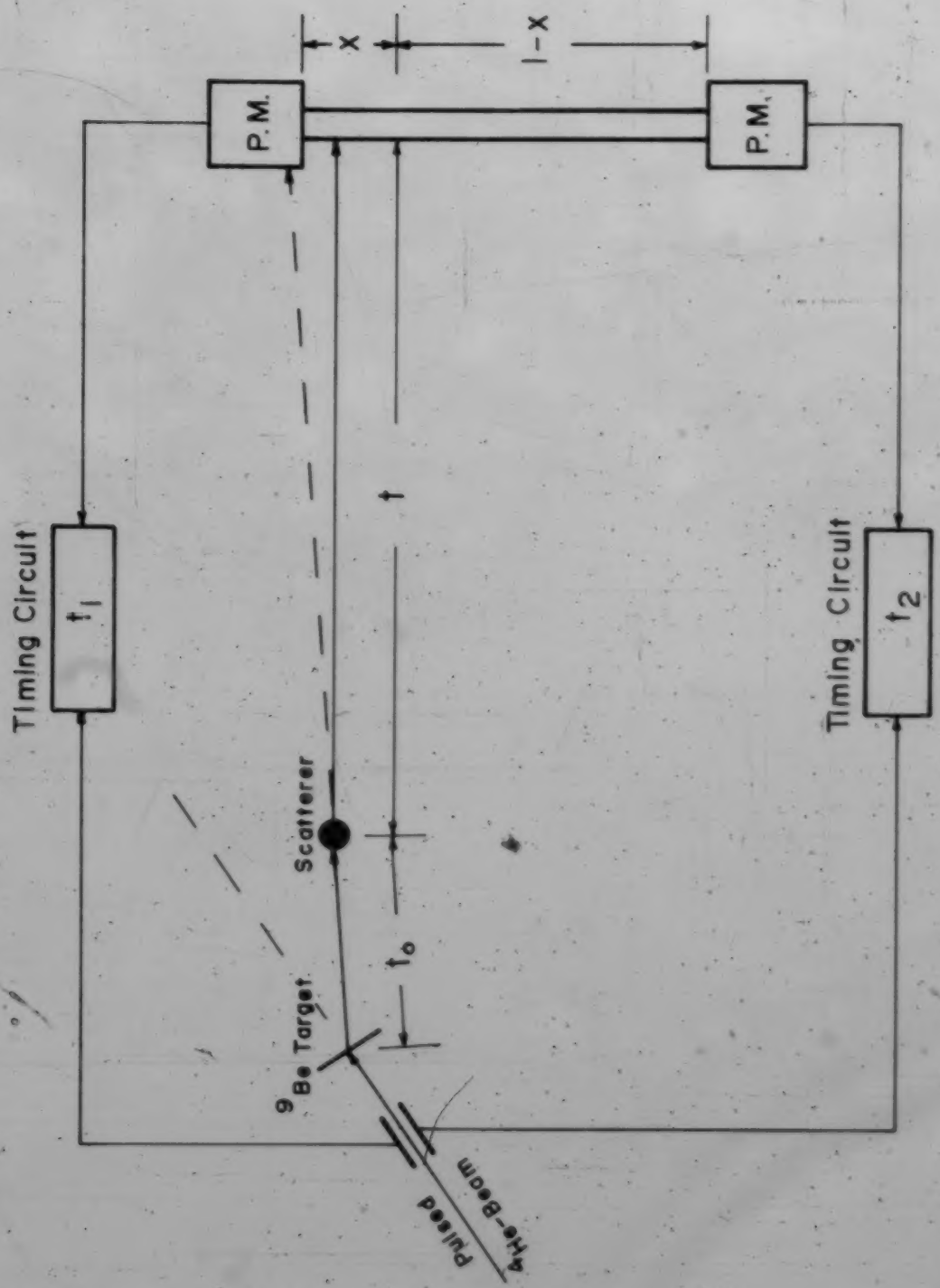
x
l-x
P.M.
P.M.
Timing Circuit
t_1
t_2
Timing Circuit
t
Scatterer
t_0
^{9}Be Target
Pulsed
^{4}He-Beam

Similarly "t_2" is the sum of "t_o", "t" and the light transit time "$t_{(\ell-x)}$" over "ℓ-x" where ℓ is the length of the scintillator, i.e.

$$t_1 = t_o + t + t_x$$

$$t_2 = t_o + t + t_{(\ell-x)} \quad .$$

This gives

$$\Delta t = t_1 - t_2 = t_x - t_{(\ell-x)}$$

since

$$t_{(\ell-x)} = t_\ell - t_x$$

then

$$t_x = \frac{1}{2} (\Delta t + t_\ell) \quad . \qquad (5.1)$$

The measured times t_1 and t_2 were digitized and fed to an on-line computer. The computer then computed t_x and the corresponding time "t". The whole time spectrum was then divided into 16 bins. Each bin so selected contained time of flight information for neutrons hitting 16 successive sections of the scintillator each two inches in diameter and 2.5 inches long. If the scintillator is 130 inches away from the scatterer, then the scintillator will act as 16 small detectors separated from each other by one degree. The main advantage of this type of detector is that the electronics necessary to operate it is almost the

same as the electronics needed to operate a single detector placed at a single angle. Unfortunately, when the first bin, of the long detector, was placed at 2°, relative to the direction of the incident neutron beam, the unscattered neutron beam hit the photomultiplier tube. This resulted in a large number of neutrons being scattered from the photo tube into the scintillator resulting in a background which made it impossible to obtain any useful information from the first seven bins which covered the region of interest.

Three small detectors were eventually used to collect the data presented in this thesis. They were NE 213 liquid scintillators each 3" high by 2" diameter. Each was viewed by an RCA 8575 photomultiplier tube. The aluminum plate shown in figure 5.2 was used to fix the relative position of the three detectors and to move them together without any change in their relative position. An aluminum bar, $\frac{1}{4}$" × 2" × 150" was coupled to the edge of the plate. The end of the bar, in turn, hinged at a point directly below the scatterer. When the center of detector #1 (figure 5.2) was 112.5" away from the center of the scatterer, the relative angular positions of the detectors are

Figure 5.2 - Detectors' holder for small angle scattering measurements.

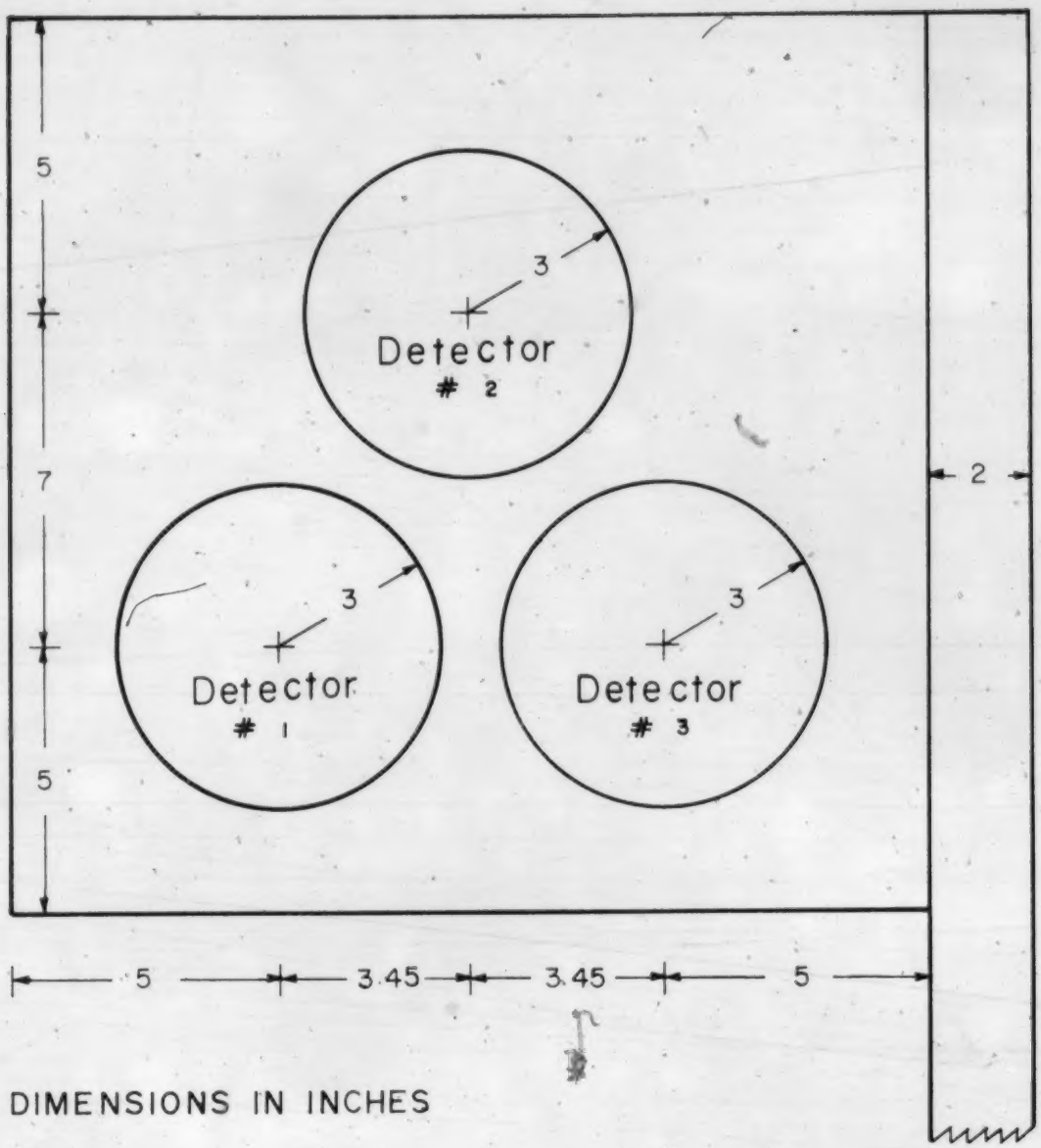

DIMENSIONS IN INCHES

$$\theta_2 = \theta_1 + 1.5°$$

$$\theta_3 = \theta_1 + 3.5° \qquad (5.2)$$

where θ_1, θ_2 and θ_3 are the angles which detectors #1, #2 and #3 make with the direction of the incident neutron beam, respectively.

A fourth detector at -30° relative to the incident neutron beam was used as a monitor. It was also an NE 213 liquid scintillator, 2" long by 3.5" diameter.

A block diagram of the electronics used with each detector is shown in figure 5.3. For a complete description of a similar circuit see Hussein (Hu 70). Two analog signals from each detector, one for n-γ discrimination and the other for time of flight, were digitized by Analog-to-Digit converters. The digitized signals were fed to a Honeywell DDP-516 on-line computer. The signals from the n-γ discrimination system were used to gate the time of flight spectrum in the following way. A digitized window, set on the neutron peak in the n-γ spectrum, was used by a special code "SORT" (Da 72) to select those events which lie within the window and route them, as neutron events, into a 1024 channel spectrum. Those events which lay outside the window were channeled to another 1024 channel region.

Figure 5.3 - Block diagram of time-of-flight electronics with n-γ separation.

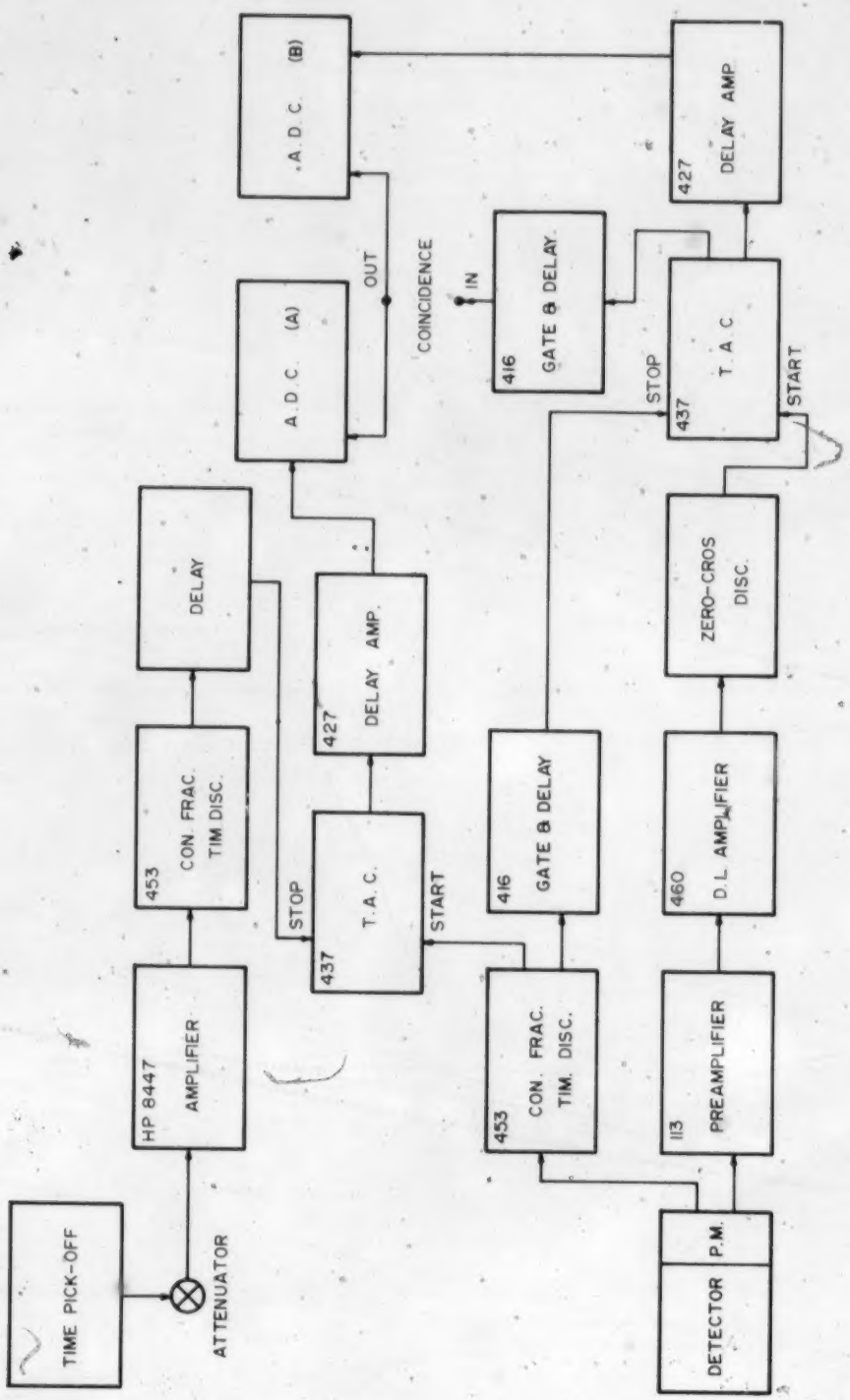
TIME PICK-OFF
ATTENUATOR
HP 8447 AMPLIFIER
453 CON. FRAC. TIM DISC.
DELAY
STOP
437 T. A. C.
START
427 DELAY AMP.
A. D. C. (A)
OUT
COINCIDENCE
IN
A. D. C. (B)
416 GATE & DELAY
453 CON. FRAC. TIM. DISC.
416 GATE & DELAY
STOP
437 T. A. C.
START
427 DELAY AMP
ZERO-CROS DISC.
460 D. L. AMPLIFIER
113 PREAMPLIFIER
DETECTOR
P.M.

The large angle measurements were taken using two identical detectors. The detectors were NE 213 scintillators 3.5" diameter and 2" long. One of these detectors, placed inside the detector shield of figure 3.5, was rotated around the scatterer to detect scattered neutrons at different angles between 15 and 65°. The other detector was fixed at -30° relative to the incident neutron beam and was used as a monitor. The electronics used was identical to that used in the small angle measurements.

Figure 5.4 shows the examples of the following time of flight spectra. (a) is an unsorted (i.e. without n-γ separation) spectrum with the scatterer in. (b) is the sorted neutron spectrum with the scatterer in. (c) is the same as (b) with the scatterer out. (d) is the difference between (b) and (c) (i.e. (In-out) spectrum). This last spectrum is shown magnified in figure 5.5. The solid line under the 10 MeV peak is the linear background used. All these spectra were taken with the magnetic field on.

5.4 Angular Calibration

To use equation (5.2) to determine the angular position of the detectors one has to determine the position of the incident neutron beam which passed

Figure 5.4 - Typical time-of-flight spectra for the elastic scattering of 10 MeV polarized neutrons from Pb at scattering angle of 1.5°.

a) Unsorted spectrum taken with scatterer in.

b) Sorted spectrum with scatterer in.

c) Sorted spectrum with scatterer out.

d) In-out spectrum.

Each spectrum is offset by a certain amount, so that the number indicated at the right must be subtracted from the ordinate to obtain the correct magnitude.

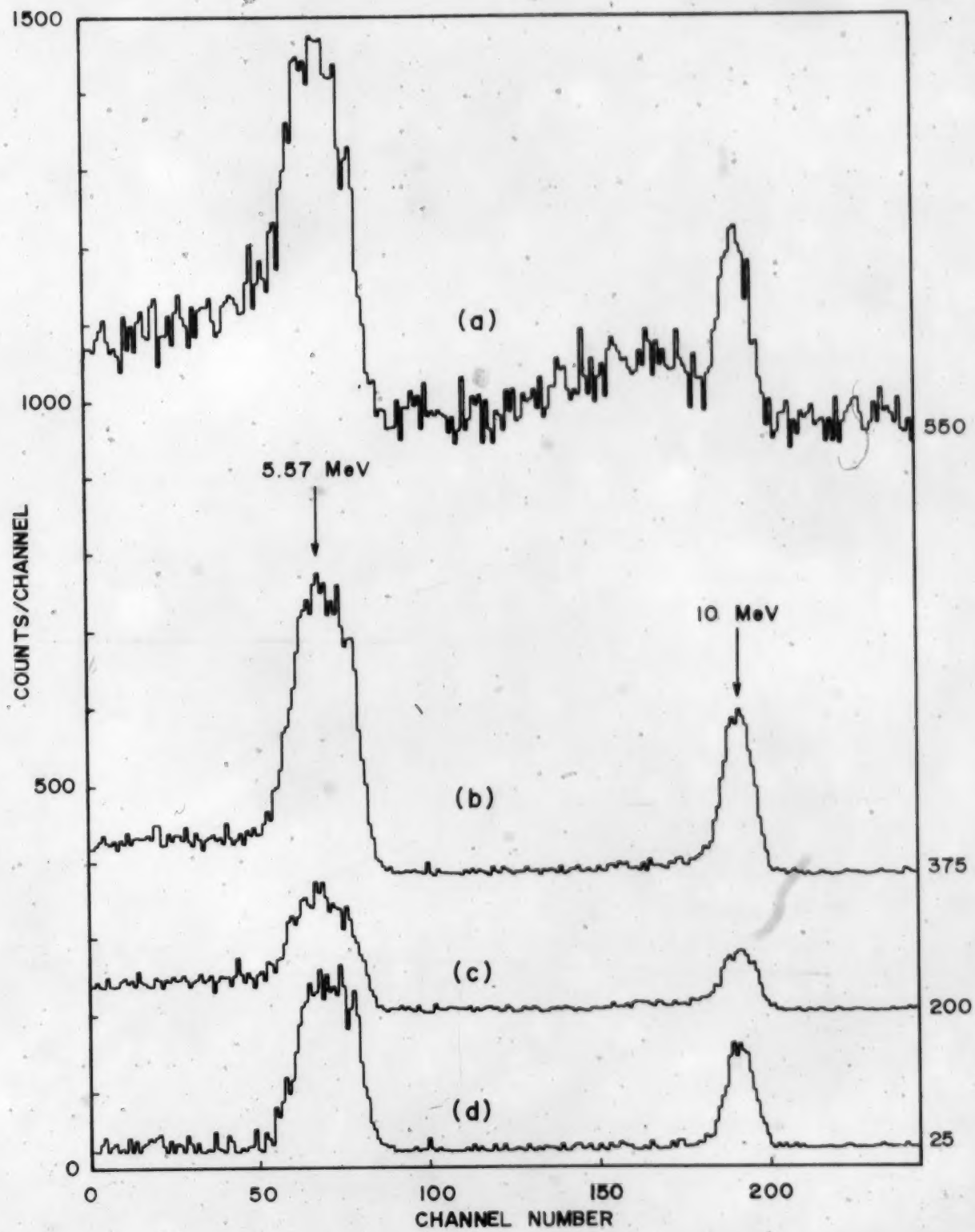
1500
1000
500
0
COUNTS/CHANNEL
(a)
550
5.57 MeV
10 MeV
(b)
375
(c)
200
(d)
25
0
50
100
150
200
CHANNEL NUMBER

Figure 5.5 - This is the same spectrum shown in figure 5.4d. The straight line under the 10 MeV peak is the average linear background.

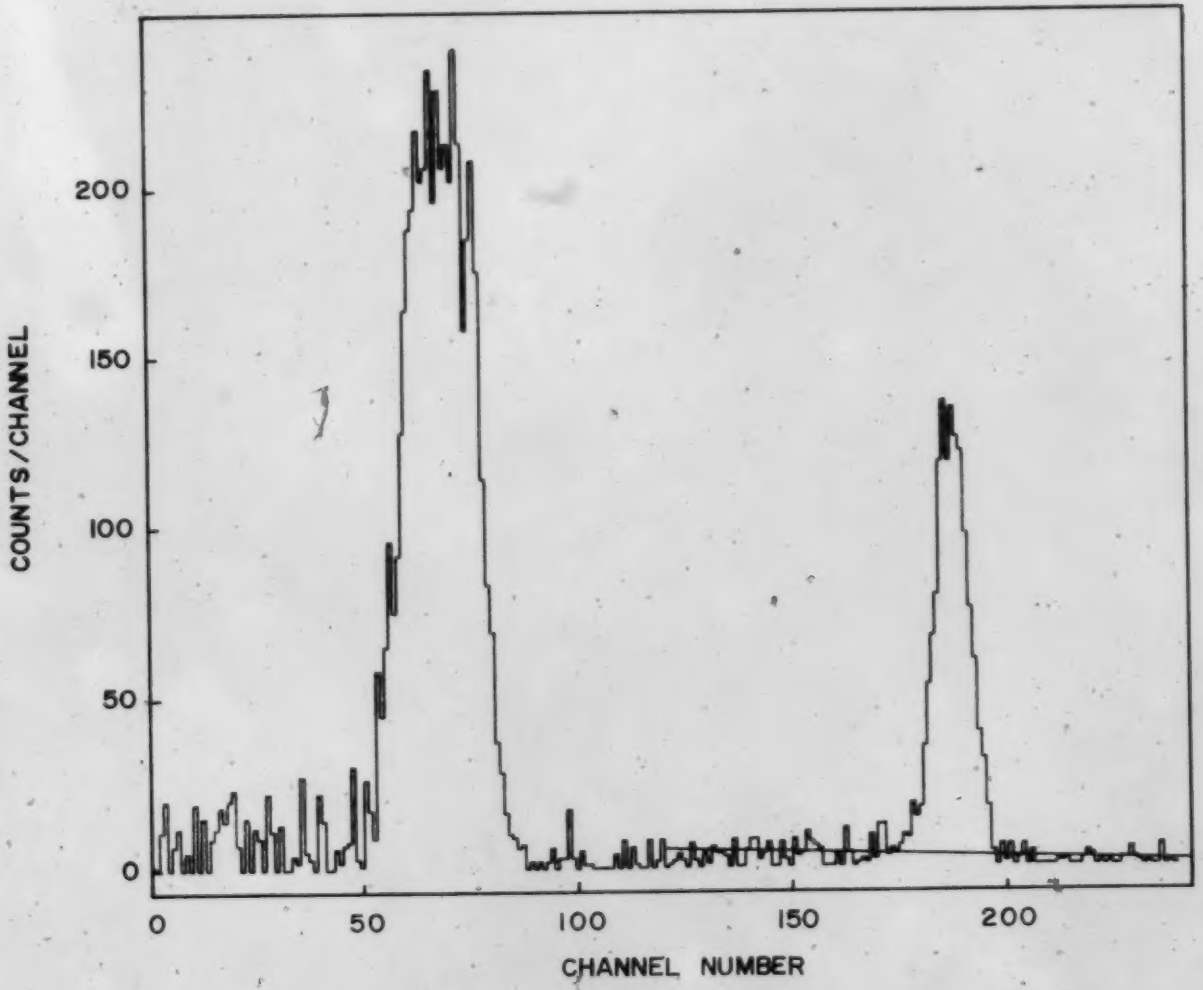
COUNTS/CHANNEL
200
150
100
50
0
0
50
100
150
200
CHANNEL NUMBER

through the center of the scatterer. The following method was used to determine that position. Detector #1 was used to record neutrons at different positions measured from an arbitrary point on the arc of rotation of the detectors. The number of counts was recorded twice at each position, once with the scatterer "in" and once with the scatterer "out". The ratio R given by

$$R = \frac{N_{out} - N_{in}}{N_{out}}$$

is plotted against the detector position in figure 5.6. N_{out} and N_{in} are the number of neutrons recorded with the scatterer "out" and "in" respectively. These numbers were normalized to a monitor at 0° relative to the incident α-beam. The ratio R is the fraction of the incident neutron beam absorbed in the scatterer and will take its maximum value when the detector center and the scatterer center are along the direction of the incident neutron beam. As shown in figure 5.6 the position "6.85" is the center at half maximum and was taken as the direction of the incident neutron beam. The error in determining that position is $\pm\frac{1}{4}$" which correspond to ±0.13° an error much smaller than the angular acceptance of the detector.

Figure 5.6 - Neutron absorption in the scatterer as a function of detector position.

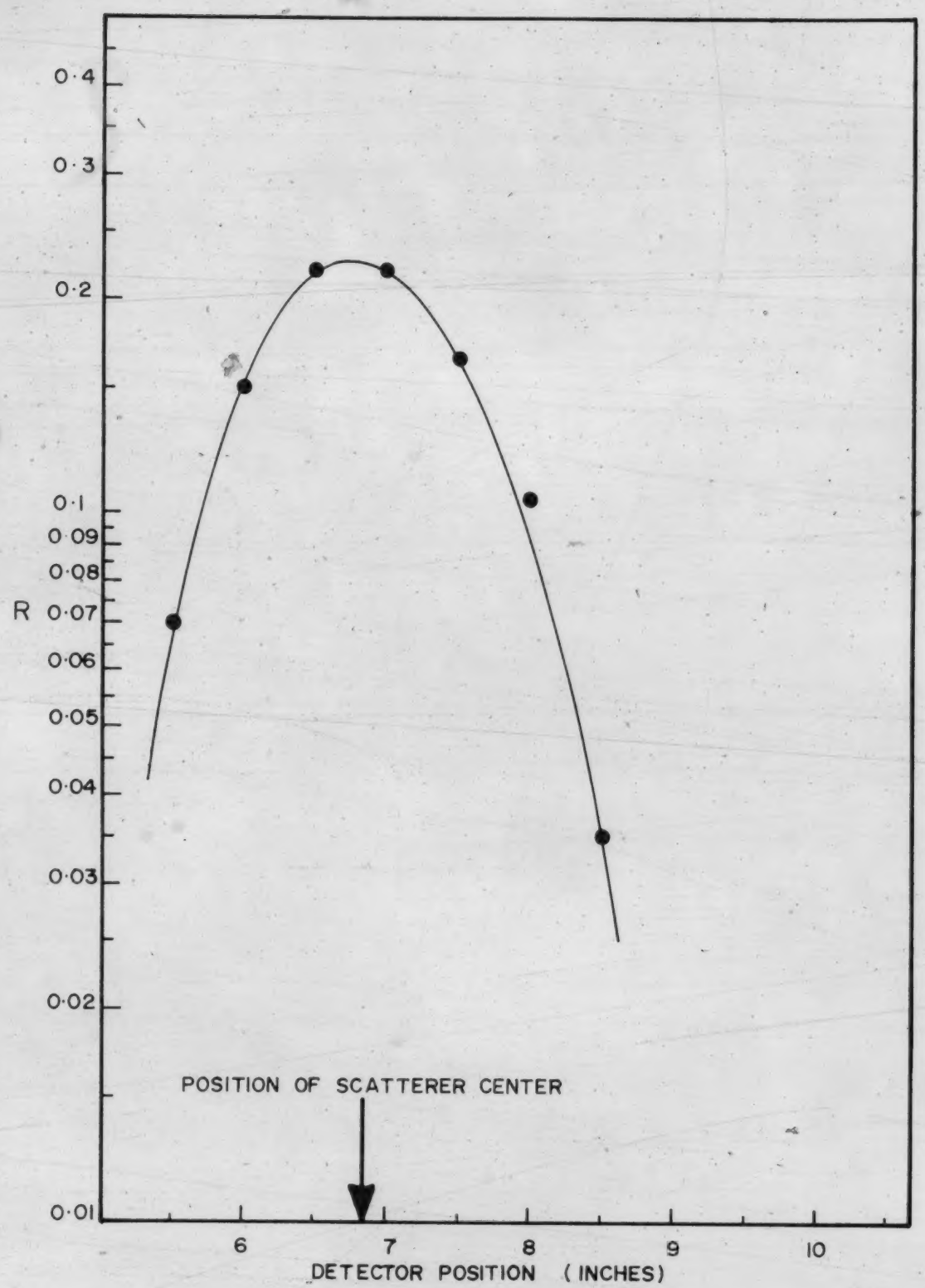
0·4
0·3
0·2
0·1
0·09
0·08
R 0·07
0·06
0·05
0·04
0·03
0·02
0·01
POSITION OF SCATTERER CENTER
6
7
8
9
10
DETECTOR POSITION (INCHES)

5.5 Experimental Results

Small angle data were taken at two detector settings. In the first detector #1 was at an angle of 1.6° and in the second setting detector #1 was at 2.8°. At the first position data were taken in the following order:

1) Pb scatterer in position and magnetic field off,
2) Pb scatterer in position and magnetic field on,
3) scatterer out and magnetic field on,
4) scatterer out and magnetic field off,
5) Bi scatterer in position and field off, and
6) Bi scatterer in position and field on.

After detectors were moved to the second position the data were taken in the reverse order i.e. starting with step 6 and end up with step 1. In this way it was ensured that the scatterer was in the same position with the field on and off, also time was saved by taking only one background run (scatterer out) for the two scatterers. The data were collected over three series of runs. The total data collection time per series was about 36 hours for each "scatterer-in" run and 24 hours for each "scatterer-out" run.

The data reduction was performed as follows. First, all sorted data were normalized to the monitor at -30°. The background under each peak was determined by linear extrapolation between the average number of

counts per channel on each side of the peak. Using Madison convention, as described in Chapter 2, one can write

$$\varepsilon = P_o P = \frac{(N_{in}^{on} - N_{out}^{on}) - (N_{in}^{off} - N_{out}^{off})}{(N_{in}^{on} - N_{out}^{on}) + (N_{in}^{off} - N_{out}^{off})}$$

where ε is the asymmetry of the scattered neutrons, P_o is the polarization of the incident neutron beam, P is the analysing power of the scatterer or the polarization of the scattered beam and N is the final number of counts obtained under the conditions defined by the subscripts and superscripts. "On" and "off" refer to the magnetic field and "in" and "out" refer to the scatterer.

As described in section 3.1, $^{9}Be(^{4}He,\vec{n})$ reaction gave two well resolved, neutron groups. The ground state group was at 10 MeV, having a polarization of 0.44±0.03 (De 73). The next group was at 5.57 MeV, having a polarization of 0.07±0.02 (De 73). Both groups were observed in the time spectra of the elastically scattered neutrons. Since $\varepsilon = P_o P$ and since P could not exceed unity then the asymmetry of the scattered 5.57 MeV neutrons could not exceed the value of P_o (0.07). This, thus, provided a check on the asymmetry of the scattered 10 MeV neutrons.

A computer program was written to calculate ε and P along with their statistical errors for both neutron groups taking into consideration all necessary normalizations.

Figure 5.7 shows the small angle polarization results for 10 MeV neutrons. The corresponding small angle cross section in absolute units is shown in figure 5.10. Figure 5.8 shows the small angle polarization after being corrected for multiple scattering effects (see Appendix A). Small angle asymmetries of the 5.57 MeV neutrons group which has been used to check on the 10 MeV results are shown in figure 5.9. In figure 5.11 the large angle polarization is shown, while the corresponding cross section is shown in figure 5.12. In all of these figures the vertical bars are the statistical errors and the horizontal bars, if any, are the combined angular acceptance due width of the detector and the scatterer.

Figure 5.7 - Small angle polarization of 10 MeV neutrons scattered from Pb and Bi.

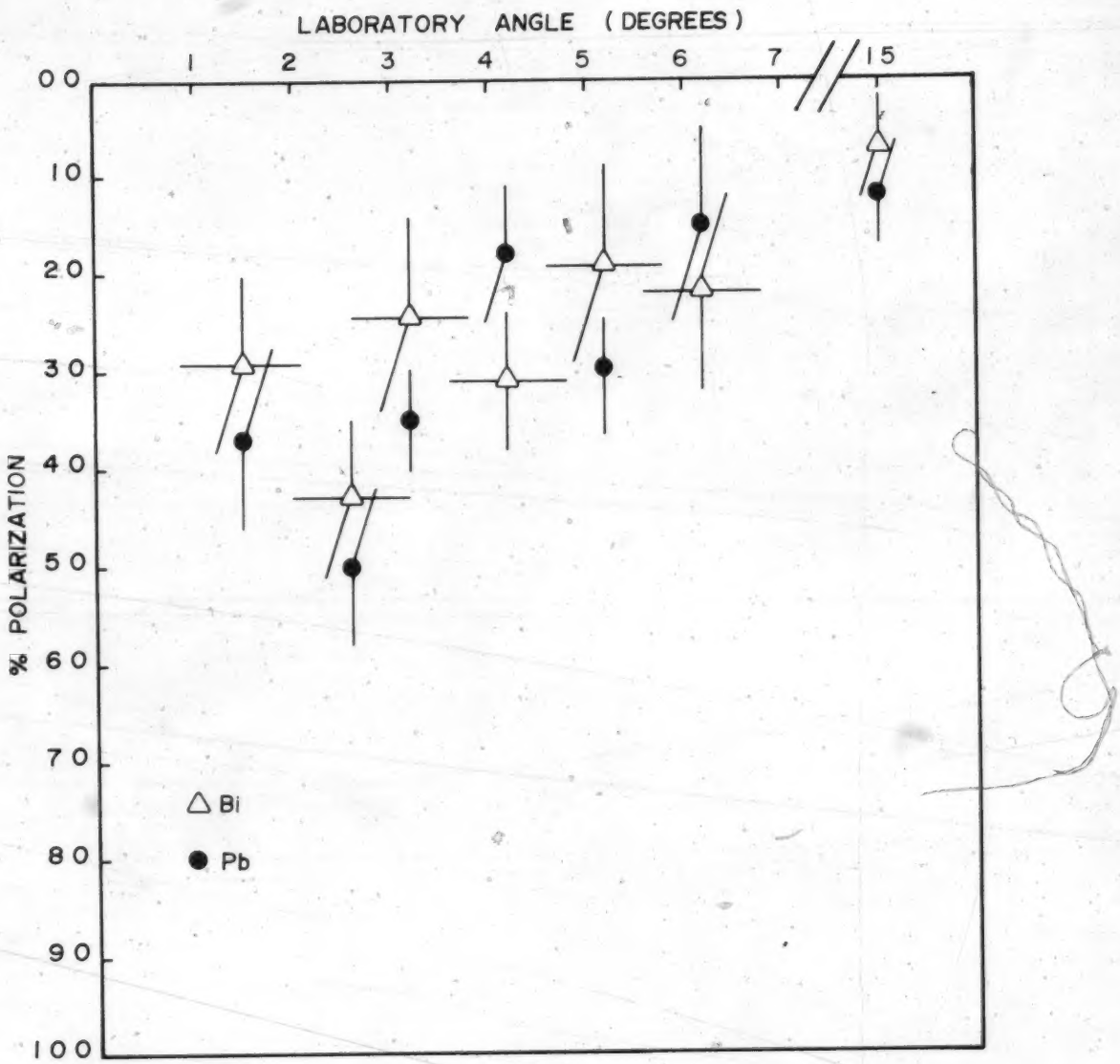
LABORATORY ANGLE (DEGREES)
1
2
3
4
5
6
7
15
00
10
20
30
40
50
60
70
80
90
100
% POLARIZATION
△ Bi
● Pb

Figure 5.8 - Small angle polarization of 10 MeV neutrons scattered from Pb and Bi corrected for multiple scattering and finite geometry effects.

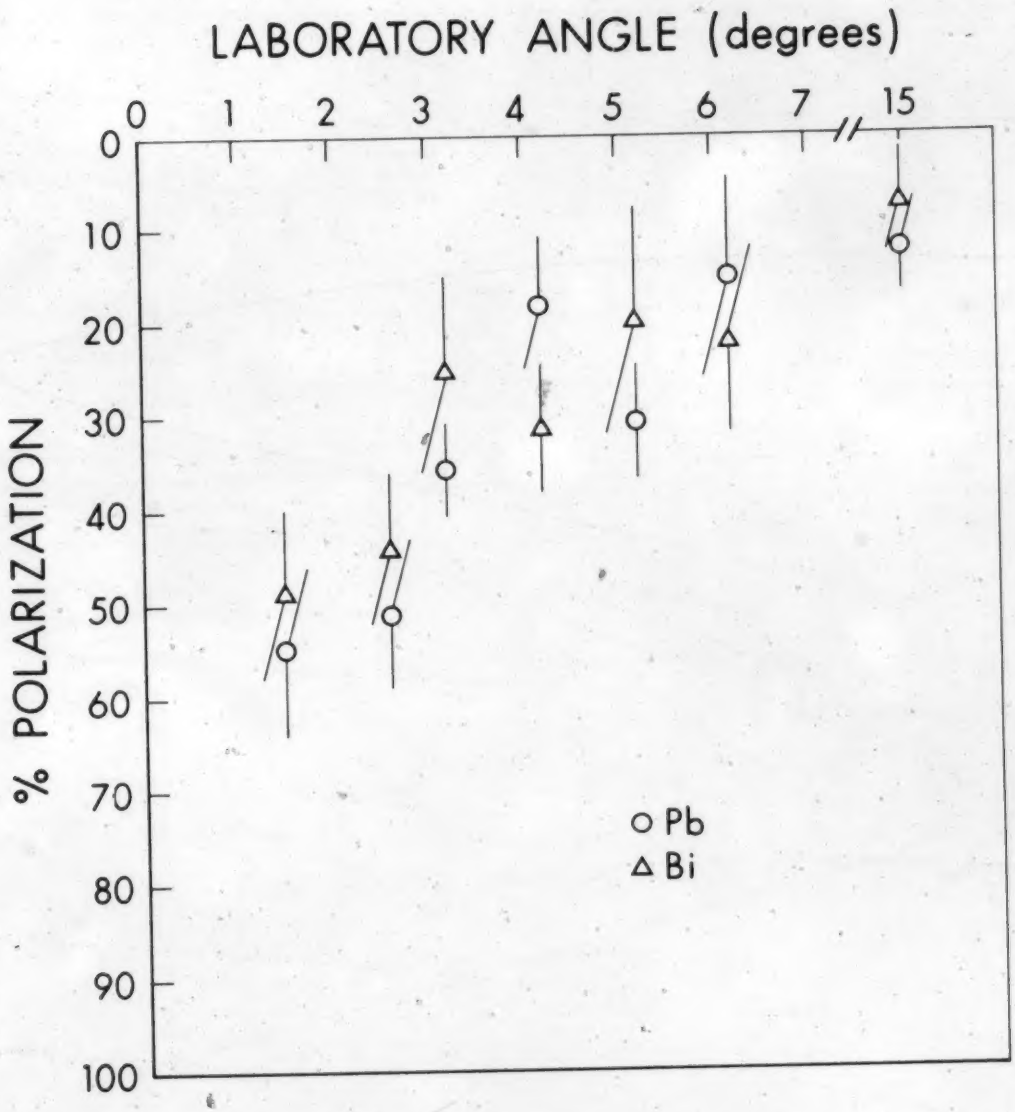
LABORATORY ANGLE (degrees)
0
1
2
3
4
5
6
7
15
% POLARIZATION
0
10
20
30
40
50
60
70
80
90
100
Pb
Bi

Figure 5.9 - Small angle asymmetry of 5.57 MeV neutrons scattered from Pb and Bi.

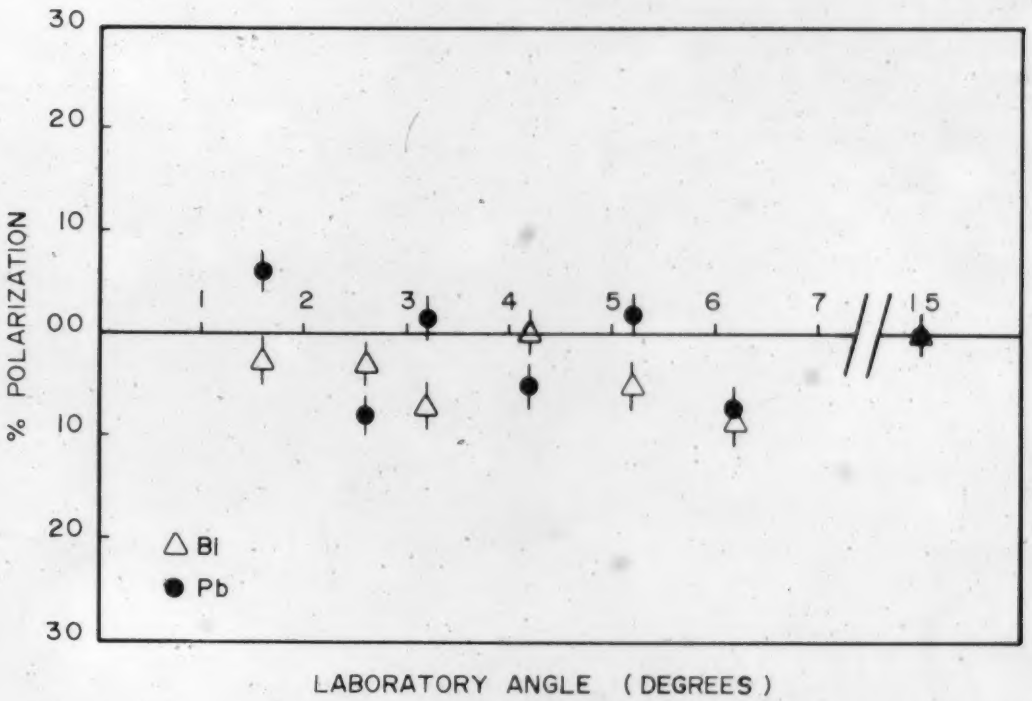
30
20
10
00
10
20
30
% POLARIZATION
1
2
3
4
5
6
7
15
Bi
Pb
LABORATORY ANGLE (DEGREES)

Figure 5.10 - Small angle differential cross section of 10 MeV neutrons scattered from Pb and Bi.

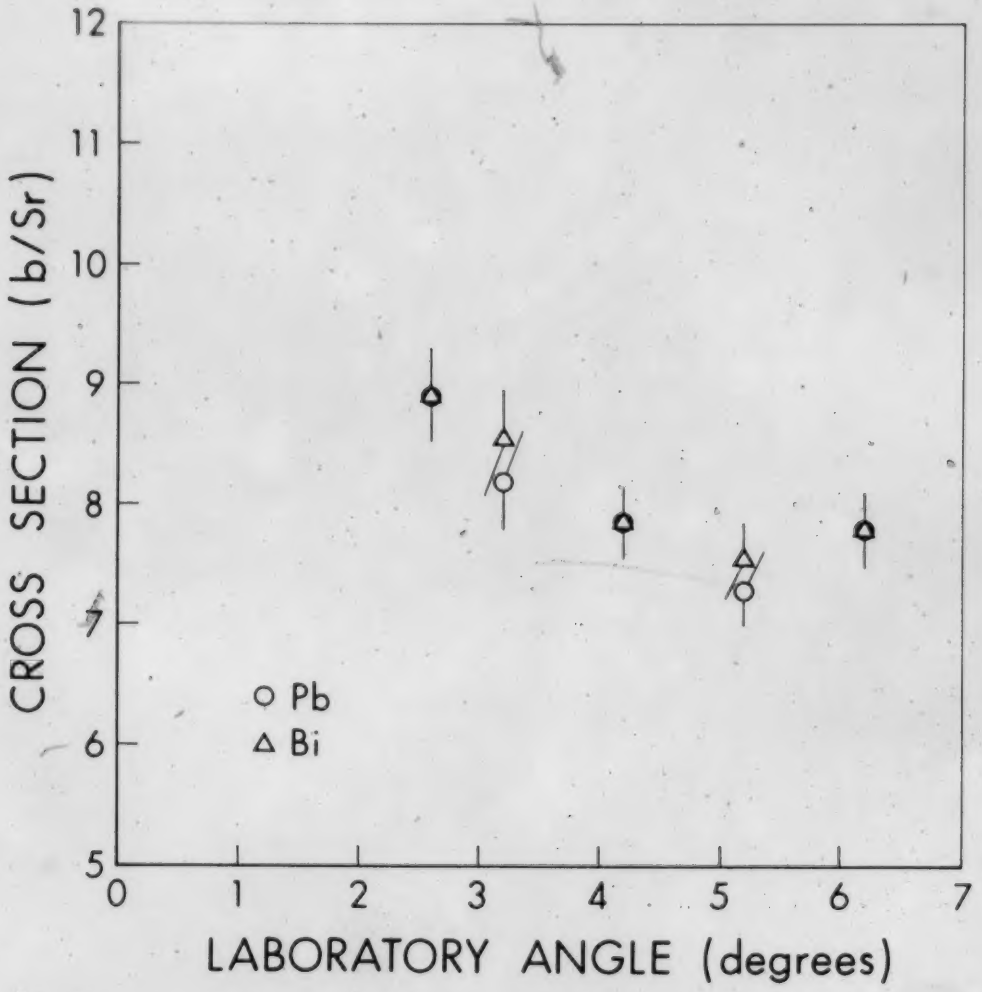
CROSS SECTION (b/Sr)
LABORATORY ANGLE (degrees)
12
11
10
9
8
7
6
5
0
1
2
3
4
5
6
7
○ Pb
△ Bi

Figure 5.11 - Large angle polarization of 10 MeV neutrons scattered from Pb and Bi.

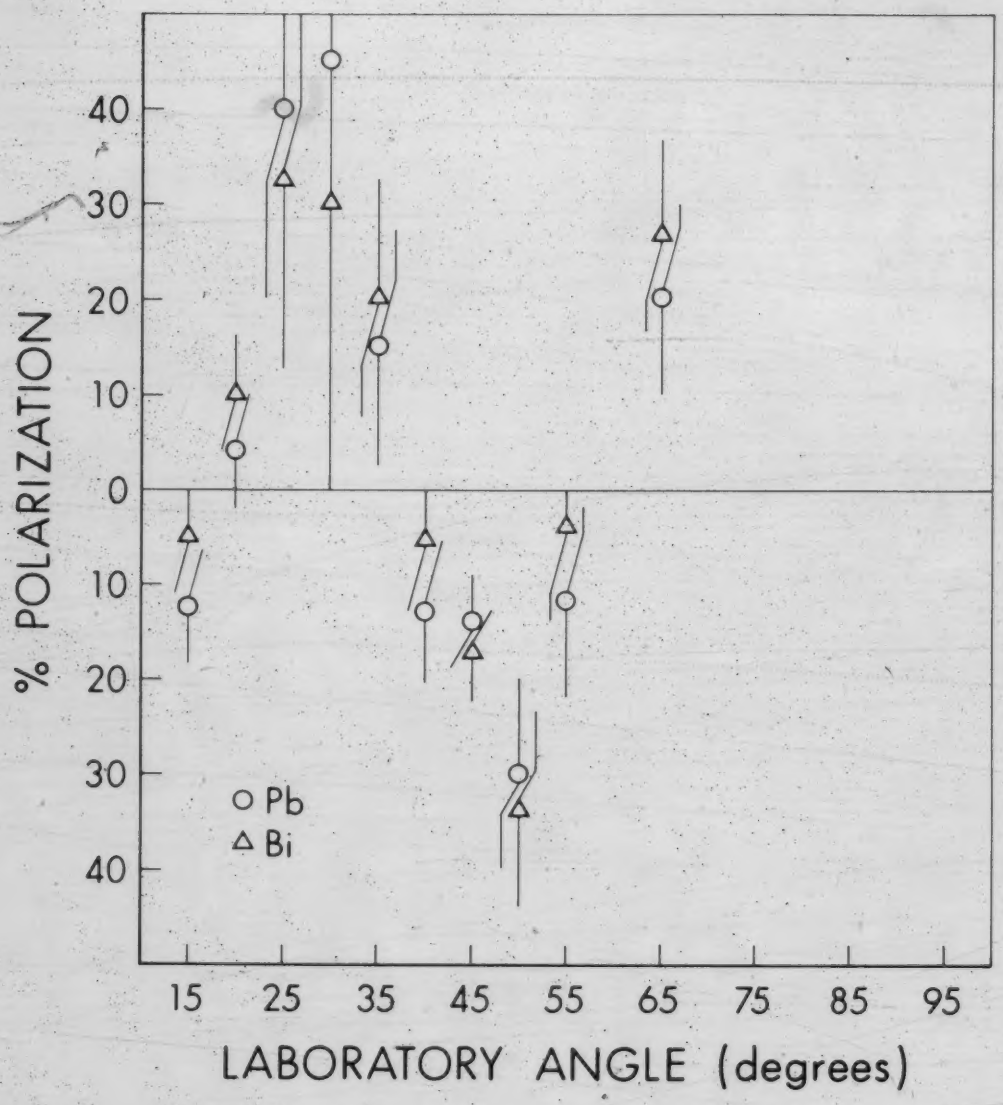
40
30
20
10
0
10
20
30
40
% POLARIZATION
○ Pb
△ Bi
15
25
35
45
55
65
75
85
95
LABORATORY ANGLE (degrees)

Figure 5.12 - Large angle differential cross section of 10 MeV neutrons scattered from Pb and Bi.

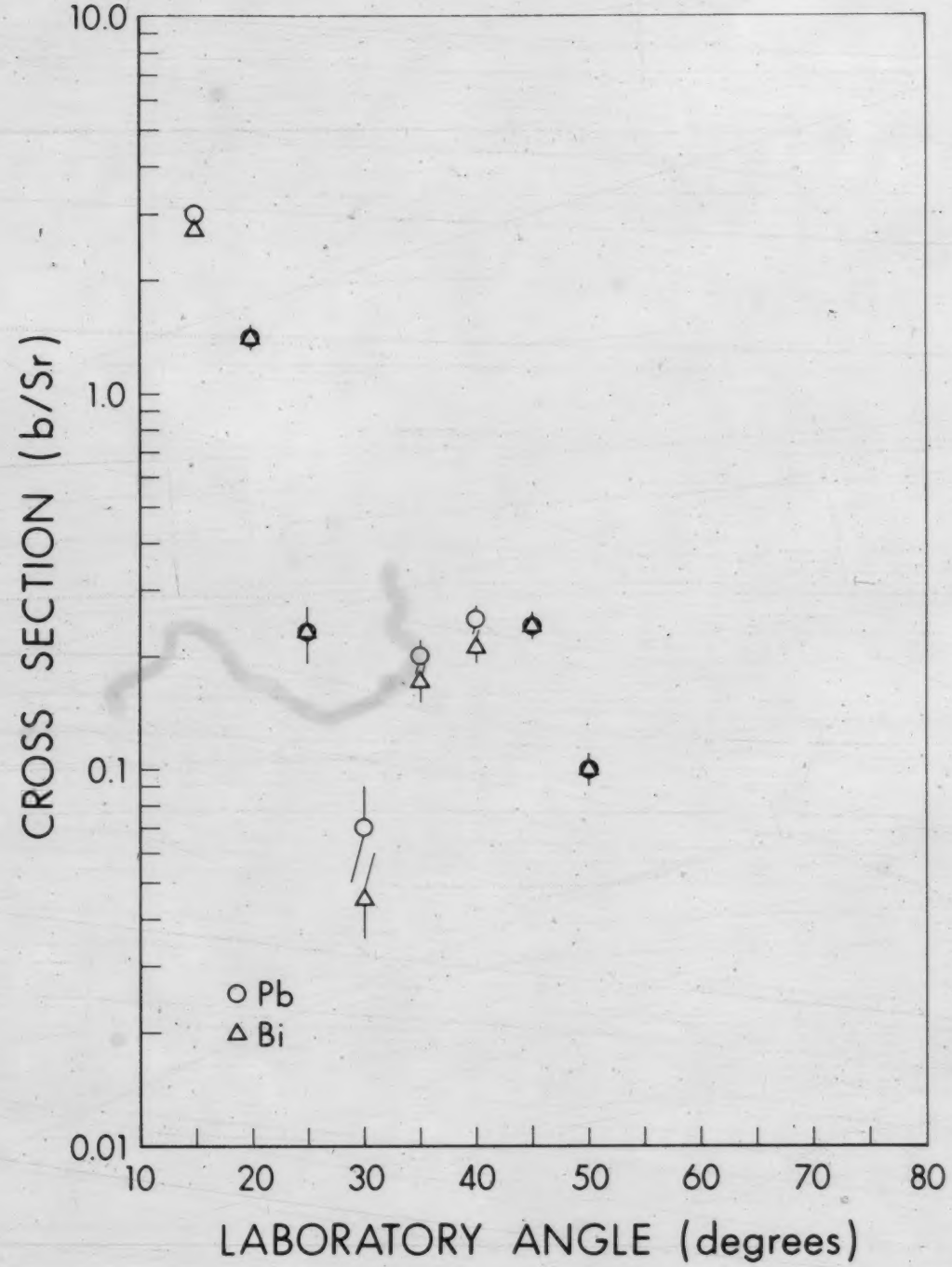
10.0
1.0
0.1
0.01
CROSS SECTION (b/Sr)
10
20
30
40
50
60
70
80
LABORATORY ANGLE (degrees)
○ Pb
△ Bi

CHAPTER 6

COMPARISON WITH THEORETICAL CALCULATIONS

6.1 Introduction

The DWBA calculations of the cross section and polarization for neutrons elastically scattered from a nucleus require the optical model potential of the scattering nucleus. There are two different types of optical potentials, local and non-local potentials. The local potential is normally written as

$$U(r) = Vf(X_v) + i(W + 4a_w W_s \frac{d}{dX_w}) f(X_w)$$

$$- (V_{so} + iW_{so}) \frac{1}{r} \frac{d}{dr} f(X_{so}) \vec{L}\cdot\vec{\sigma} \qquad (6.1)$$

with $f(X) = (1 + e^{X})^{-1}$ and

$$X_i = \frac{r - r_i A^{1/3}}{a_i} \quad , \quad i \text{ can be v, w or so}$$

where

V, r_v and a_v are the depth, radius and diffuseness of the real part of the potential,

W, W_s, r_w and a_w are the volume depth, surface depth, radius and diffuseness of the imaginary part of the potential, and

V_{so}, W_{so}, r_{so} and a_{so} are the real depth, imaginary depth, radius and diffuseness of the spin-orbit part of the potential.

A non-local potential operating on a wave function has the form (Pe 62)

$$V\psi(\vec{r}) = \int V(\vec{r},\vec{r}')\psi(\vec{r}')d\vec{r}' \ .$$

To facilitate numerical calculations a separable form could be chosen for the non-local potential kernel function as

$$V(\vec{r},\vec{r}') = U(\frac{\vec{r}+\vec{r}'}{2})H(\frac{\vec{r}-\vec{r}'}{\beta})$$

where β is the range of non-locality. "H" is normally chosen to be a Gaussian function

$$H(|\vec{r}-\vec{r}'|) = \frac{Exp[-(\frac{\vec{r}-\vec{r}'}{\beta})^2]}{\pi^{3/2}\beta^3}$$

which is normalized such that

$$\int H(|\vec{r}-\vec{r}'|)d\vec{r}' = 1 \ .$$

If we define

$$p = \frac{1}{2}|\vec{r}+\vec{r}'|$$

then U(p) can take exactly the same form as U(r) defined in equation (6.1) with p replacing r. The spin-orbit term will stay as a function of r. Wilmore and Hodgson (Wi 64) developed a potential which is equivalent to a non-local potential i.e. it produces the same results as the non-local potential but at the same time it could be used by any optical model computer program which accepts local potentials only.

In general, the optical potential for a particular nucleus at a certain energy is found by varying in the computer program the ten parameters mentioned above, until a best fit, between the theoretical calculation and experimental results, is indicated by a χ^2 minimization procedure.

There are three commonly used sets of parameters, for neutron elastic scattering from Pb and Bi for neutrons in the 10 MeV energy range. They are:

a) the local potential of Rosen et al (Ro 65). The parameters of this potential were obtained by fitting proton data and then modified for neutrons.

b) the equivalent local potential of Wilmore and Hodgson (Wi 64), and

c) the local potential of Beccetti and Greenlees (Be 69).

From now on these potentials will be referred to by the symbols RO for potential (a), WH for potential (b) and BG for potential (c).

The parameters of these three potentials are given in table 6.1.

It is often assumed that these potentials will give equally good fits to experimental data. However, recently, Bucher and Hollandsworth (Bu 75 and Bu 75a) have found that the WH potential fits their data for small angle scattering of neutrons from Pb and Bi much

Table 6.1

Optical model parameter used in the theoretical calculations

Parameter	Rosen et al (Ro 65)	Wilmore & Hodgson (Wi 64)	Becceti & Greenlees (Be 69)
V(MeV)	46.30	44.22	48.02
r_v(fm)	1.25	1.26	1.17
a_v	0.65	0.65	0.75
W (MeV) W_s	5.75	4.22	7.98 0.64
r_w(fm)	1.25	1.24	1.26
a_w	0.70	0.48	0.58
V_{so}(MeV)	5.50	7.29	6.2
W_{so}(MeV)	0.00	0.00	0.00
r_{so}(fm)	1.25	1.22	1.01
a_{so}	0.65	0.65	0.75

better than the RO potential.

6.2 The Program Code "TASHTASH"

This program was written by Sherif to calculate the cross section and polarization of neutrons or protons elastically or inelastically scattered from nuclei using a DWBA approach. This program takes into account both the nuclear and M-S interaction in the manner described in Chapter 4 (Sh 71). This program has been used to calculate the polarizations and cross sections for the scattering of 10 MeV neutrons from Pb and Bi reported in this work. The three optical model sets of parameters shown in table 6.1 were used and the results are shown in figures 6.1-6.4.

Figure 6.1 shows that the three potentials fit the small angle polarization with almost the same quality. However, figure 6.2 shows that the BG potential gives the best fit for the small angle cross section while the WH potential is the worst of the three potentials. If we look now at the large angle polarization in figure 6.3 we see again that the BG potential fits the data much better than the other potentials and also the WH potential provides the poorest fit. For the large angle cross section data all three potentials fit the forward peak in a reasonable way but they differ

Figure 6.1 - Comparison between theoretical calculations and small angle polarization measurements.

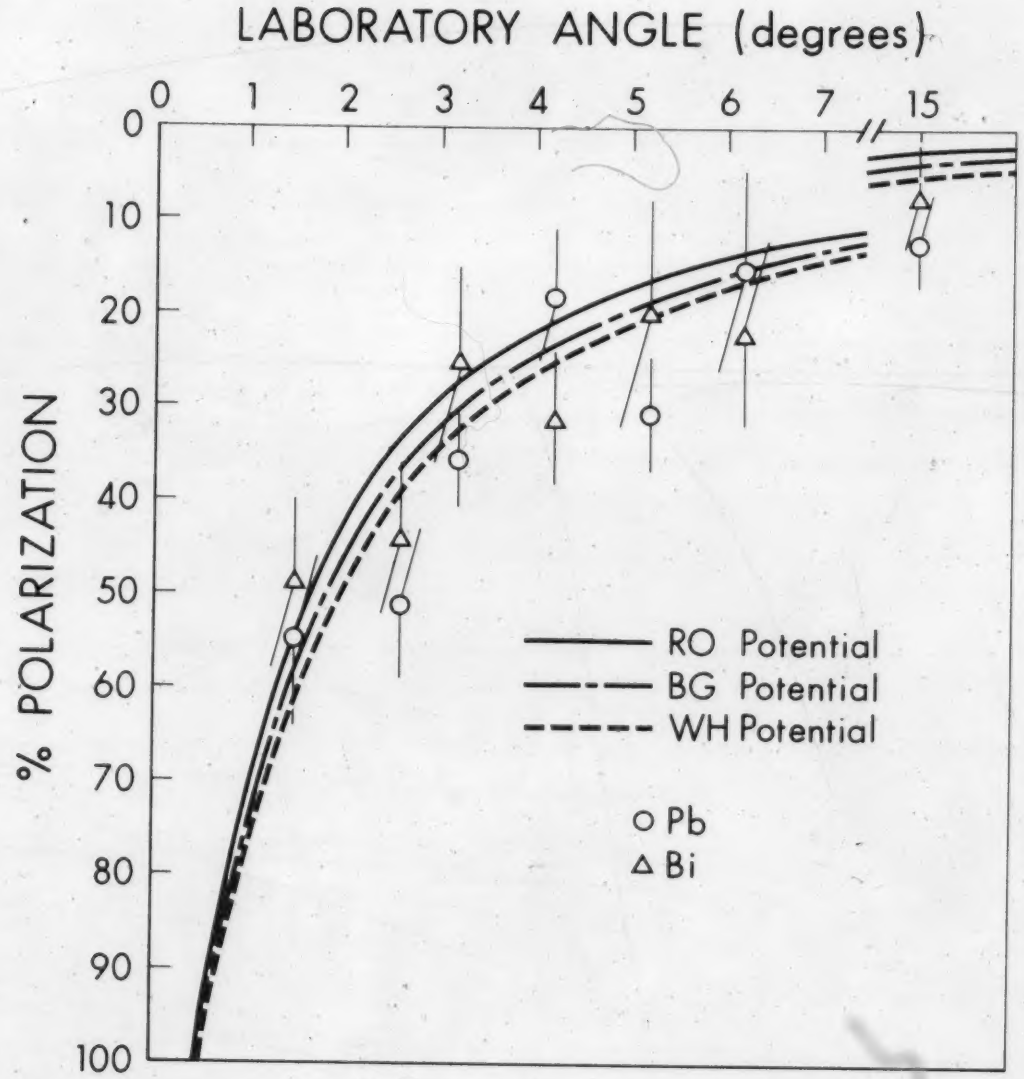
LABORATORY ANGLE (degrees)
0
1
2
3
4
5
6
7
15
% POLARIZATION
0
10
20
30
40
50
60
70
80
90
100
RO Potential
BG Potential
WH Potential
Pb
Bi

Figure 6.2 - Comparison between theoretical calculations and small angle differential cross section.

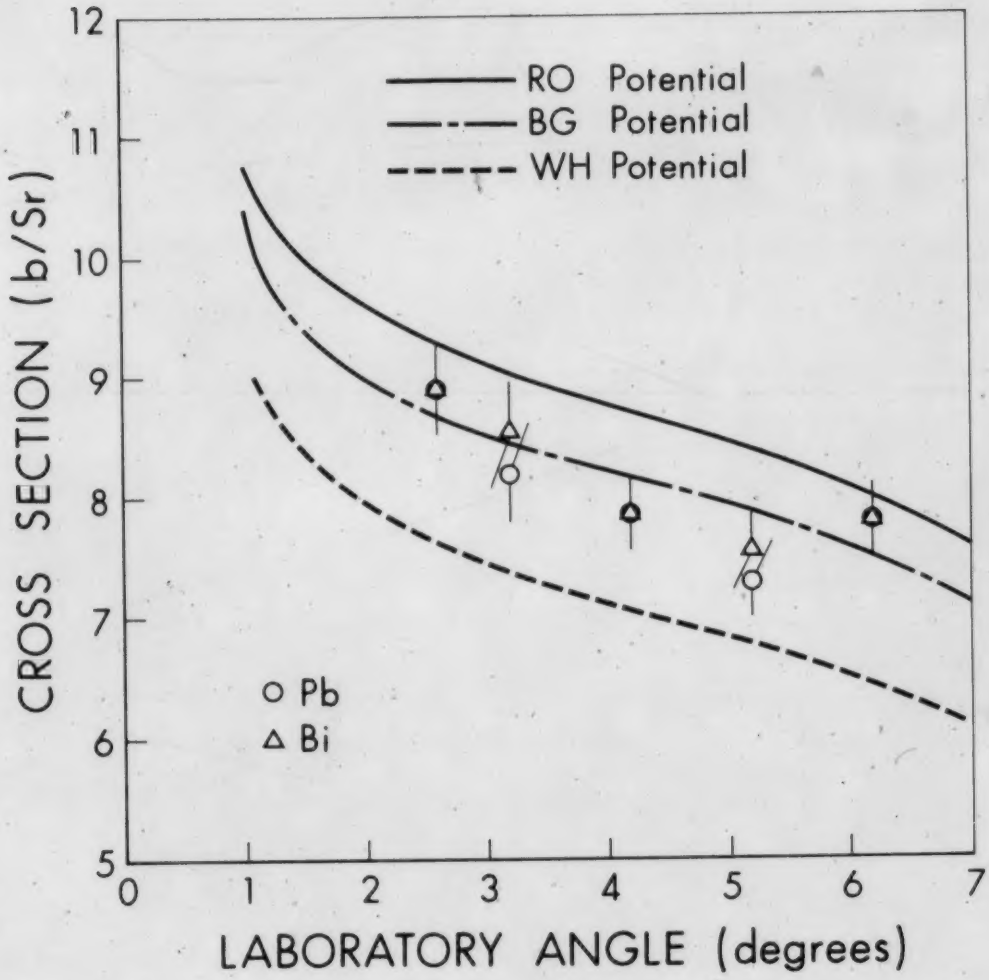
RO Potential
BG Potential
WH Potential
Pb
Bi
CROSS SECTION (b/Sr)
LABORATORY ANGLE (degrees)
12
11
10
9
8
7
6
5
0
1
2
3
4
5
6
7

Figure 6.3 - Comparison between theoretical calculations and large angle polarization measurements.

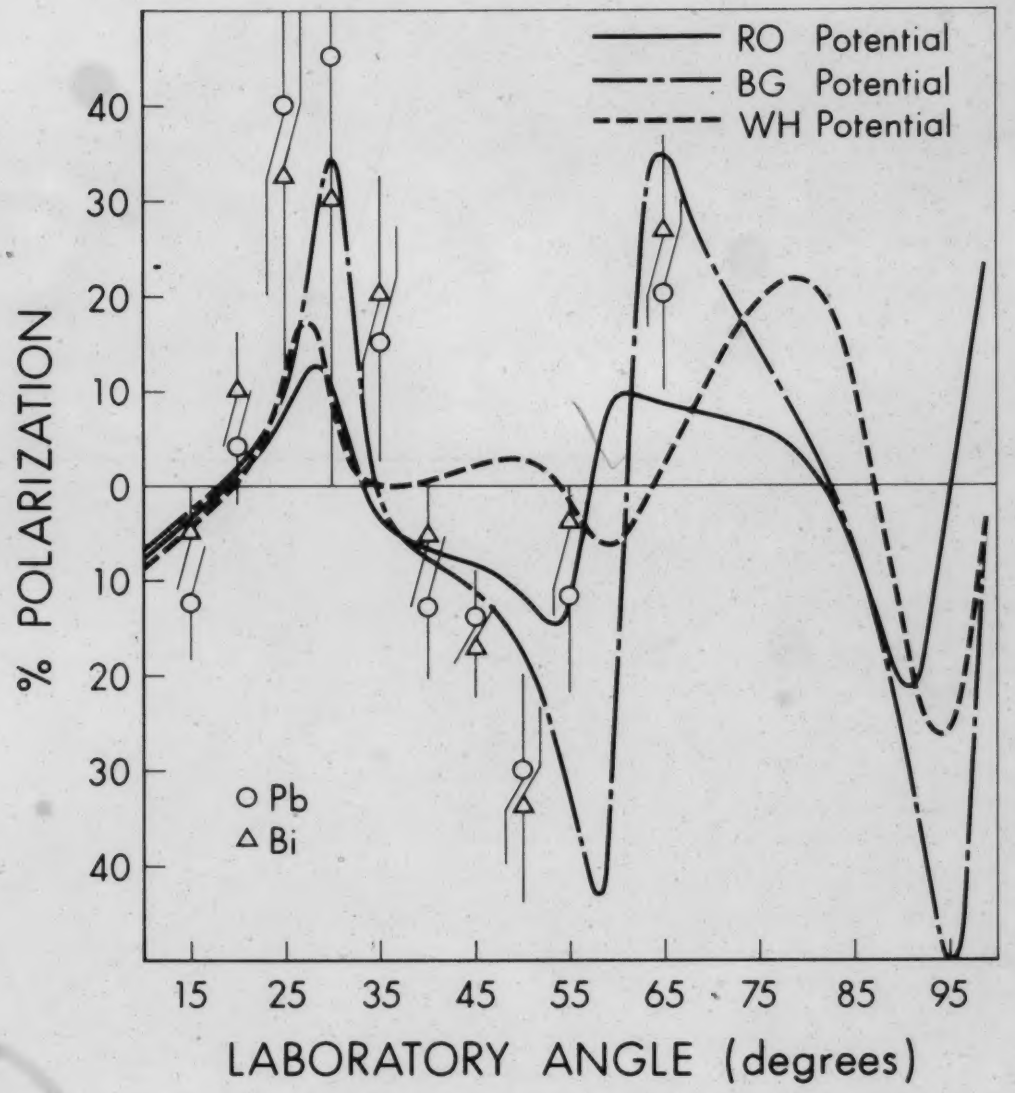
RO Potential
BG Potential
WH Potential
% POLARIZATION
40
30
20
10
0
10
20
30
40
Pb
Bi
15
25
35
45
55
65
75
85
95
LABORATORY ANGLE (degrees)

Figure 6.4 - Comparison between theoretical calculations and large angle differential cross section.

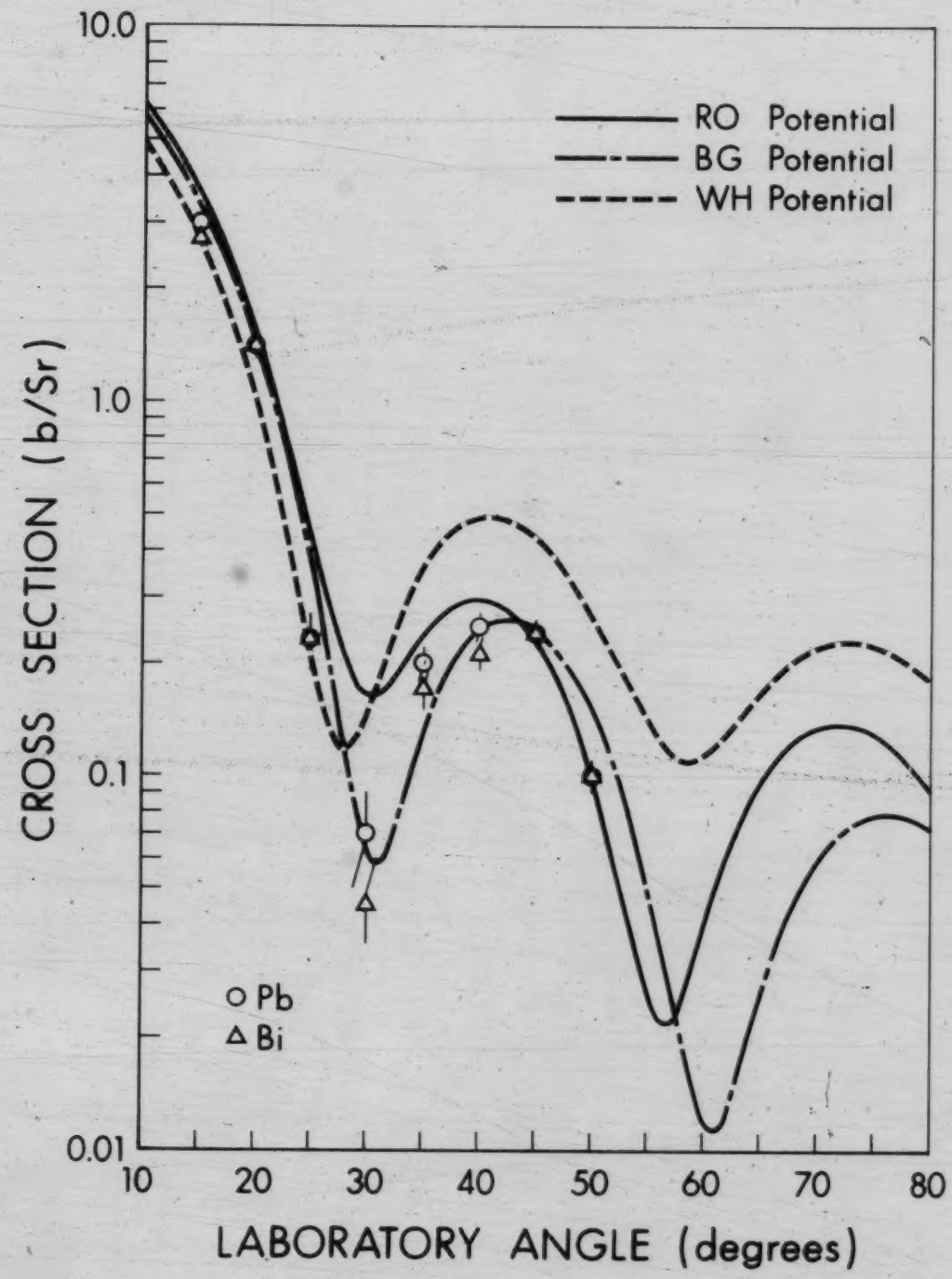
10.0
1.0
0.1
0.01
CROSS SECTION (b/Sr)
RO Potential
BG Potential
WH Potential
O Pb
Δ Bi
10
20
30
40
50
60
70
80
LABORATORY ANGLE (degrees)

drastically at the second maximum where once again the BG potential provides the best fit and the HW potential is the poorest. Thus, one can conclude that the Beccetti and Greenlees (Be 69) potential is the best potential available to describe neutron elastic scattering data at 10 MeV on Pb and Bi. One reason for the poor fit produced by the equivalent local potential of Wilmore and Hodgson (Wi 64) is that they derived the spin-orbit parameters by fitting the cross section at backward angles rather than fitting both cross section and polarization data.

CHAPTER 7

CONCLUSIONS

A facility for the production of 10 MeV polarized neutrons has been designed and built as described in Chapter 3. In this facility a combination of source and detector shielding along with a superconducting spin rotation magnet makes it possible to measure the polarization and cross section of scattered neutrons over the angular range of 2-100°. A Monte Carlo computer program to correct the polarization data for finite geometry and multiple scattering effects was modified to include the M-S effects.

The facility has been used to measure the polarization and cross section of 10 MeV neutron scattered from Pb and Bi in the angular range of 1.5-65°.

A comparison of the results of small angle measurements on Pb and Bi do not show any significant differences. This is in contrast to the situation reported by Drigo et al (Dr 73) at 2.45 MeV where systematic variation was claimed. This does not rule out the possibility that the difference at 2.45 MeV is a real one. This difference could be due to some effect such as compound nucleus formation which may be more important

at that energy. It would be useful to repeat the experiment at 2.45 MeV and, if the differences reported are confirmed, to study further their energy dependence.

Where the M-S force dominates the interaction between the incident neutron and the scattering nucleus, only contributions from high partial waves will be significant. This means that the choice of the optical potential should have little effect on the magnitude of the polarization and the cross section in this region (Sh 71). In the case of scattering from heavy nuclei, this will hold true in the angular range below 10° for polarization measurements and below 2° for cross section. This conclusion has been confirmed by the present work. The agreement between the polarization measurements and theoretical calculations in the small angle region is good and there is little dependence on the optical model potential used. Thus, one can have confidence in the polarization predictions using the M-S interaction. This will facilitate the use of small angle scattering in neutron polarimeters. Galloway and Maayouf (Ga 72) argued that a well designed small angle polarimeter will be as efficient as helium polarimeters. With the confidence gained in the theoretical calculations, the small angle scattering polarimeter will have the advantage that the energy dependence of the analysing power of the polarimeter's scattering nucleus could be

accurately calculated.

The three optical potentials used (Table 6.1) are actually global potentials obtained by fitting scattering data for a large number of nuclei over a wide range of energies. The RO potential was obtained by fitting proton polarization data only. The WH potential is the local equivalence of the non-local potential of Perey and Buck (Pe 62) and was generated by fitting cross sections only. The spin orbit term was obtained by fitting the cross section at backward angles. The BG potential is a local global potential obtained by fitting cross section and polarization.

The cross sections of 10 MeV neutrons scattered from Pb or Bi in the angular range of 2 to 50° should be very sensitive to the choice of the optical potential. Thus, one can use these cross section measurements and the polarization measurement in the interval of 15-65° to test the optical potentials available to describe the data. The BG potential produced the best fit to all the data presented in this work. The RO potential fit is not as good as the BG fit but it is definitely better than the WH potential. In particular, the small angle cross section is best described by the BG potential. All three potentials fitted the forward maximum of the large angle cross section data reasonably well but at the second maximum the BG potential provided

a better fit. The large angle polarization is also fitted very well by the BG potential and the poorest fit was obtained with the WH potential. This is in contrast to the result reported by Bucher and Hollandsworth (Bu 75 and Bu 75a) who got a superior fit, to the small angle scattering of 7.14 MeV neutrons from Pb and Bi, using the WH potential compared to the fit obtained using the RO potential.

APPENDIX A

MULTIPLE SCATTERING CORRECTIONS

A.1 Introduction

Neutron scattering experiments suffer from a severe restriction on the flux of incident neutrons. To illustrate this one might compare the neutron flux typically used in a neutron scattering experiment with that of a proton scattering experiment. As has been mentioned in Chapter 3 the reaction $^{9}Be(^{4}He,\vec{n})^{12}C$ has been used as a neutron source. The neutron flux coming of this reaction at 30° is about 6×10^{6} neutron/sec.μa.sr. In case of a proton beam provided by a charged particle accelerator the proton flux is 6×10^{12} protons/sec.μa. If the neutron and proton scattering cross sections are of the same order of magnitude then, to achieve the same statistical accuracy in both experiments, one has to run the neutron experiment over a period of time much larger than that of a proton experiment. This situation can be eased by using large size scatterers. This will result in an increase in solid angle and number of scattering nuclei. Consequently, the number of scattered neutron/sec will increase with a corresponding cut in the running time required to achieve a reasonable statistical accuracy. Fortunately, in neutron scattering experiments one can use as much as 2 moles of scattering

material without compromising the energy spread of the scattered neutrons. Since nature is not always that nice, this simple solution of the flux problem is not without serious consequences. Two problems will impose themselves due to the use of a large scatterer:

1) If the cross section and polarization angular distributions of the neutron source are not isotropic, then different sections of scatterer surface will be illuminated by different number of neutrons with different energies and polarizations. This problem is known as a "finite geometry" problem.

2) If the scatterer thickness is of the same order of magnitude as the mean free path of the neutron in the scatterer material, then the neutron will have a very good chance to scatter more than once before emerging out of the scatterer. This problem is called the "multiple scattering" problem.

The seriousness of these problems will be recognized once one remembers that all formulae and theoretical relationships are based on the assumption that neutrons are scattered from a point scatterer only once before being recorded as an event in the detector. In particular, equation (2.37) will provide meaningful numbers from experimental data only in the absence of the problems mentioned above, otherwise, these numbers have to be corrected.

Correcting the experimental data for multiple scattering can be achieved by calculating the observables, under investigation, for ideal condition and for real conditions. The ratio between these two estimations can provide a correction factor for experimental data. Several authors have tried an analytical solution for this problem. The analytical solutions involve a complex multidimensional integrals which can be performed either analytically under certain approximations or more accurately by numerical methods (see, for example, Mo 61). Aspelund and Gustafsson (As 67) have shown that Monte Carlo method is much superior to the analytical method in accuracy, computing time and computer storage. Moreover, the Monte Carlo method will in principle incorporate the essential experimental features by a computer simulation of the experiment. Finally, the Monte Carlo method makes it possible to estimate the error in the correction factors by calculating their standard deviations.

In what will follow we will restrict ourselves to the process of correcting the left-right asymmetry in elastic scattering experiments using a Monte Carlo technique.

Two Monte Carlo programs were available for use at the University of Alberta, PMS1 (Mi 70) and MULTPØL (As 67). These two programs are basically

dcing the same job using the same mathematical formalism to track down the polarization of individual neutrons scattered more than once inside the scatterer. Neither program could be used for scattering angles as small as 1° where the Mott-Schwinger scattering is dominant. It was found that the program PMS1 was easier to modify to include the Mott-Schwinger interaction.

A.2 The Program PMS1

The program simulates the experimental geometry as shown in figure A.1. Thousands of neutron are created at the point (x_s, y_s, z_s) which defines the location of the neutron source relative to an origin at the center of the scatterer. These neutrons fly between the source and points located at random inside the scatterer. These neutrons were assigned the experimental value of the energy and an arbitrary initial polarization of unity perpendicular to the scattering plane. The program then traces the scattering histories of these neutrons from which an estimate of the value of multiple scattering asymmetry can be obtained along with its standard deviation.

In order to perform the above process, the polarization dependence of the scattering cross section should be incorporated in the program. This is simple

Figure A.1 - Experimental geometry simulated by the Monte Carlo code PMS1.

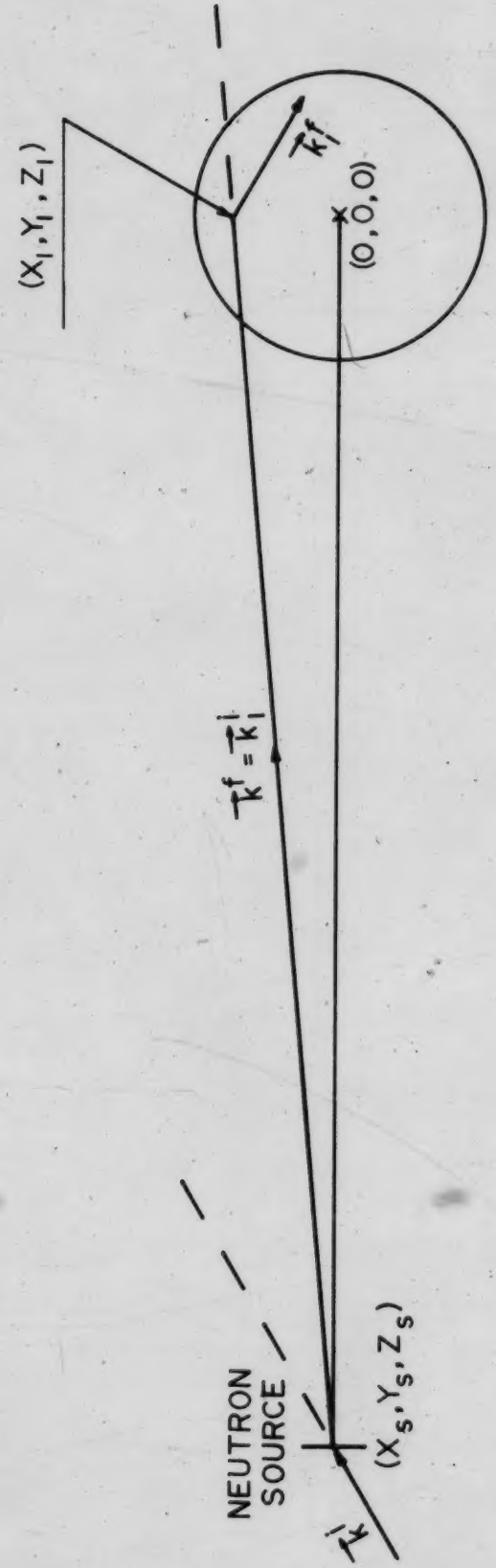
(X_1, Y_1, Z_1)
$\vec{k}_1^f$
$(0,0,0)$
$\vec{k}^f = \vec{k}_1^i$
NEUTRON SOURCE
(X_s, Y_s, Z_s)
$\vec{k}^i$

for the first scattering, since, according to equation (2.33) only the incident polarization and the analysing power of the scattering nucleus need to be known. If, now, we go to the second scattering the situation will become much more complicated. A total of seven parameters will be needed to perform the calculations. However, in case of a spinless target the following parameters will be needed:

1) the unpolarized cross section,

2) the initial polarization,

3) the analysing power of the scatterer, and

4) the rotation angle as defined in Chapter 2,

as functions of angle and energy. It is very difficult to get all this information experimentally. Moreover, if it is available it will need correction for multiple scattering and finite geometry before it can be used in the program. The alternative is then to provide the program with theoretically calculated information. Equations (2.41-2.45) tell us what we need to calculate the scattering amplitudes A and B. These amplitudes can be defined in terms of scattering phase shifts as:

$$A = \frac{1}{2ik} \sum_{\ell=0} [(\ell+1)(e^{2i\delta_+} - 1) + \ell(e^{2i\delta_-} - 1)]P_\ell(\theta) \qquad (A.1)$$

$$B = \frac{i}{2k} \sum_{\ell=1} \sqrt{\ell(\ell+1)}[e^{2i\delta_+} - e^{2i\delta_-}]P_\ell^1(\theta) \qquad (A.2)$$

where k is wave number, δ_+ for $j = \ell+\frac{1}{2}$ and δ_- for $j = \ell-\frac{1}{2}$

are the phase shifts, $P_\ell(\theta)$ is legender polynomial and P_ℓ^1 is the associated legender polynomial. The phase shifts can be either obtained directly by fitting the experimental data or can be calculated using the optical model potential whose parameters are obtained by fitting experimental data. The program takes phase shifts as functions of energy and uses them to calculate A and B which in turn are used in equations (2.41-2.45). Here the program is allowed to accept only real phase shifts. This condition restricts the usefulness of the program to only light nuclei. The cross sections are calculated as functions of the cosine of the scattering angle in the range from +1 to -1 at 41 steps which means that the program cannot be used where the Mott-Schwinger interaction is dominating.

For the purpose of tracing the polarization of a neutron undergoing several collisions inside the scatterer, the following process is used.

The axes of the system are defined as:-

$$\hat{x} = \frac{\hat{z} \wedge \vec{k}^i}{|\hat{z} \wedge \vec{k}^i|} = \frac{-\vec{k}^i \cos\theta_1 + \vec{k}^f}{\sin\theta_1} \qquad (A.3)$$

$$\hat{y} = - \vec{k}^i \qquad (A.4)$$

$$\hat{z} = \frac{\vec{k}^i \wedge \vec{k}^f}{|\vec{k}_i \wedge \vec{k}_f|} = \frac{\vec{k}^i \wedge \vec{k}^f}{\sin\theta_1} \qquad (A.5)$$

where $\hat{x}$, $\hat{y}$, $\hat{z}$ are unit vectors along the axis, $\vec{k}^i$ is the wave vector of the incident neutron, $\vec{k}^f$ is that of the scattered neutrons and θ_1 is the scattering angle. It should be mentioned here that this axes system is different from that used in Chapter 2. The axes system used in Chapter 2 is consistent with the Madison convention. In Chapter 2 the z-axis is taken along the direction of the incident neutron while here it is taken normal to the scattering plane. Now a neutron is created at the point (x_s, y_s, z_s) with polarization of

$$\vec{P}_1 = \vec{P}_1(\theta) = P_1(\theta)\hat{z} = P_1(\theta)\,\frac{\vec{k}^i \wedge \vec{k}_1^i}{\sin\theta} \,. \qquad (A.6)$$

If this neutron undergoes a scattering through an angle θ_1 at a randomly chosen point (x_1, y_1, z_1) inside the scatterer, then the initial polarization of this first scattering process is given by:

$$P^i_{x_1} = \vec{P}_1 \cdot \hat{x}_1 = \vec{P}_1(\theta)\,\frac{\vec{k}^i \cdot (\vec{k}_1^i \wedge \vec{k}_1^f)}{\sin\theta\,\sin\theta_1} \qquad (A.7)$$

$$P^i_{y_1} = \vec{P}_1 \cdot \hat{y} = 0 \qquad (A.8)$$

$$P^i_{z_1} = \vec{P}_1 \cdot \hat{z} = P_1(\theta)\,\frac{\cos\theta\,\cos\theta_1 - \cos\eta_1}{\sin\theta\,\sin\theta_1} \qquad (A.9)$$

where $\vec{k}^i$ is the unit wave vector of the charged particles used in the neutron source, $\vec{k}_1^i$ is the unit wave vector of the incident neutron in scattering #1, $\vec{k}_1^f$ is that for scattered neutron in scattering #1.

$$\cos\eta_1 = (\vec{k}^i \wedge \vec{k}_1^f)$$

$$\cos\theta_1 = \vec{k}_1^i \wedge \vec{k}_1^f$$

$$\cos\theta = \vec{k}^i \wedge \vec{k}_1^i \quad .$$

The polarized differential cross section for scattering #1 is:

$$\left(\frac{d\sigma}{d\Omega}\right)^1 = \left(\frac{d\sigma}{d\Omega}\right)_0^1 [1 + P_{z_1}^i P^{(1)}(\theta_1)]$$

$$= \left(\frac{d\sigma}{d\Omega}\right)_0^1 \left(1 + P^{(1)}(\theta_1) P_1(\theta) \frac{\cos\theta \cos\theta_1 - \cos\eta_1}{\sin\theta \sin\theta_1}\right) \quad (A.10)$$

where $\left(\frac{d\sigma}{d\Omega}\right)_0^1$ is the unpolarized cross section of scattering #1, and $P^{(1)}(\theta_1)$ is the polarization acquired by unpolarized beam upon scattering on the same scatterer.

Now we are ready to use equations (2.41) of Chapter 2, with the following equalities:

$$P_x = P_{x_1}^i \qquad P_y = P_{z_1}^i \qquad P_z = -P_{y_1}^i$$

$$P_x' = P_{x_1}^f \qquad P_y' = P_{z_1}^f \qquad P_z' = -P_{y_1}^f$$

and $$P_y' = P^{(1)} \quad .$$

The final polarization after scattering #1 will be given by:

$$P^f_{x_1} = \frac{\sqrt{1 - P^{(1)^2}(\theta_1)}\; P_1(\theta)\; \frac{(\vec{k}^i \cdot [\vec{k}^i_1 \wedge \vec{k}^f_1])}{\sin\theta\, \sin\theta_1}\; \cos(\theta_1 - \beta^{(1)})}{1 + P_1(\theta) P^{(1)}(\theta_1)\; \frac{\cos\theta\, \cos\theta_1 - \cos\eta_1}{\sin\theta\, \sin\theta_1}} \tag{A.11}$$

$$P^f_{y_1} = \frac{\sqrt{1 - P^{(1)^2}(\theta_1)}\; P_1(\theta)\; \frac{(\vec{k}^i \cdot [\vec{k}^i_1 \wedge \vec{k}^f_1])}{\sin\theta\, \sin\theta_1}\; \sin(\theta_1 - \beta^{(1)})}{1 + P_1(\theta) P^{(1)}(\theta_1)\; \frac{\cos\theta\, \cos\theta_1 - \cos\eta_1}{\sin\theta\, \sin\theta_1}} \tag{A.12}$$

$$P^f_{z_1} = \frac{P^{(1)}(\theta_1) + P_1(\theta)\; \frac{\cos\theta\, \cos\theta_1 - \cos\eta_1}{\sin\theta\, \sin\theta_1}}{1 + P_1(\theta) P^{(1)}(\theta_1)\; \frac{\cos\theta\, \cos\theta_1 - \cos\eta_1}{\sin\theta\, \sin\theta_1}} \tag{A.13}$$

The program now tests if the neutron can scatter again inside the scatterer. If the answer is yes, then the coordinates of the scattering point will be calculated along with the scattering angle and energy. Let the second scattering point be (x_2, y_2, z_2) and scattering angle is θ_2. The incident polarization of the second scattering will be:

$$P^i_{x_2} = (P^f_{x_1} \cdot \hat{x}_1 + P^f_{z_1} \cdot \hat{z}_1) \cdot \hat{x}_2 = -P^f_{z_1} (\hat{x}_1 \cdot \hat{z}_2) + P^f_{x_1} (\hat{x}_1 \cdot \hat{x}_2)$$

$$= P^f_{x_1} \frac{\cos\theta_1\, \cos\theta_2 - \cos\eta_{1,2}}{\sin\theta_1\, \sin\theta_2} + P^f_{z_1} \frac{\vec{k}^i_1 \cdot [\vec{k}^i_2 \wedge \vec{k}^f_2]}{\sin\theta_1\, \sin\theta_2} \tag{A.14}$$

$$P^{i}_{y_2} = \vec{P}^{f}_{y_1} \tag{A.15}$$

$$P^{i}_{z_2} = (P^{f}_{x_1} \cdot \hat{x}_1 + P^{f}_{z_1} \cdot \hat{z}_1) \cdot \hat{z}_2 + P^{f}_{x_1} (\hat{x}_1 \cdot \hat{z}_2) + P^{f}_{z_1} (\hat{x}_1 \cdot \hat{x}_2)$$

$$= -P^{f}_{x_1} \frac{\vec{k}^{i}_1 \cdot [\vec{k}^{i}_2 \wedge \vec{k}^{f}_2]}{\sin\theta_1 \sin\theta_2} + P^{f}_{z_1} \frac{\cos\theta_1 \cos\theta_2 - \cos\eta_{1,2}}{\sin\theta_1 \sin\theta_2} \tag{A.16}$$

where

$$\cos\eta_{1,2} = \vec{k}^{i}_1 \cdot \vec{k}^{f}_2 \ .$$

The differential cross section is:

$$\left(\frac{d\sigma}{d\Omega}\right)^2 = \left(\frac{d\sigma}{d\Omega}\right)_0 \left(1 + P^{i}_{z_2} \, P^{(2)}(\theta_2)\right) \ . \tag{A.17}$$

Now the state of the polarization after scattering #2 can be described by:

$$P^{f}_{x_2} = \frac{\sqrt{1 - P^{(2)^2}}}{1 + P^{i}_{z_2} P^{(2)}} \left[P^{i}_{x_2} \cos(\theta_2 - \beta^{(2)}) + P^{i}_{y_2} \sin(\theta_1 - \beta^{(2)})\right] \tag{A.18}$$

$$P^{f}_{y_2} = \frac{\sqrt{1 - P^{(2)^2}}}{1 + P^{i}_{z_2} P^{(2)}} \left[-P^{i}_{x_2} \sin(\theta_2 - \beta^{(2)}) + P^{i}_{y_2} \cos(\theta_2 - \beta^{(2)})\right] \tag{A.19}$$

$$P^{f}_{z_2} = \frac{P^{i}_{z_2} + P^{(2)}}{1 + P^{i}_{z_2} P^{(2)}} \ . \tag{A.20}$$

We can now use equations (A.7-A.20) to gereralize the state of the polarization before and after any number of scatterings. Let scattering m take place at the point (x_m, y_m, z_m) while (m-1) will denote the preceding scattering then:

$$P^{i}_{x_m} = \frac{\cos\theta_{(m-1)}\ \cos\theta_m - \cos\eta_{(m-1),m}}{\sin\theta_{(m-1)}\ \sin\theta_m} P^{f}_{x_{(m-1)}}$$

$$+ \frac{\vec{k}^{i}_{(m-1)} \cdot [\vec{k}^{i}_{m} \wedge \vec{k}^{f}_{m}]}{\sin\theta_{(m-1)}\ \sin\theta_m} P^{f}_{z_{(m-1)}} \qquad (A.21)$$

$$P^{i}_{y_m} = P^{f}_{y_{(m-1)}} \qquad (A.22)$$

$$P^{i}_{z_m} = -\frac{\vec{k}^{i}_{(m-1)} \cdot [\vec{k}^{i}_{m} \wedge \vec{k}^{f}_{m}]}{\sin\theta_{(m-1)} \cdot \sin\theta_m} P^{f}_{x_{(m-1)}}$$

$$+ \frac{\cos\theta_{(m-1)}\ \cos\theta_m - \cos\eta_{(m-1),m}}{\sin\theta_{(m-1)}\ \sin\theta_m} P^{f}_{z_{(m-1)}} \qquad (A.23)$$

and

$$P^{f}_{x_m} = \frac{\sqrt{1 - P^{(m)^2}}}{1 + P^{i}_{z_m} P^{(m)}} [P^{i}_{x_m} \cos(\theta_m - \beta^{(m)}) + P^{i}_{y_m} \sin(\theta_m - \beta^{(m)})] \qquad (A.24)$$

$$P^{f}_{y_m} = \frac{\sqrt{1 - P^{(m)^2}}}{1 + P^{i}_{z_m} P^{(m)}} [-P^{i}_{x_m} \sin(\theta_m - \beta^{(m)}) + P^{i}_{y_m} \cos(\theta_m - \beta^{(m)})] \qquad (A.25)$$

$$P^{f}_{z_m} = \frac{P^{i}_{z_m} + P^{(m)}}{1 + P^{i}_{z_m} P^{(m)}} \qquad (A.26)$$

and finally

$$\left(\frac{d\sigma}{d\Omega}\right)^{m} = \left(\frac{d\sigma}{d\Omega}\right)^{m}_{0} [1 + P^{i}_{z_m} P^{(m)}] \quad . \qquad (A.27)$$

We turn our attention now to the detection process. At each collision point in the scatterer, the

program calculates the probability that the neutron will scatter to each of the two detectors on each side of the incident neutron beam and each makes the same scattering angle with the incident beam direction. The product of the weight of neutron and its probability of reaching the detector form an estimate of the flux at the detector. The neutron flux at a point $\vec{r}$ in the detector resulting from a collision at $\vec{r}'$ in the scatterer is given by

$$F = WA_m P(E,\Omega)\,\Delta\Omega\ \mathrm{Exp}\left(-\int_0^{|\vec{r}-\vec{r}'|} \Sigma^t(E)\,ds\right) \qquad (A.28)$$

where

$$P(E,\Omega) = E\ \frac{\sigma(\theta)}{\int_0^{2E}\int_0^{\pi}\sigma(\theta)\ d\theta\ d\phi}\ .$$

E is the laboratory energy of the neutron after scattering, $\sigma(\theta,\phi)$ is the unpolarized differential cross section. $\Delta\Omega$ is the solid angle subtended by the detector at the scattering point,

$$\Sigma^t(E) = \rho \int_0^{2\pi}\int_0^{\pi} \sigma(\theta,\phi)\ d\theta\ d\phi\ ,$$

ρ is the density of the scatterer,
s is the distance from scattering point $\vec{r}'$ to an arbitrary point along the path from $\vec{r}'$ to $\vec{r}$,

A is a factor to correct the cross section from that of an unpolarized beam to that of a polarized one. A is given by:

$$A = 1 + P_{z_D} \, P^D(\theta_D)$$

where

$$\cos\theta_D = \vec{r}' \cdot \vec{r} / |\vec{r}' \wedge \vec{r}|$$

and P_{z_D} is calculated by using equation (A.23) where θ_D replaces θ_m and $P^D(\theta_D)$ is calculated theoretically from equation (2.44) of Chapter 2 at angle θ_D. Finally W is the statistical weight which is equal to 1.0 for collision #1 and given by:

$$W = \prod_{1}^{m} [1 + P^f_{z_m} \, P^m(\theta_m)]$$

for subsequent collisions.

The asymmetry can now be calculated using the flux at both detectors and the actual experimental conditions. Comparing the asymmetry to the one calculated under ideal condition will yield the correction factor for the experimental points.

A.3 The Modified Program

The first modification to the program is to include the contribution of the Mott-Schwinger interaction to the scattering amplitude. This contribution is given by:

$$B_1 = B - 2.93 \times 10^{-3} \frac{M}{m+M} Z \cot(\theta/2)$$

where B is the scattering amplitude defined in equation (A.2), M is the scattering nucleus mass, m is the neutron mass and θ is the scattering angle. In calculating cross sections and polarizations a provision has to be made for the inclusion of angles as small as 0.1°. In the original program the angular range (0-180°) was divided into 41 equal steps in the range of +1 to -1 for the cosine of the scattering angle and this means that the smallest scattering is 18°. This has been changed, such that the range (+1 to -1) has been divided into 134 unequal steps in the following way:

$$\begin{aligned}
\cos\theta &= 1 - [2.0 \times 10^{-6} \times (I-1)] && 1 \leq I \leq 51 \\
&= 1 - [5.0 \times 10^{-5} \times (I-49)] && 52 \leq I \leq 69 \\
&= 1 - [5.0 \times 10^{-4} \times (I-67)] && 70 \leq I \leq 87 \\
&= 1 - [5.0 \times 10^{-3} \times (I-85)] && 88 \leq I \leq 95 \\
&= 1 - [5.0 \times 10^{-2} \times (I-94)] && 96 \leq I \leq 134
\end{aligned}$$

Finally the program has been changed so that it can accept complex nuclear scattering amplitudes, A and B, rather than real phase shifts, as functions of energy whose range can be defined externally. These scattering amplitudes have been calculated using the optical model by a special program (SH 74).

To test the performance of the program in the large angle region the output of the new program was compared to the output of the old one for the scattering of 5.0 MeV polarized neutron on ^{12}C. The geometry and phase shifts for this experiment were given by Weil (We 73). The results of both programs were in very good agreement. In the small angle region several runs have been performed on the geometry of the present experiment on the scattering of 10.0 MeV neutrons on ^{208}Pb. In these runs the scattering angles of 1.0, 2.3 and 5.0° have been considered and for each angle three scattering radii of 0.5, 1.27, 2.5 cm were considered. As one should expect, the correction factor for a certain scatterer thickness decreases with the increase of the angle. Meanwhile, the correction factor for a certain angle increases with an increase in the scatterer thickness.

APPENDIX B

THE SUPERCONDUCTING SOLENOID SYSTEM

B.1 The Solenoid and the Persistent Switch

Table B.1 summarizes the characteristics of the solenoid and the switch. Fig. B.1 shows a schematic circuit diagram for the solenoid and the switch. Three things will be considered here, the action of the persistent switch, the calibration of the solenoid and, finally, the calculation of the required integrated field.

1) The persistent switch is a simple superconducting wire made of the same material as the solenoid with a normal resistance of 15 Ω. The switch is electrically connected in parallel with the solenoid. Its physical position is adjusted such that both the solenoid and the switch can be cooled down simultaneously to the liquid helium temperature of 4.2°K. In addition, a normal wire, called switch heater with a resistance of 100 Ω, surrounds the superconducting wire. A current of 2.25 ma, at 2.25 V, passing through the switch heater will produce enough heat to change the state of superconducting wire to normal. This combination of the superconducting wire and the heater acts as a switch in that it can conduct current when it is closed (zero

Table B.1

Specification of the superconducting solenoid system
(supplied by the manufacturer)

Bore diameter (room temperature)	1.5 inches
Overall winding length	22.61 cm
Overall width of cryostat	10.0 inches
Overall length of cryostat	12.0 inches
Minimum guaranteed field	70.0 KG
Number of turns in coil	17207
Inside diameter of coil	6.71 cm
Outside diameter of coil	10.45 cm
Liquid helium evaporation rate	∿250 cc/hour
Capacity of liquid helium reservoir	∿3.6 liters
Quench current at 4.2°K	80 A
Switch heater resistance	∿100 Ω
Switch normal state resistance	15 Ω
Solenoid inductance	6.9 H
Voltage to open switch	2.25 V

Figure B.1 - Schematic circuit diagram for the superconducting solenoid and the persistent switch.

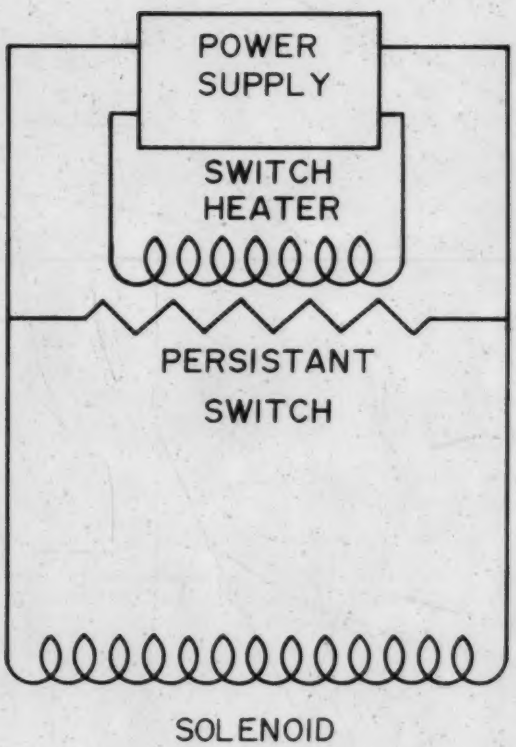
POWER
SUPPLY
SWITCH
HEATER
PERSISTANT
SWITCH
SOLENOID

resistance) and block it when it is open (very large resistance). The actual process of putting the solenoid in the persistent mode is as follows.

a) With the heater off the solenoid and the superconducting wire is cooled to liquid helium temperature.

b) Putting the switch heater on, the superconducting wire will become normal with 15 Ω resistance, infinitely large compared to the solenoid resistance (zero Ω). The switch now is "open".

c) Connecting the system to the power supply the desired current will flow through the solenoid.

d) Switching the heater off, the switch wire will be cooled down and become superconducting. The switch now is "closed". The current in the solenoid will then flow through a zero resistance loop formed by the switch superconducting wire and the solenoid.

e) It is possible now to turn the power supply off without affecting the current in the loop. This will mean that the magnetic field produced by the current in the loop will stay on as long as the loop is kept under its critical temperature.

f) To change the magnitude of the magnetic field, the power supply should be switched on and adjusted to provide (within $\frac{1}{4}$ to $\frac{1}{2}$ amps) the same current as in the loop, open the switch by turning the switch heater on.

The current in the solenoid will flow through the power supply and could be changed and the process could be repeated to put the solenoid back in the persistent mode.

2) Three different kinds of magnetic probes have been used to measure the magnetic field as a function of the current and distance along the axis of the solenoid.

The first probe was a "MistoR", MRA11 produced by American Aerospace Controls, Inc. This probe is a solid state, thin magnetic flux-sensitive film, that changes resistance as a function of the applied magnetic field. The second probe was a Hall generator HA-12 produced by the same company. When a fixed electric current passes through the thin film, of the Hall generator, while it is exposed to a magnetic field, a Hall voltage will develop across the terminals of the thin film. This voltage is a function of the applied magnetic field. The main advantage of these probes is their size. The MistoR, for example, measures $\frac{3}{32} \times \frac{3}{16}$". Unfortunately, we have found, contrary to the manufacturer's claim, these probes are not linear above about 10 KV.

The third probe used was a rotating coil. Unfortunately, the geometry of the rotating coil available made it impossible to insert it inside the solenoid to trace the field profile. As a result,

the ratio $H(x)/H_o$, where $H(x)$ is the magnetic field at a distance x from the center and H_o is the magnetic field at the center, is plotted as a function of x. The resulting profile is shown in fig. B.2. The values of $H(x)$ and H_o are those provided by the manufacturer. As shown in fig. B.2, two points A and B were chosen for measuring the magnetic field as a function of the current. Point A is the closest point to the edge of cryostat the rotating coil could reach. Point B is a point at which the magnetic field does not change very rapidly with the change in the distance. A series of measurements of the magnetic field have been taken at these two points as a function of the current I. Table B.2 shows these results. In this table H(A) and H(B) are the magnetic fields measured in KG at points A and B respectively. $H_o(A)$ is the value of the magnetic field at the center of the solenoid calculated from the profile of fig. B.2 and the corresponding H(A). $H_o(B)$ is the same as $H_o(A)$ at point B. R_o is the ratio H_o/I, and R is the ratio H/I. The average value of R_o is 0.908 KG/amp. The ratio of the magnetic field at the center to the current could also be calculated from

$$R_{oc} = \mu_o n$$

where R_{oc} is the calculated ratio, μ_o is the permeability

Figure B.2 - The profile of the axial magnetic field of the superconducting solenoid.

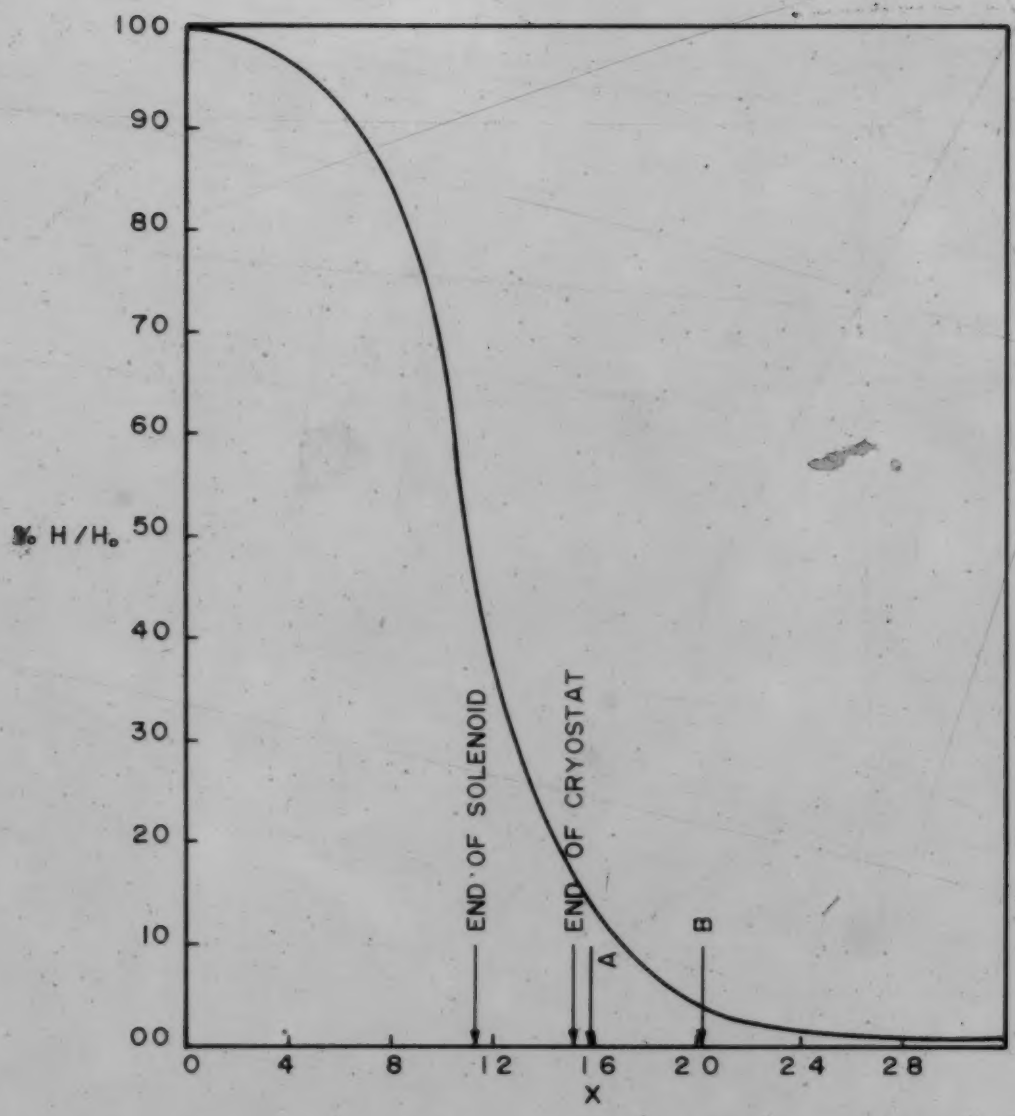
100
90
80
70
60
% H/H₀ 50
40
30
20
10
00
0
4
8
12
16
20
24
28
X
END OF SOLENOID
END OF CRYOSTAT
A
B

Table B.2

Measurements of the magnetic field along the axis of the solenoid at two different points

I (amp.)	Point A X = 15.9 cm				Point B X = 20.3 cm			
	H(A) (KG)	H_o(A) (KG)	R = H(A)/I (KG/amp)	R = H_o(A)/I (KG/amp)	H(B) (KG)	H_o(B) (KG)	R = H(B)/I (KG/amp)	R = H_o(B)/I (KG/amp)
70	9.112	62.841	0.1302	0.8977	3.179	63.58	0.0454	0.9083
60	7.867	54.255	0.1311	0.9043	2.711	54.22	0.0452	0.9037
50	6.539	45.097	0.1308	0.9019	2.240	44.80	0.0448	0.8960
40	5.261	36.283	0.1315	0.9071	1.822	36.44	0.0456	0.9110
30	3.945	27.207	0.1315	0.9069	1.368	27.36	0.0456	0.9120
26	3.426	23.628	0.1318	0.9088	1.189	23.78	0.0457	0.9146
20	2.633	18.159	0.1317	0.9080	0.919	18.38	0.0460	0.9190
10	1.315	9.069	0.1315	0.9060	0.462	9.24	0.0462	0.924

of the air and n is the number of turns in the solenoid per unit length. Using the information given in table B.1 we get

$$R_{oc} = 0.956 \quad \text{KG/amp} .$$

One can see that R_o and R_{oc} agree within 5.3% which means that the profile provided by the manufacturer of the solenoid is good enough to be used in setting up the required integrated field.

3) The fact that, the magnetic field, produced by the solenoid, is not a homogeneous field has the advantage that the stray field outside the solenoid is small enough to disturb neither the charged particle beam nor the photomultiplier tubes in the detectors. However, this inhomogeneity makes it difficult to set up the required integrated field. The current which produces a certain integrated field can be calculated from:

$$I = \frac{H_t}{a \cdot R_o} \qquad \text{(B.1)}$$

where H_t is the integrated field in KG-cm and can be calculated for each neutron energy using equation (2.47), a is double the area under the magnetic field profile of fig. B.2. For 10.0 MeV neutrons the integrated field as given by equation (2.48) is 751.8 KG-cm, a was found to be 24.048 and R_o is 0.908. The current

required to produce enough magnetic field to rotate the spin of 10.0 MeV neutrons by 180.0° is then 34.43 amp.

B.2 The Power Supply

The power supply is a model D.P.S. A/100/4.5/1, manufactured by Didcot Inst. Co. Ltd., Oxford, England. It is capable of providing 100 amperes at ±5 volts. The current can be swept up and down automatically to a preset value in times as short as 1 minute and as long as 100 minutes. It, also, provides the switch heater with the necessary current. This power supply is provided with an ampere/volt meter for measuring the solenoid current.

B.3 The Cryostat

Fig. B.3 shows a schematic diagram of the cryostat which has been manufactured by Thor Cryogenics, Brinsfield, Oxford, England. The upper part of the helium reservoir is surrounded by a liquid nitrogen jacket which is connected to a thermal radiation shield surrounding the lower part of the liquid helium reservoir. The helium reservoir is separated from the nitrogen jacket and shield by vacuum. The capacity of the helium reservoir is about 3.6 liters. According to the manufacturer's specifications the evaporation

rate of liquid helium should be about 300 cc/hour. After six months the evaporation rate started to increase very rapidly until it was more than one liter per hour which made the magnet impractical to use in neutron experiments. Examination of the inside of the cryostat in the Nuclear Research Center showed that the liquid nitrogen shield and the top of the lower section of the helium reservoir were touching each other. The nitrogen shield was realigned solving the problem, for some time, but it then reoccurred. It was then decided to glue some nylon hemispheres to the liquid helium reservoir at the positions indicated by A, B, C, and D in fig. B.3. The hemisphere shape was chosen to minimize the area of contact between the nitrogen shield and the helium reservoir. The radius of these hemispheres is slightly less than 5 mm so that contact will not take place unless there is a large misalignment of the nitrogen shield. This misalignment might result from any rough handling of the cryostat because the connection between the liquid nitrogen jacket and shield is established by a flexible stainless steel screen. As a consequence of these modifications the evaporation rate of the liquid helium has been improved to about 250 cc/hour.

Figure B.3 - Schematic diagram of the liquid helium cryostat.

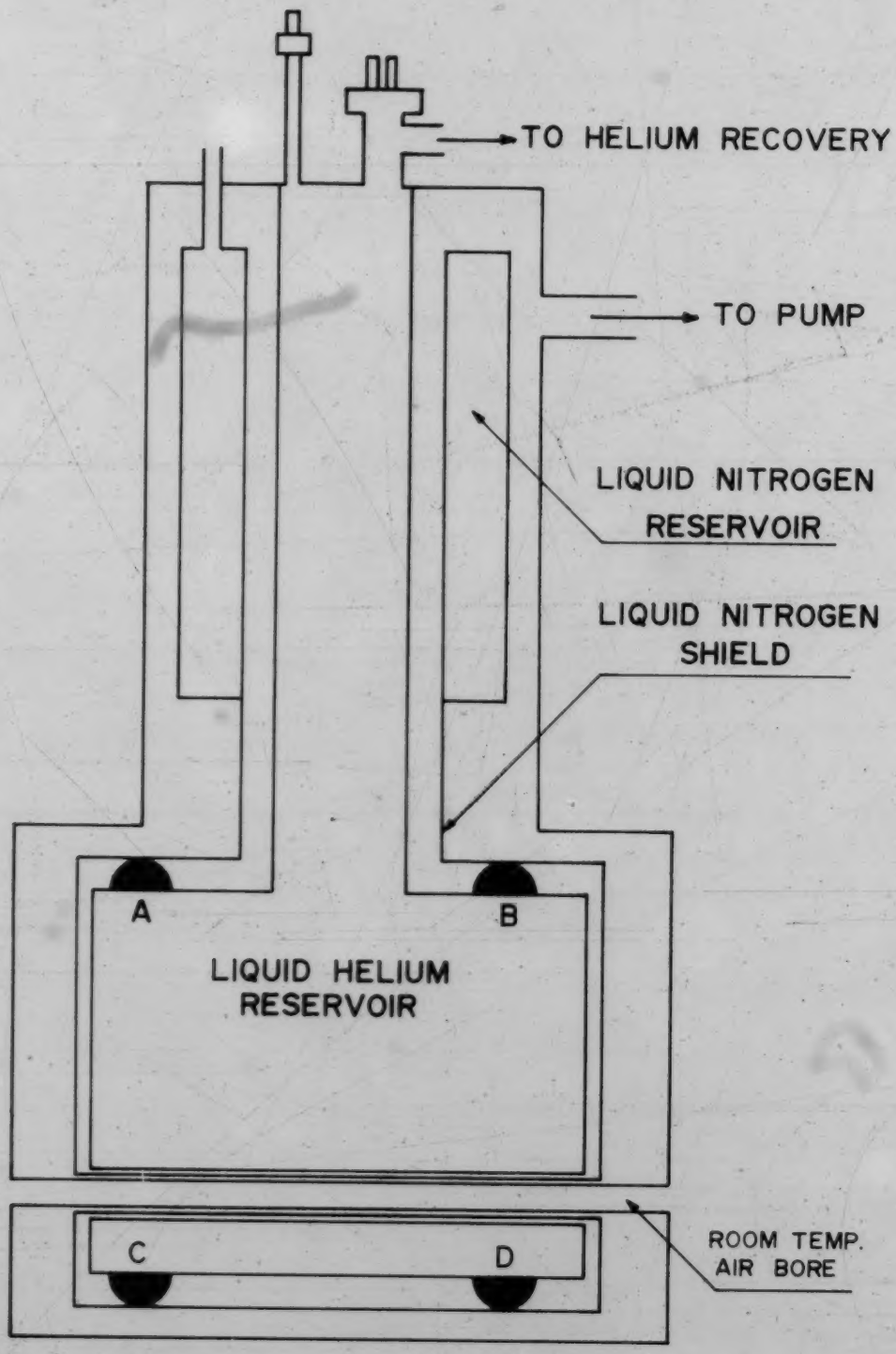
TO HELIUM RECOVERY
TO PUMP
LIQUID NITROGEN RESERVOIR
LIQUID NITROGEN SHIELD
A
B
LIQUID HELIUM RESERVOIR
C
D
ROOM TEMP. AIR BORE

The final feature of the cryostat is the liquid helium level meter. The level meter is a superconducting wire placed vertically in the liquid helium reservoir. So when the cryostat is full with liquid helium, a large portion of the wire will be superconducting. By applying a very small voltage across the superconducting wire a small current will flow in the circuit. This current will be proportional to the resistance of the wire, which in turn is proportional to the length of that portion of the wire which is not superconducting. The current will then be a measure of the height of the liquid helium in the cryostat.

REFERENCES

Ad 68 A. Ádám, F. Deak, L. Jéki, A. Kiss, Z. Kövessy, G. Palla and P. Harasko, Yad. Fiz 8 (1968) 439. [Translation: Soviet J. Nucl. Phys. 8 (1969) 255].

Al 56 IU. A. Aleksandrov and I.I. Bondarenko, J. Exptl. Theoret. Phys. (U.S.S.R.) 31 (1956) 726. [Translation: Soviet Phys. JETP 4 (1957) 612].

Al 57 IU. A. Aleksandrov, J. Exptl. Theoret. Phys. (U.S.S.R.) 33 (1957) 294. [Translation: Soviet Phys. JETP 6 (1958) 228].

Al 61 Yu. A. Aleksandrov, G.V. Anikin and A.S. Soldetov, J. Exptl. Theoret. Phys. (U.S.S.R.) 40 (1961) 1878. [Translation: Soviet Phys. JETP 13 (1961) 1319].

An 70 G.V. Anikin and I.I. Kotukhov, Yad. Fiz 12 (1970) 1121. [Translation: Soviet J. Nucl. Phys. 12 (1971) 614].

An 71 G.V. Anikin and I.I. Kotukhov, Yad. Fiz 14 (1971) 269. [Translation: Soviet J. Nucl. Phys. 14 (1972) 152].

As 67 O. Aspelund and B. Gustafsson, Nucl. Inst. Meth. 57 (1967) 197.

Ba 57 S.J. Bame, Jr. and J.E. Perey, Jr., Phys. Rev. 107 (1957) 1616.

Ba 57a V.S. Barashenkov, I.V. Stakhnov and IU. A. Aleksandrov, J. Exptl. Theoret. Phys. (U.S.S.R.) 32 (1957) 154. [Translation: Soviet Phys. JETP 5 (1957) 144].

Be 69 F.D. Becctti, Jr. and G.W. Greenlees, Phys. Rev. 182 (1969) 1190.

Be 73 R.E. Benenson, K. Rimawi, E.H. Sexton and B. Center, Nucl. Phys. A212 (1973) 147.

Br 71 W.B. Brost, Los Alamos Scientific Laboratory Report LA-4596.

Bu 73 W. Bucher, C. Hollandsworth and R. Lamoreaux, Nucl. Inst. Meth. 111 (1973) 237.

Bu 75 W. Bucher and C. Hollandsworth, Phys. Lett. 58B (1975) 277.

Bu 75a W. Bucher and C. Hollandsworth, Phys. Rev. Lett. 35 (1975) 1419.

Co 58 J.H. Coon, R.W. Davies, H.E. Felthauser and D.B. Nicodemus, Phys. Rev. 111 (1958) 250.

Da 72 W.K. Dawson, Nuclear Research Center, University of Alberta Internal Report UAE-NPL-39 (1972) 30.

De 64 S. De Bendetti, "Nuclear Interaction", John Wiley & Sons Inc., New York, 1964, p.

De 73 D.C. De Martini, C.R. Soltesz and T.R. Donoghue, Phys. Rev. 7C (1973) 1824.

Dr 73 L. Drigo, C. Manduchi, G. Moschini, M.T. Russo-Munduchi, G. Tornielli and G. Zannoni, Il Nuovo Cimento 13A (1973) 867.

Du 61 P.S. Dubbeldam and R.L. Walter, Nucl. Phys. 28 (1961) 414.

Du 63 Yu. V. Dukarevich and A.N. Dyumin, J. Exptl. Theoret. Phys. (U.S.S.R.) 44 (1963) 130. [Translation: Soviet Phys. JETP 17 (1963) 89].

El 66 A.J. Elwyn, J.E. Monahan, R.O. Lane, A. Langsdrof, Jr., and F.P. Mooring, Phys. Rev. 142 (1966) 758.

Er 56 T. Eriksson, Nuclear Phys. 2 (1956) 91.

Er 67 H.J. Erramuspe, Nuclear Phys. A91 (1967) 75.

Ga 72 R.B. Galloway and R.M.A. Maayouf, Nucl. Inst. Meth. 105 (1972) 561.

Ga 73 R.B. Galloway and R.M.A. Maayouf, Nucl. Phys. A212 (1973) 182.

Ga 75 R.B. Galloway and M. Lugo, Contribution to the Fourth International Symposium on Polarization Phenomena in Nuclear Reactions, Zurich, Switzerland, Aug. 25-29, 1975.

Go 61 M.D. Goldberg and J.M. Le Blanc, Phys. Rev. 122 (1961) 164.

Go 63 M.D. Goldberg, Progress In Fast Neutron Physics, (Eds.: G.C. Phillips, J.B. Marrion and J.R. Risser, University of Chicago Press, 1963) p. 3.

Go 67 G.V. Gorlov, N.S. Lebedeva and V.M. Morosov, Phys. Letters 25B (1967) 197.

Go 68 G.V. Gorlov, N.S. Lebedeva and V.M. Morosov, Yad. Fiz. 8 (1968) 1086. [Translation: Soviet J. Nucl. Phys. 8 (1969) 630].

Ha 60 W. Haeberli, Proc. 1st International Symp. on Polarization Phenomena of Nucleons, Basel, 1963 (Eds.: P. Huber and K.P. Meyer, Kirkhauser Verlag Basel, 1961) p. 149.

Ha 63 W. Haeberli, Progress In Fast Neutron Physics, (Eds.: G.C. Phillips, J.B. Marrion and J.R. Risser, University of Chicago Press, 1963) p. 307.

He 56 W. Heckrotte, Phys. Rev. 101 (1956) 1406.

Hi 56 P. Hillman and G.H. Stafford, Il Nuovo Cimento 3 (1956) 633.

Hi 56a P. Hillman, G.H. Stafford and C. Whitehead, Il Nuovo Cimento 4 (1956) 67.

Ho 69 W.S. Hogan and R.G. Seylor, Phys. Rev. 117 (1969) 1706.

Hu 70 A.H. Hussein, M. Sc. Thesis, University of Alberta, Edmonton, Alberta, Canada, 1970.

Ku 68 F.T. Kuchnir, A.J. Elwyn, J.E. Monahan, A. Langsdrof, Jr. and F.P. Mooring, Phys. Rev. 176 (1968) 1405.

Ma 70 P. Marmier and E. Sheldon, Physics of Nuclei and Particles Vol. II (Academic Press, 1970).

Ma 71 K. Masood Ali, R.B. Galloway and D.G. Vass, Nucl. Inst. Meth. 92 (1971) 553.

Ma 73 P.W. Martin, R. McFadden and B.L. White, Can. J. Phys. 51 (1973) 2197.

Mi 70 T.G. Miller, F.P. Gibson and G.W. Morrison, Nucl. Inst. Meth. 80 (1970) 325.

Mo 29 N.F. Mott, Proc. Roy. Soc. (London) A124 (1929) 425.

Mo 61 J.E. Monahan and A.J. Elwyn, Nucl. Inst. Meth. 14 (1961) 348.

Mo 64 J.E. Monahan and A.J. Elwyn; Phys. Rev. 136 (1964) 1678.

Mu 71 G.S. Mutcher, W.B. Broste and J.E. Simmons, Phys. Rev. 3C (1971) 1031.

Na 72 R. Nath, F.W.K. Firk, R.J. Molt and H.L. Schultz, Nucl. Inst. Meth. 98 (1972) 365.

Ne 70 G.C. Neilson, C. Glavina, W.K. Dawson, K.V.K. Ivengar and W.J. McDonald, Nucl. Inst. Meth. 81 (1970) 301.

Ob 72 A.W. Obest, T.B. Grandy and J.S. Weil, Phys. Rev. 5C (1972) 738.

Oh 72 G.G. Ohlsen, Rep. Prog. Phys. 35 (1972) 717.

Pa 71 G. Palla, Phys. Lett. 35B (1971) 477.

Pe 62 F. Perey and B. Buck, Nucl. Phys. 32 (1962) 353.

Pe 74 C.M. Perey and F. Perey, Atomic Data and Nuclear Data Tables 13 (1974) 293.

Re 65 R.F. Redmond, Phys. Rev. 140 (1965) 1267.

Ro 65 L. Rosen, J.G. Beery and A.S. Goldhabor, Annals of Phys. 34 (1965) 96.

Sa 56 J.T. Sample, Can. J. Phys. 34 (1956) 36.

Sa 67 G.R. Satchler, Nucl. Phys. A91 (1967) 75.

Sc 48 J. Schwinger, Phys. Rev. 73 (1948) 407.

Sh 71 H. Sherif, Can. Assoc. Phys. Bull. 27 (1971) 70.

Sh 74 H. Sherif, University of Alberta, Edmonton, Alberta, Canada, Private communications.

So 71 J. Soukup et al, Nuclear Research Center, University of Alberta Progress Report 1971 and 1974, also to be published in Nucl. Inst. Meth.

Ta 65 T. Tamura, Rev. Mod. Phys. 37 (1965) 679.

Th 59 R.H. Thaler, Phys. Rev. 114 (1959) 827.

Vo 56 R.G.P. Voss and R. Willson, Phil. Mag. 1 (1956) 175.

Wa 65 M. Walt and D.B. Fossan, Phys. Rev. 137 (1965) 629.

Wa 70 R.L. Walter, Proc. 3rd Int. Symp. on Polarization Phenomena in Nuclear Reactions, Madison, 1970 (Eds.: H.H. Barschall and W. Haeberli, University of Wisconsin Press, Madison, 1970) p. 317.

We 59 V.F. Weisskopf and H. Feschbach (Private communication with R.H. Thaler Th 59).

We 73 J.S. Weil, Dept. of Physics, Univ. of Kentucky, Private communications.

Wi 64 D. Wilmore and P.E. Hodgson, Nucl. Phys. 55 (1964) 673.

Wo 62 C. Wong, J.D. Anderson, J.W. McClure and B.D. Walker, Phys. Rev. 128 (1962) 2339.